Blocking Protein Phosphatase 2Cm to prevent pancreatic cancer cell growth

Elin Jessie Hollseter

Master thesis

Molecular Biology and Biochemistry

60 credits

Department of Biosciences

Faculty of Mathematics and Natural Sciences

University of Oslo

November 2023

Thesis for the Master´s degree in Bioscience

Main field of study in Molecular biology and biochemistry

Blocking Protein Phosphatase 2Cm to prevent pancreatic cancer cell growth

2023

Blocking Protein Phosphatase 2Cm to prevent pancreatic cancer cell growth

Elin Jessie Hollseter

http://www.duo.uio.no/

Print productions: Reprosentralen, University of Oslo

ACKNOWLEDGEMENTS

This thesis is the culmination of my master's degree at the Department of Biosciences, University of Oslo. Laboratory work was conducted at the Department of Medicinal Biochemistry at Rikshospitalet from January 2022 to September 2023.

I want to extend my heartfelt appreciation and gratitude to my supervisors Dr. Bjørn Dalhus and Prof. Lars Eide for allowing me to be a part of this project and write this thesis. I have learned so much and truly grown my interest in research because of you. Bjørn, thank you for your patience, calmness, and simplification in your learning, and your invaluable guidance and expert mentorship throughout this project. Your wisdom and dedication have been instrumental in shaping this thesis, I am forever grateful. Thank you for teaching me several molecular and biochemical methods in the lab, and for your critical reading of my thesis. I want to thank my co-supervisor, Lars, for your valuable insights, constructive feedback, and willingness to invest your time and expertise in this project. Thank you for taking the time to help me understand challenging results, and for reading my thesis with a critical eye.

Furthermore, I want to thank Pernille Blicher, Marte Eikenes, Georgina Fura Munoz, and Viktoria Holsvik. You are all inspiring women I look up to. Pernille, thank you for always being there to help me in the lab and for always bringing fun and good conversations. I want to thank Marte for teaching me methods in the cell lab and helping me understand challenging details. Thank you for all the enjoyable conversations and support. Gina, thank you for your motivational speeches, supporting words, and good mood. Also, I thank Viktoria for calming and motivational words and for cheering me through the writing. I am forever grateful to you all.

To my friends and family, I extend my deepest gratitude for your unwavering encouragement, understanding, and belief in my abilities. Your support provided me with motivation and strength through this project. Last, but not least, I want to thank my boyfriend, Ashkan, for all your love and encouragement. You have been my constant source of motivation.

ABSTRACT

The mitochondrial phosphatase PP2Cm is a central protein in the catabolism of branched-chain amino acids (BCAA), regulating the activity of the BCKDH complex. Cancer cells often use BCAAs for energy and metabolites, causing alterations in BCAA catabolism. This is especially seen within the mitochondria of pancreatic ductal adenocarcinoma (PDAC). The BCKDH complex plays a crucial role in PDAC, thus targeting PP2Cm is a promising strategy for suppressing BCKDH complex activity and, consequently, cancer cell growth and proliferation. This master thesis aimed to target mitochondrial metabolism to combat pancreatic cancer by identifying and characterizing novel molecules inhibiting the activity of human PP2Cm.

The identification and profiling of compounds were established by conducting activity and cytotoxicity assessments on a selection of 15 compounds identified through high-throughput screening of PP2Cm. The compounds were subjected to biochemical and cellular analyses to determine their IC_{50} and LD_{50} values. Among these compounds, the lowest IC_{50} values were found to be 64 μM, 162 μM, and 147 μM for compounds 1, 2, and 12, respectively. IC_{50} values for compounds 3, 4, 7, 10, and 13 could not be determined as their highest tested concentration failed to inhibit enzyme activity by 50%. It was estimated that the IC_{50} values of these compounds exceed the tested concentration range. For the remaining compounds, their IC_{50} values fell within the range of 280-990 μM. Cellular testing revealed high cytotoxicity for most compounds, with LD_{50} values below 10 μM for compounds 1, 2, 3, 10, 13, and A4 in PANC-1 cells. Additionally, compounds 5, 9, 11, and 12 were also highly cytotoxic with estimated LD_{50} values below 50 μM. The least cytotoxic compounds were compounds 4, A2, and A3, as their highest tested concentrations did not reduce cell viability to below 50%. Comparing IC_{50} and LD_{50} values, no compound stood out as significantly better than the others. Additional cellular testing was conducted to measure the intracellular inhibition of PP2Cm. The results revealed that cells exposed to compounds secreted less BCKAs than the control cells, which contradicts the expected behavior of a potent PP2Cm inhibitor. More potent compounds are needed to achieve more favorable IC_{50} and LD_{50} values. However, these results provide information about the PP2Cm enzyme and the tested compounds which can be used as a guide to future research of better inhibitors.

ABBREVIATIONS

3D	Three-dimensional
α-KIC	α-ketoisocaproate
α-KIV	α-ketoisovalerate
α-KMV	α-keto-β-methylvalerate
β-ME	β-Mercaptoethanol
Å	Angstrom
Abs	Absorbance
AA	Amino acid
ADME	Absorption, Distribution, Metabolism, and Excretion
ADP	Adenosine diphosphate
ATP	Adenosine triphosphate
BCAA	Branched-chain amino acids
BCAT	Branched-chain aminotransferase
BCKA	Branched-chain α-keto acids
BCKDH	Branched-chain α-keto acid dehydrogenase
BCKDHA	Branched-chain α-keto acid dehydrogenase E1 subunit α
BCKDHB	Branched-chain α-keto acid dehydrogenase E1 subunit β
BCKDK	Branched-chain α-keto acid kinase
CAF	Cancer-associated fibroblasts
CHD	Congenital heart diseases
CoA	Coenzyme A
CRISPR-Cas9	Clustered regularly interspaced short palindromic repeats-Cas9
DBT	Dihydrolipoamide branched-chain transacylase E2
DLD	Dihydrolipoamide dehydrogenase
DMEM	Dulbecco´s Modified Eagle´s Medium
DMSO	Dimethyl sulfoxide
DNA	Deoxyribonucleic acid
DTT	Dithiothreitol
E. coli	*Escherichia coli*
EDTA	Ethylenediaminetetraacetic acid
ETC	Electron transport chain

E1α	α-subunit of BCKDH complex
E1β	β-subunit of BCKDH complex
ε	Molar extinction coefficient
$FADH_2$	Flavin adenine dinucleotide
FBS	Fetal bovine serum
FL	Full-length
FPLC	Fast protein liquid chromatography
His-tag	Hexa histidine tag
HTS	High throughput screening
IC_{50}	Inhibitory concentration at 50%
IEC	Ion exchange chromatography
IMAC	Immobilized metal affinity chromatography
IPTG	Isopropyl-β-D-1-thiogalactopyranosid
kDa	Kilodalton
KICA	α-ketoisocaproic acid
LB	Luria Broth
LD_{50}	Lethal dose 50%
LDH	Leucine dehydrogenase
MOPS	3-(N-morpholino) propane sulfonic acid
$MnCl_2$	Manganese(II) chloride
MQ	MilliQ
MSUD	Maple syrup urine disease
NaCl	Natrium chloride
NAD^+	β-Nicotinamide adenine dinucleotide, oxidized
NADH	β-Nicotinamide adenine dinucleotide, reduced
NC	Negative control
NCMM	The Norwegian Centre for Molecular Medicine
Ni^{2+}	Nickel ion
NMR	Nuclear magnetic resonance
$NH4^+$	Ammonium ion
NTA	Nitrilotriacetic acid
OD	Optical density
PANC-1	Pancreatic ductal adenocarcinoma cells
X	

PBS	Phosphate-buffered saline
PC	Positive control
PDAC	Pancreatic ductal adenocarcinoma
PEG	Polyethylene glycol
pH	Potential of hydrogen
pNP	para-nitrophenol
PNPP	p-nitrophenyl phosphate
PPM1K	Protein phosphatase Mn^{2+} dependent 1 kinase
PP2Cm	Protein phosphatase 2C, mitochondrial
RM	Reaction mix
RNA	Ribonucleic acid
RNAi	RNA interference
rpm	Revolutions per minute
SBDD	Structure-based drug design
SDS-PAGE	Sodium dodecyl-sulfate polyacrylamide gel electrophoresis
SEC	Size exclusion chromatography
SOC	Super Optimal broth with Catabolite repression
SUMO	Small Ubiquitin-like Modifier
SUMO-PP2Cm	Small Ubiquitin-like Modifier-Protein phosphatase 2C
TCA	Tricarboxylic acid
TEV	Tobacco etch virus
U	Unit
UV	Ultraviolet

TABLE OF CONTENTS

1 INTRODUCTION

The figures and illustrations are made with Biorender.com.

1.1 Proteins and catabolism of branched-chain amino acids

Proteins are organic macromolecules made up of building blocks called amino acids (AAs). There are over 300 known AAs, however, only 20 of these serve as building blocks for proteins. The AAs have different functions and biochemical properties due to variations in their side chains. In mammals, some of the AAs cannot be synthesized by the body and thus need to be obtained through the diet, these are classified as essential AAs (1). Leucine, isoleucine, and valine, the three branched-chained amino acids (BCAA), are examples of essential AAs (2). The BCAAs are unique by having a small hydrophobic and branched functional R group making them important in protein synthesis and other biological processes such as metabolism and immunity (3).

The BCAAs are catabolized by highly reversible enzymes, and many of these enzymes can use all three BCAAs as substrates and thus affect the levels of the BCAAs in the body. The catabolic enzymes of BCAAs are widely distributed in body tissues, such as the liver and muscle tissues. The catabolic reactions take place in the mitochondria, except for the reaction in the central nervous system (4). The catabolic reaction of BCAAs is shown in **Figure 1.1**.

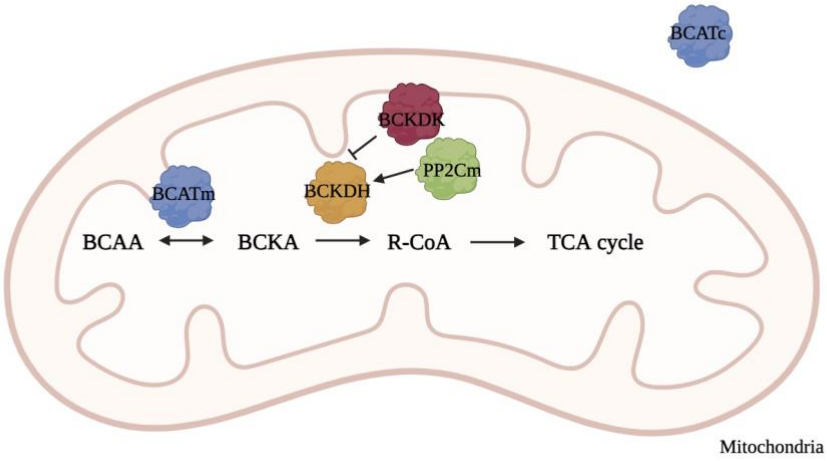

Figure 1.1. Simplified illustration of the catabolic reaction of BCAAs in mitochondria. *Mitochondrial BCAT catalyzes the first reversible reaction of the BCAA catabolism, forming the respective BCKAs of leucine, isoleucine, and valine. BCKAs are oxidatively decarboxylated to their respective acyl-CoA derivatives (R-CoA) by an active BCKDH complex. These acyl-CoA derivatives can be further catabolized and enter the TCA cycle. The illustration is inspired by (5).*

Two of the most essential catabolic enzymes are the branched-chain aminotransferase (BCAT) and branched-chain α-keto acid dehydrogenase (BCKDH). BCAT initiates the first reversible reaction by transamination of the BCAAs. The deamination of leucine, isoleucine, and valine forms their respective branched-chain α-keto acid (BCKA) α-ketoisocaproate (α-KIC), α-keto-β-methylvalerate (α-KMV), and α-ketoisovalerate (α-KIV), respectively (6). Following transamination, the BCKDH complex catalyzes the irreversible oxidative decarboxylation of the BCKAs together with various cofactors and enzymes, generating isovaleryl-coenzyme A (CoA) from α-KIC, 2-methylbutyryl-CoA from α-KMV, and isobutyryl-CoA from α-KIV. These acyl-CoA derivatives can be further catabolized to acetyl-CoA or succinyl-CoA and utilized as energy sources or to synthesize other molecules such as lipids and glucose. Acetyl-CoA and succinyl-CoA can for instance enter the tricarboxylic acid (TCA) cycle where they can be oxidized to provide reduced β-nicotinamide adenine dinucleotide (NADH) and flavin adenine dinucleotide ($FADH_2$) that feed the electron transport chain (ETC) (2).

The catabolism of BCAAs has been associated with cancer growth and progression (7), and it is reported a continuous accumulation of BCAAs in patients with insulin resistance (8) and type 2 diabetes (9). Impaired BCAA catabolism can be caused by enzyme deficiencies or certain disorders, leading to metabolic disorders requiring medical attention and specialized dietary management (10). An example of such a disorder is maple syrup urine disease (MSUD) which can have severe consequences including coma, convulsions, and mitochondrial dysfunction (11). Therefore, enzymes like the BCKDH complex must have optimal functionality to avoid disease.

1.1.1 Regulation of BCKA catabolism – the BCKDH complex

The liver is the organ with the highest metabolic efficiency in the catabolism of BCKAs, although the catabolism is carried out in other tissues as well. The oxidative decarboxylation step catalyzed by the BCKDH complex is a rate-controlling process in BCAA catabolism, where a block in this step leads to the accumulation of BCAAs and BCKAs. The BCKDH complex consists of three subunits: E1, E2, and E3. Subunit E1 functions as a thiamin-dependent decarboxylase, E2 acts as a lipoate-dependent dihydrolipoyl transacylase that transfers the acyl groups to coenzyme A (CoA), and the E3 subunit is a FAD-dependent dihydrolipoyl dehydrogenase that transfers the released electrons to NAD^+. The three subunits are encoded by the genes branched-chain keto acid dehydrogenase E1 subunit α (BCKDHA) and branched-chain keto acid dehydrogenase E1 subunit β (BCKDHB), dihydrolipoamide branched-chain transacylase E2 (DBT), and dihydrolipoamide dehydrogenase (DLD), respectively (5). The activity of the BCKDH complex is regulated by BCKDH kinase (BCKDK) and mitochondrial protein phosphatase 2C (PP2Cm). BCKDK suppresses the activity by phosphorylation of BCKDHA and is regulated by the level of BCKAs or by the BCKDH complex, where high concentrations of BCKAs will inhibit the activity of BCKDK. PP2Cm catalyzes the dephosphorylation that activates the BCKDH complex (12). **Figure 1.2** shows the regulation of the BCKDH complex by PP2Cm and BCKDK.

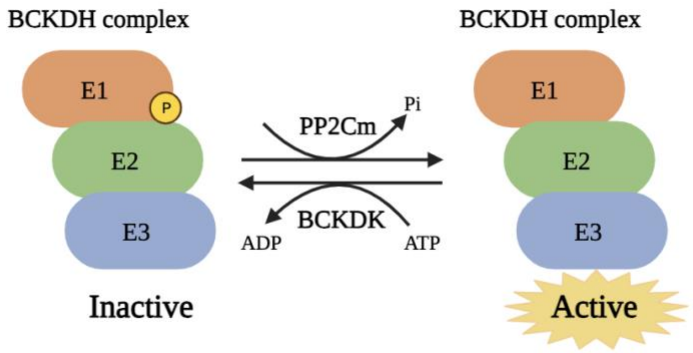

Figure 1.2. The regulation of the BCKDH complex by PP2Cm and BCKDK. *The activity of the BCKDH complex is regulated by phosphorylation and dephosphorylation of the E1 subunit. BCKDK uses ATP to phosphorylate the BCKDH complex, making it inactive, while dephosphorylation by PP2Cm restores its active state. The figure is inspired by (13).*

1.2 Mitochondrial protein phosphatase 2C

PP2Cm, also known as protein phosphatase Mn^{2+} dependent 1 kinase (PPM1K), plays an important role in regulating protein phosphorylation (14). PP2Cm specifically functions as a protein phosphatase, removing phosphate groups from phosphorylated proteins. This dephosphorylation activity helps regulate several cellular processes, including cell division, cell growth, and signal transduction pathways. It also regulates the activity of protein kinases, which add phosphate groups to proteins, by removing the phosphate groups and thus balancing the overall level of protein phosphorylation and preventing excessive phosphorylation that can lead to cellular dysfunction (15). PP2Cm is a serine/threonine protein phosphatase specifically targeted to the mitochondrial matrix where its primary role is modulating mitochondrial function. It is encoded by the PPM1K gene and belongs to the protein phosphatase 2C family (16). It is highly conserved among vertebrates, indicating its essential role in mitochondrial function, and the human PP2Cm has 372 residues with a predicted molecular mass of 40.9 kDa (17). The protein exhibits enriched expression in key organs such as the brain, heart, and liver, underscoring its importance in these tissues (16).

PP2Cm has a broader role as a mitochondrion-targeting protein phosphatase that participates in vital functions such as activating stress-signaling pathways, regulating the mitochondrion

permeability transition pore, and other processes crucial for developmental and cardiac functions (17). Moreover, based on the existing structural and biochemical information it seems to be the primary enzyme responsible for the dephosphorylation of the BCKDH complex. The E1 subunit of the BCKDH complex is heterotetrameric and consists of an alpha (E1α) and beta (E1β) subunit. PP2Cm activates BCKDH by specifically dephosphorylating the E1α subunit, which promotes BCAA catabolism to further degrade BCKA (18), as illustrated in **Figure 1.1** and **Figure 1.2**.

1.3 PP2Cm and diseases

PP2Cm has been implicated in important cellular and physiological processes, such as insulin signaling (19), DNA damage response (20), and cell death regulation (15). Hence, a disruption in the function of PP2Cm can lead to cellular dysfunction, which in turn can contribute to the development and progression of various diseases. A defective PP2Cm function has been linked to several diseases, including cancer, maple syrup urine disease (MSUD), type 2 diabetes, neural disorders, and cardiovascular diseases (13, 21). This makes PP2Cm an important target for therapeutic intervention.

1.3.1 PP2Cm and cancer

It is of particular interest to investigate PP2Cm in the context of cancer due to its unique role and potential implications in cancer biology. Mitochondria are essential for energy production and are known to play a role in cancer metabolism (22). PP2Cm's unique localization in the mitochondria and its involvement in the regulation of various mitochondrial processes can provide insight into cancer biology. PP2Cm is involved in metabolic processes, including the metabolism of AAs. Often, cancers have altered metabolic pathways to support their rapid growth and proliferation, and it is known that amino acids serve as both energy sources and metabolite providers in oncogenesis (23). Many cancers overexpress amino acid-degrading enzymes, which the tumors utilize as immunosuppressive factors, enhancing their ability to survive. It is also shown that tumors preferentially use BCAAs for protein synthesis or energy purposes and that the metabolism of BCAAs is altered in many solid tumors, such as melanoma, pancreatic cancer, and breast cancer (24). The BCKDH complex has a crucial role in BCAA

catabolism, thus there are emerging studies and theories regarding its role in the context of cancer. PP2Cm is one of the two enzymes regulating the activity of the BCKDH complex, thus understanding how PP2Cm contributes to this regulation can provide insight into cancer biology.

In addition, some studies suggest that PP2Cm may act as a tumor suppressor and loss or inactivation of tumor suppressors can contribute to cancer development (25). If it is found to have a significant role in promoting or inhibiting cancer growth, PP2Cm could potentially serve as a therapeutic target by modulating its activity. Research also suggests that PP2Cm may regulate immune responses in tumors (26), making it interesting for immunotherapy.

1.3.2 PP2Cm and pancreatic cancer

Pancreatic cancer is one of the most lethal cancers in the world, being the seventh leading cause of cancer-related deaths (27), with a five-year survival rate of only 10% (28). Pancreatic ductal adenocarcinoma (PDAC) arises in the exocrine glands of the pancreas and is the most common form of pancreatic cancer. The cancer lacks symptoms at its early stages; thus, it is often detected at a late stage giving a poor prognosis for the patients (29). Cancer treatments such as surgery, chemotherapy, and radiotherapy are used to relieve symptoms and extend survival, however, there is still no definite cure for the disease. Thus, it is urgent to identify factors that can diagnose the cancer early and give a better prognosis. The identification of potential molecular markers of PDAC can for instance be through high-throughput sequencing (30).

Recent research has revealed that PDAC is particularly dependent on the degradation of BCAAs inside the mitochondria and that increased levels of BCAAs are correlated with an increased risk of PDAC. They found that the level of BCAAs is elevated in the early stage of PDAC due to increased catabolism of tissue protein, and the consumption of circulating BCAAs is reduced in these tumors (31). BCAAs supply pancreatic cancer cells with both carbon and nitrogen (31), which supports cancer growth and proliferation (32). As mentioned, the degradation of BCAAs is initiated by BCAT, followed by further degradation via the BCKDH complex regulated by the enzymes PP2Cm and BCKDK. In mammals, BCAT is present as two isoforms, where the human isozymes are called BCAT1 and BCAT2, being the cytosolic and mitochondrial forms,

respectively (33). BCAT1 is mainly expressed in cancer-associated fibroblasts (CAFs), while BCAT2 and the BCKDH complex are primarily expressed in PDAC cells. The BCKA production in CAFs is catalyzed by BCAT1. CAFs secrete BCKAs that are taken up by PDAC cells within the tumor microenvironment. Once taken up by PDAC cells, BCKAs can either be re-aminated to BCAAs by BCAT2, supporting de novo protein synthesis and cell proliferation, or oxidized by the BCKDH complex contributing to the generation of important biomacromolecules (31).

A study from 2019 showed that BCAAs sustain pancreatic cancer cell growth by regulating lipid metabolism. By suppressing the metabolism of BCAAs the levels of fatty acids were significantly reduced, demonstrating that the BCAAs provide a carbon source for the biosynthesis of fatty acids, which support the proliferation of cancer cells. In the study, the crucial role of the BCKDH complex in PDAC cells was demonstrated, where a knockdown of the E1α subunit of the complex led to inhibition of cancer cell proliferation both *in vitro* and in mice (34).

Considering that the BCKDH complex is required for the proliferation of pancreatic cancer cells, targeting PP2Cm is highly interesting for suppressing BCKDH activity, and consequently suppressing cancer cell growth and proliferation in PDAC patients.

1.3.3 PP2Cm and maple syrup urine disease

The cytotoxicity of the BCAAs and BCKAs is shown in the metabolic disorder called maple syrup urine disease (MSUD). This is an inherited disorder resulting from deficient catabolic enzymes of the BCAAs. The enzyme deficiency leads to an accumulation of leucine, isoleucine, valine, and their byproducts in the blood and the urine. This accumulation leads to a range of different symptoms, including mitochondrial dysfunction, brain damage, coma, intellectual disability, and death if left untreated (35). MSUD is characterized by the accumulation of BCAAs in the urine with a smell of maple syrup (36). Dietary therapy with limited protein in the diet, especially BCAA restriction, and liver transplantation are current therapies used as treatment (37). The treatments partially restore the activity of the BCKDH complex, improving the circulating levels of BCAAs and thus increasing the survival rate of the patients. However,

dietary therapy is challenging to implement and manage, and liver transplantation does not improve cognitive deficits and psychiatric morbidities, such as anxiety and attention deficit disorders (38). Thus, there is a high need for better and safer treatments.

Patients diagnosed with MSUD have a mutated BCKDH complex where the activity of the complex is decreased, meaning that BCKAs are not oxidized. This leads to elevated levels of BCAAs and BCKAs (38). Studies have found that the three genes encoding the different subunits of the BCKDH complex are mutated in MSUD, namely the BCKDHA, BCKDHB, and the DBT gene (37). BCKDHA encodes the E1α subunit of the BCKDH complex, which is dephosphorylated by PP2Cm to activate the complex. The activity of PP2Cm has also been shown to be affected by changes in the levels of BCAAs, indicating a relation of PP2Cm to MSUD. A study revealed that accumulation of BCAAs in MSUD leads to increased protein phosphorylation and reduced activity of PP2Cm, contributing to the development of symptoms of the disease. The study revealed that loss of PP2Cm expression or activity prevents dephosphorylation of the E1α subunit in response to BCKA stimulation *in vivo*. Also, PP2Cm knock-out mice manifested elevated BCAA and BCKA levels. When fed a high-protein diet, the mice exhibited characteristics similar to the intermittent or intermediate MSUD phenotype, including oxidative stress and neonatal lethality, representing a predicted variant form of MSUD (12). This variant was recently confirmed in an MSUD patient carrying a homozygous p.His139fs null mutation in the PP2Cm protein, providing direct evidence that PP2Cm is the endogenous phosphatase component of the BCKDH complex and documents the occurrence of type 5 MSUD caused by a deficiency in PP2Cm (14).

The findings of these studies suggest that PP2Cm plays a crucial role in the regulation of MSUD, and changes in its activity may contribute to the development and progression of the disease. Thus, PP2Cm should be considered as a potential target for therapeutic intervention in the case of MSUD.

1.3.4 PP2Cm and congenital heart diseases

Congenital heart diseases (CHD) are abnormalities in the heart structure that occur before birth and can cause problems in blood circulation, heart failure, and eventually lead to death (39).

Although some medications and treatments can reduce mortality rates by repairing heart defects, such as catheters and surgery, CHD is still the leading cause of mortality among birth defects. This condition affects around 0.8-1.2% of newborns worldwide and is among the most commonly diagnosed congenital disorders (40). Only 15% of CHD cases have known causes among thousands diagnosed. Thus, identifying underlying genetic factors contributing to these conditions can help find new treatments, such as gene therapy, to get a better understanding of the genetic mechanisms and to manage CHD in patients (40).

Researchers have found that cell death occurs during heart failure and thus may have a role in this. In addition, heart failure and cardiomyocyte hypertrophy have been linked to mitochondrial dysfunction. As previously mentioned, PP2Cm has an essential role in mitochondrial regulation and cell survival, where the downregulation of PP2Cm has been linked to cardiac diseases (16). There is evidence that suggests that loss of PP2Cm is a significant contributor to the pathogenesis of heart failure, linking BCAA catabolism to cardiac pathophysiology. A defect in the PP2Cm-mediated catabolism of BCAAs can be a potential novel mechanism for CHD and heart failure. PP2Cm is highly expressed in cardiac muscle, and a study found that its expression is diminished in the heart under pathologic stress (17). Moreover, phenotypic heart failure characteristics, such as cardiac contractility, are observed in zebrafish embryos lacking PP2Cm, and PP2Cm-deficient mice developed accelerated heart failure at an early age when exposed to mechanical overload. These findings indicate that PP2Cm is a significant contributor to the pathogenesis of heart failure, where BCAA catabolism plays a significant role in maintaining normal cardiac function (41), supporting the important role of PP2Cm.

1.4 Drug design

The process of drug design is the discovery and development of new medications, where the goal is to create effective and safe drugs to treat or prevent specific diseases or medical conditions. It offers several significant advantages, such as targeted therapy, personalized medicine, increased success rate, and better, safer, and more efficient disease management. The drug design process uses insights about a biological target to develop a novel drug, involving

several stages to design a molecule that aligns in terms of both charge and shape with the specific biological target it intends to interact and bind to (42). The drug design process is very expensive and time-consuming, taking on average more than a decade, thus new technologies are necessary. Fortunately, there are already some technologies such as high throughput screening (HTS) and structure-based drug design (SBDD) that reduce time and expenses (43, 44). The process is illustrated in a schematic overview in **Figure 1.3** and typically consists of the following stages: target identification and validation, hit discovery, lead discovery and optimization, preclinical testing, and clinical development (45). If the clinical development is successful, the drug must pass regulatory approval to be launched to the market and distributed to healthcare providers and patients (42, 46).

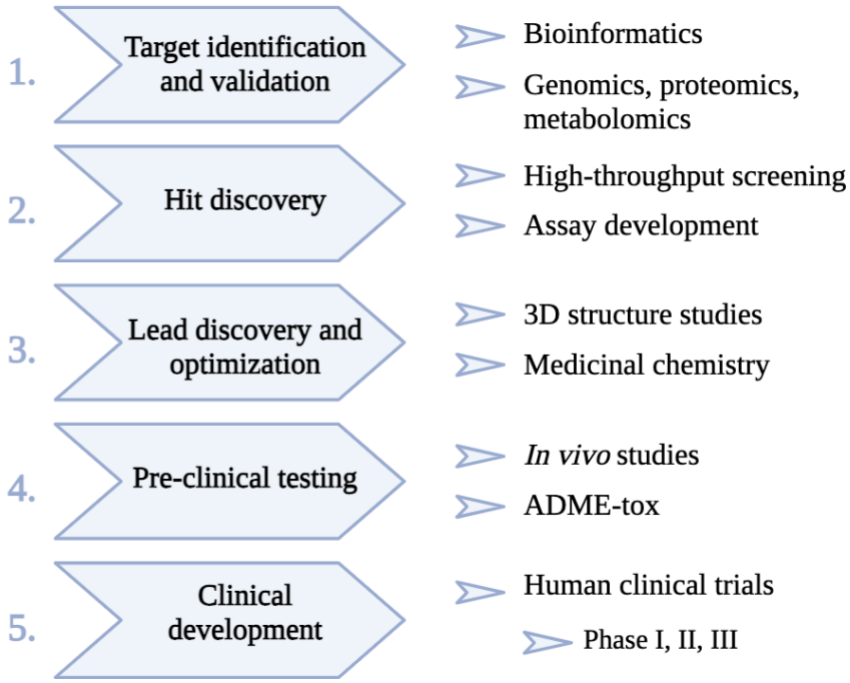

Figure 1.3. The different stages of the drug design process. *The drug design process involves several steps, including target identification, hit discovery, lead optimization, pre-clinical testing, and clinical development. There are several different methods in each step and some of the methods are listed. The illustration is inspired by (45).*

1.4.1 Target identification and validation

The first step in a drug design process is target identification. Proteomic and genomic data are used to identify potential biological targets within the body, such as a protein, enzyme, receptor,

or genetic sequence, that plays a key role in a disease. The target should have a known or highly anticipated connection to the disease and be validated to ensure that it likely has a therapeutic effect, meaning that the potential drug can access the target and thus create a biological response (47). Ideal targets are those whose functionality is dependent on the binding of a small molecule, such as a ligand binding in its binding pocket. Also, the target should be unique, meaning that no alternative pathway can substitute for the target's function and overcome the presence of an inhibitor (48). Validation of the target consists of laboratory research and (often) animal studies to investigate its functional role in the specific disease. Overexpression or suppression of the gene encoding the target using knock-in or knock-out organisms by clustered regularly interspaced short palindromic repeats-Cas9 (CRISPR-Cas9) technology or RNA interference (RNAi) are common methods for target validation (49).

1.4.2 Hit discovery

The second step in the process of designing a new drug is hit discovery where the aim is to identify compounds (hits) that will interact with the target. A high-throughput screening (HTS) is performed to find potential hits, where a library of thousands to millions of compounds are screened against the molecular target (47). The selection of hits is often found by using computational methods where virtual libraries are used to screen many molecules. For example, virtual screening uses virtual libraries to calculate and find potential hits (50). However, this requires a structure of the target which will be used to calculate the predicted binding between the target and small molecules. Although virtual screening reduces time and costs, it has some drawbacks that must be avoided to not produce false results (51). The most promising compounds are ranked by the highest scores, where the score is calculated by the free energy difference between the target and the molecule (52). Along with HTS and virtual screening, fragment-based discovery is used, which also has a much higher hit rate. In fragment-based discovery, the hits are compounds with a much lower molecular mass compared to the hits from HTS (53). The compounds have a high ligand efficiency, meaning that the binding affinity per atom in the fragment is high. However, it is necessary to screen the fragment-based hits at a high concentration due to their tendency to be relatively weak binders (54).

In this master project, a total of 15 initial compounds were tested. An assay with the target protein, PP2Cm, was used to screen against approximately 28,000 compounds at the NOR

OpenScreen platform to identify potential compounds. The HTS gave 44 potential candidates that were subsequently re-screened through a dose-response analysis. Out of the 44 potential candidates, 15 validated compounds were ordered for this project to be tested for PP2Cm inhibition. Three of these compounds were suggested to work as activators of PP2Cm, thus this was investigated.

1.4.3 Lead discovery and optimization

In lead discovery and optimization, the most promising hits are selected as lead compounds. These compounds have demonstrated an ability to interact with the target molecule, but they may require significant optimization for efficacy and safety. Target selectivity, toxicological analyses, and binding mechanisms are examples of lead properties that are investigated. The compounds are modified to enhance their pharmacological properties, such as potency, selectivity, bioavailability, and safety. While beneficial properties are optimized, the unfavorable traits are minimized, achieved by inducing changes in the lead structure (55). Nuclear magnetic resonance (NMR) and X-ray crystallography are used to investigate lead binding affinities and study the 3D structure of the protein-inhibitor complex (53). The lead discovery and optimization also involve synthesizing and testing various analogs of the initially prioritized lead compounds to reach candidate status (56).

The inhibition efficacy of the hits resulting from HTS of PP2Cm was analyzed by a PP2Cm activity assay used to determine the IC_{50} values of the hits. The next step would have been to investigate the structure and binding properties with X-ray crystallography. However, this part of the project was unsuccessful due to problems with crystallization.

1.4.4 Preclinical testing

After optimization of the lead compound, it is tested for efficiency and safety in animal models to indicate a human response to the drug. Preclinical testing involves toxicological testing of the lead compound both *in vitro* and *in vivo*. However, *in vitro* testing is often performed earlier in the drug design process to identify undesirable off-target effects. Ensuring the safety and effectiveness of a drug before it enters the clinical phase is crucial. One important aspect is the drug's ability to be absorbed, distributed, metabolized, and eliminated (55). *In vitro* studies

focus on key factors that can impact drug release *in vivo* and can be performed on sample tissue, bacteria, or cells. For instance, evaluating the drug's effect on cells such as phenotype, proliferation, and mechanisms of action can be done by testing it in cell cultures. On the other hand, *in vivo* experiments are essential in assessing the drug's interactions and physical and biochemical characteristics within a living organism, which cannot be observed *in vitro*. Measuring drug toxicity, both qualitatively and quantitatively, is an example of in *vivo testing*. Choosing the right animal model is important, due to the drug's specificity to different species; thus selecting an animal model that most accurately resembles the pharmacokinetics and pharmacodynamics of the human body is important (57). Even though animal models indicate the human response to the drug, there are physiological differences between human and animal models that can affect the drug's accuracy and reproducibility. There is a new potential technology, called Organ-on-a-Chip that mimics the physiological environment and function of human organs on a small chip. This technology has the potential to replace the animal model or at least reduce the need for animal testing and can be used for drug testing and disease modeling at the preclinical stage (58).

In this project, the sensitivity of PDAC cells to different PP2Cm compounds was tested with an *in vitro* cell viability assay: the Presto Blue cell viability assay. The sensitivity of the cells to the different compounds was determined as LD_{50} values. In addition, a BCKA assay was performed to analyze the *in vivo* inhibition of PP2Cm by the different compounds, meaning that the enzymatic effects of PP2Cm were studied within the cells.

1.4.5 Clinical development

If the drug candidate passes the preclinical testing it is ready for the longest and most expensive stage of the drug design process: the clinical trials. The clinical trials are conducted in human volunteers to look into the efficiency and safety of the drug (55). This is a very critical step because human and animal physiology are not identical, thus the results from preclinical testing in animals cannot predict the outcome of the drug in humans with sufficient certainty (57). The trials consist of three phases for testing where each phase needs approval before proceeding to the next phase. In phase I the trials are conducted on healthy volunteers to assess the safety, dosage, pharmacokinetics, and pharmacodynamics of the drug. Phase II is conducted in patients to evaluate the drug's efficacy and side effects. The final step, phase III, involves extensive

clinical trials with a larger patient population to confirm efficacy, monitor the side effects, and compare the drug to other existing treatments. The drug needs regulatory approval and post-marketing studies that monitor the drug's long-term safety and effectiveness in a broader population, and if it completes all stages and gains approval it is launched in the market and distributed to healthcare providers and patients (59).

1.5 Method-related theory

Different methods were performed to purify the PP2Cm protein and to analyze the effects of the selected compounds on the PP2Cm activity. The IC_{50} values of the 15 different compounds were determined by an enzymatic assay. Also, the sensitivity of PDAC cells to the compounds, as well as the compound's impact on *in vivo* accumulation of BCKAs was investigated. A concise explanation of the theoretical foundations of the methods employed in this thesis is provided in the following paragraphs.

1.5.1 Enzymatic assay

Enzymatic reactions can be used to identify enzymes and their activity (60). In general, this involves tracking the rate of the specific reaction by monitoring substrate consumption or product formation, which can be accomplished through spectroscopy (61), mass spectrometry (62), or many other methods. Furthermore, enzymatic assays are employed to evaluate drug potency, quantifying it in terms of the IC_{50} value. The IC_{50} value is the concentration of a drug at which the enzyme activity is inhibited by 50% relative to its maximum activity (63).

Maintaining consistency in factors such as temperature, assay pH, and concentrations of assay components is crucial for accurately comparing enzymatic activities. Enzymes function best under specific conditions, and any variation can affect their activity. UV-vis absorbing compounds are commonly used to monitor enzymatic reactions by measuring changes in absorbance. For accurate measurements, a spectrophotometer or colorimeter can be used. Spectrophotometric assays are preferred because of their simplicity. If photometric observation is difficult, fluorimetry can be used instead (60). A coupled reaction is also a common approach

if the reaction is difficult to detect. In coupled reactions, one easily observable reaction provides the energy or a substrate for another reaction to occur. However, optimal conditions for both reactions may be difficult to achieve, thus the primary enzyme determines the conditions of the assay. It is important that the secondary reaction does not restrict or limit the process (60).

PP2Cm is a phosphatase that relies on $MnCl_2$ for its activity (14). Its enzymatic activity can be measured spectrophotometrically at 405 nm by monitoring the consumption of the substrate p-nitrophenyl phosphate (pNPP). **Figure 1.4** illustrates how phosphatases catalyze the hydrolysis of pNPP, resulting in the release of inorganic phosphate and a yellow-colored phenolate compound (pNP) with a maximum absorbance at 405 nm. This can be used to assess the activity of various phosphatases, such as alkaline phosphatase and PP2Cm (64). The reaction of PP2Cm is dependent on $MnCl_2$, thus this was supplemented to ensure the reaction to proceed.

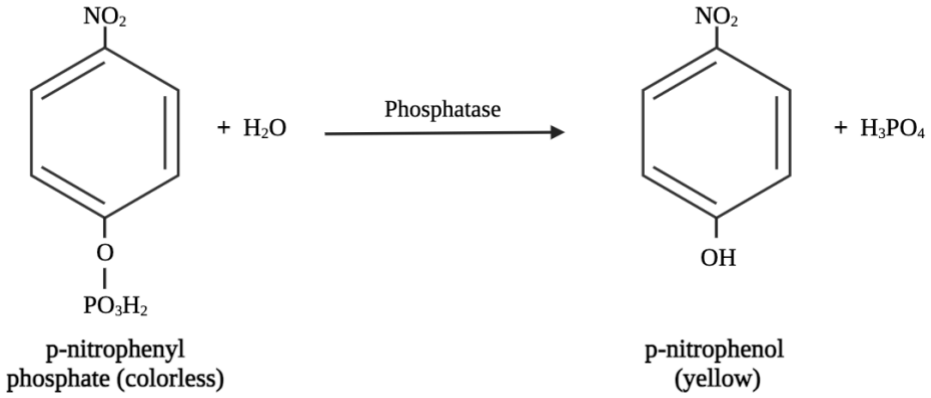

Figure 1.4. Hydrolysis of p-nitrophenyl phosphate by phosphatase enzyme. *P-nitrophenyl phosphate (pNPP) is used as a substrate to assess the activity of various phosphatases. It is hydrolyzed to p-nitrophenol by phosphatase, yielding a yellow color that can be monitored spectrophotometrically at 405 nm absorbance.*

1.5.2 Crystallization

As a part of lead discovery in the drug design process, it is important to investigate the binding affinity between the target and the lead compounds. A common and widely used method to investigate this is X-ray crystallography, which is also used to determine and study the 3D structure of the target protein and the protein-inhibitor complex. The 3D structure gives important information about the protein-inhibitor interactions and the enzymatic mechanism

(65). However, with only one copy of the target molecule, the scattering signal will be too weak, thus a crystal of the target molecule is required for 3D structure determination. The crystal is composed of many copies of the target molecule, used to amplify the scattering signal (66). In this project, no crystals were obtained of the PP2Cm target protein, thus X-ray crystallography analysis of PP2Cm in complex with the compounds was not achieved.

Protein crystallography requires a reliable homogenous protein of high quality. Necessitating an optimal protein purification protocol to get the purest protein possible. To achieve successful crystallization, it is important to test different conditions as there are many factors that can affect the process. Some of these factors include temperature, pH, buffer, protein and precipitant concentration, type of precipitant, and crystallization techniques (65). It is also important to consider any inhibitors, metal ions, and cofactors that may affect the molecular structure of the target molecule during the crystallization process (67).

The principle behind protein crystallization involves inducing the controlled precipitation of a homogenous protein from a solution to promote crystal formation. Successful crystallization relies on achieving this process at the appropriate rate; amorphous precipitation occurs if it happens too quickly (65). The crystallization process consists of two primary phases: nucleation and growth. Nucleation is the initial step of crystal formation when microcrystals are formed. When a solution contains more dissolved solute than it can hold, the molecules start arranging themselves in an ordered state, following specific symmetries, distances, and orientations (68). This leads to the formation of small crystal nuclei that act as focal points for further crystallization (67, 69). During the growth phase, molecules from the supersaturated solution keep adding onto the crystal's surface, causing it to increase in size (68). Growth stops when the system reaches equilibrium. Vapor diffusion via hanging and sitting drop, seeding, and batch are commonly used for crystal formation (67).

To find optimal crystallization conditions for PP2Cm, a screening with sitting drop vapor diffusion was used. In addition, crystallization conditions from an article (14) were tested with the hanging drop vapor diffusion method. The protein solution was mixed with the precipitant solution in a 1:1 ratio and the drop was placed on a glass coverslip and inverted over a precipitant solution-containing well. Sealing the well promotes water diffusion from the drop

into the reservoir, forcing equilibrium between the drop and the larger volume of precipitant solution in the well (70).

The dynamics within the drop can be illustrated using a phase diagram, as shown for vapor diffusion in **Figure 1.5**. This diagram describes the shift from undersaturation to a supersaturated solution, which is regulated by the concentrations of both the precipitant and protein. In a 1:1 protein-precipitation drop, it initially resides in the undersaturated phase and transitions into the supersaturated state. Within the supersaturated state, three distinct zones can be delineated. These include the precipitation zone where protein precipitation occurs, the nucleation zone characterized by the formation of small nuclei, and the metastable zone where crystal growth takes place. Equilibrium is achieved at the supersaturation-undersaturation boundary, and the crystal growth stops (67).

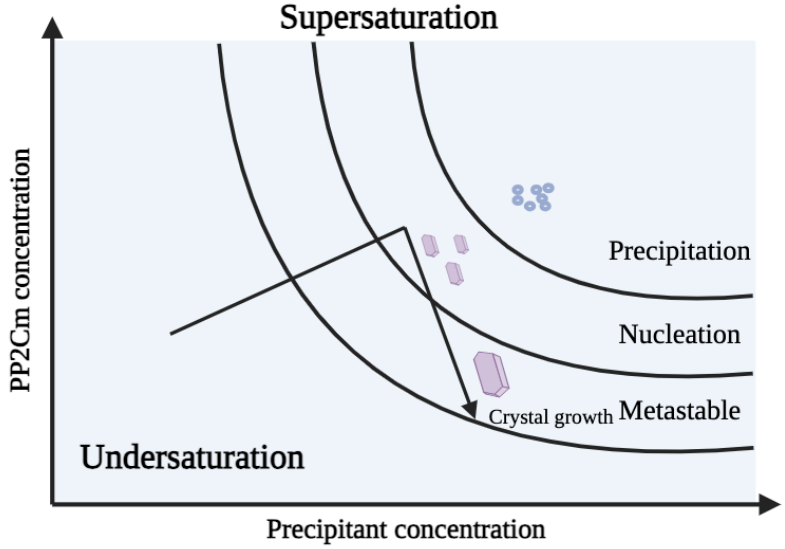

Figure 1.5. Phase diagram for vapor diffusion crystal formation. *The protein is in a soluble state in the undersaturated zone. Water evaporation from the drop leads to a more saturated solution, causing the aggregation of molecules and the formation of crystal nuclei (nucleation) under optimal conditions. When entering the metastable zone, the crystal nuclei will grow, forming larger crystals. Crystal growth stops when the system reaches equilibrium. The figure is inspired by (67, 71).*

For successful crystallization, the protein should be placed in the undersaturated zone at the start of the crystallization. As water evaporates from the drop, the concentration of protein and

precipitant increases, thereby initiating the nucleation phase. This triggers protein precipitation, nucleus formation, and potential crystal growth under optimal conditions (72).

1.5.3 Cellular testing of compounds

To investigate the toxicological effects of hit compounds, *in vitro* testing can be performed in cell cultures with the compounds to evaluate the effects on cells (55). The testing involves conducting experiments and analyses within a controlled laboratory setting, typically using isolated cells or tissues. Before testing, choosing and culturing appropriate cells or tissues relevant to the research or the compound's intended application is necessary. If cells are used, it is important to maintain a controlled environment with suitable growth media, temperature, and humidity (73). The compounds of interest are introduced to the cultured cells at various concentrations and time points, and proper controls with untreated cells, and cells treated with a vehicle, such as a solvent, are included for comparison and validation of the experiment (74). The observed effects must be specific to the compound of interest. The compound's effects on the cellular responses are tested using a range of assays. Such assays can be cytotoxicity assays where the cell viability and toxicity of the compounds are assessed, proliferation assays that measure cell division rates, and cell signaling assays that evaluate changes in molecular pathways (75). Often, microscopy and imaging are used to visualize cellular changes, such as morphological alterations, intracellular localization of the compound, or protein expression levels (76). The collected assay data are analyzed using statistical methods to determine the compound's effects and dose-response relationships.

In this project, the PANC-1 cell line was chosen to evaluate the effects of PP2Cm compounds on cells. The PANC-1 cell line is a human pancreatic cell line commonly used in pancreatic cancer-related research and drug discovery to investigate potential therapeutic agents (77). The cell line was established from the pancreatic tumor tissue of a 56-year-old male patient with pancreatic ductal adenocarcinoma (PDAC) in 1975 (78).

The Presto blue cell viability assay was conducted to test the sensitivity of PDAC cells to the hit compounds from HTS. Here, PANC-1 cells are treated with a range of concentrations of the compound, and the assay gives information about the cell viability and the cytotoxic effects on

the cells. The Presto Blue cell viability reagent quantitatively measures the proliferation of cells by using the reducing power of living cells (79). When introduced to cells, the reagent uses the reducing power of viable cells to convert resazurin to fluorescent resorufin (**Figure 1.6**). The color change can be analyzed and evaluated quantitatively on an absorbance- or fluorescence-based microplate reader. Also, qualitative analysis can be evaluated by the visual color change of the solution from blue to red (80). The data were analyzed and used to determine the lethal dose 50 (LD_{50}) of the compounds.

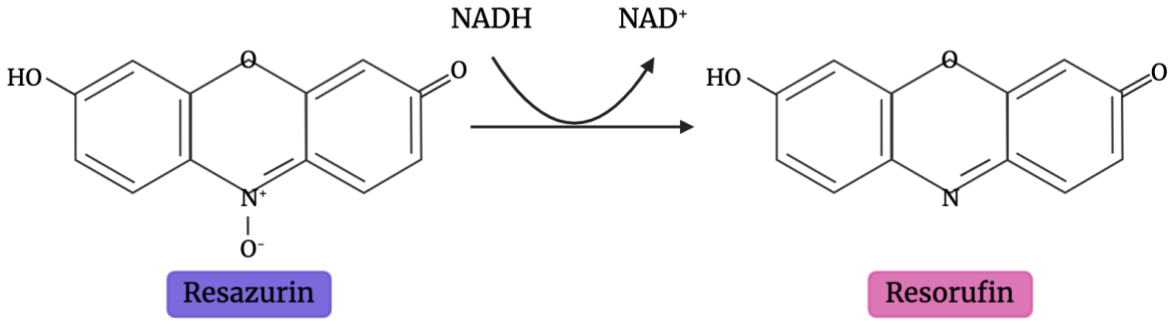

Figure 1.6. The chemical reaction of resazurin to resorufin. *Living metabolically active cells will convert resazurin to resorufin using NADH when introduced to the Presto Blue reagent.*

In addition to cell viability, another cellular assay was performed to evaluate changes in the molecular pathway of PP2Cm in compounds-treated PANC-1 cells. The assay is called BCKA assay where the amount of BCKAs is measured to investigate the effect of compounds on PP2Cm *in vivo*, i.e., inside the cells. If PP2Cm activity is inhibited by a compound, it cannot bind to the BCKDH complex and thereby activate it, meaning that the BCKDH complex cannot decarboxylate BCKAs (81). Therefore, there will be an accumulation of BCKAs when the complex is inactive. This theory is used to measure the intracellular activity of PP2Cm by measuring the quantification of extracellular BCKAs. When there is an excess of BCKAs, the leucine dehydrogenase (LDH) enzyme can convert α-KIC to L-leucine in the presence of ammonium (NH_4^+) and NADH. This LDH reaction causes stoichiometric oxidation of NADH, i.e., a decreasing absorbance, that can be monitored spectrophotometrically at 340 nm (82). When there is an excess of α-KIC the reaction is more rapid. Thus, this method uses the activity

of LDH to measure the amount of BCKAs. **Figure 1.7** provides a schematic overview of the theory behind the method, with the mitochondrial reaction in the cell.

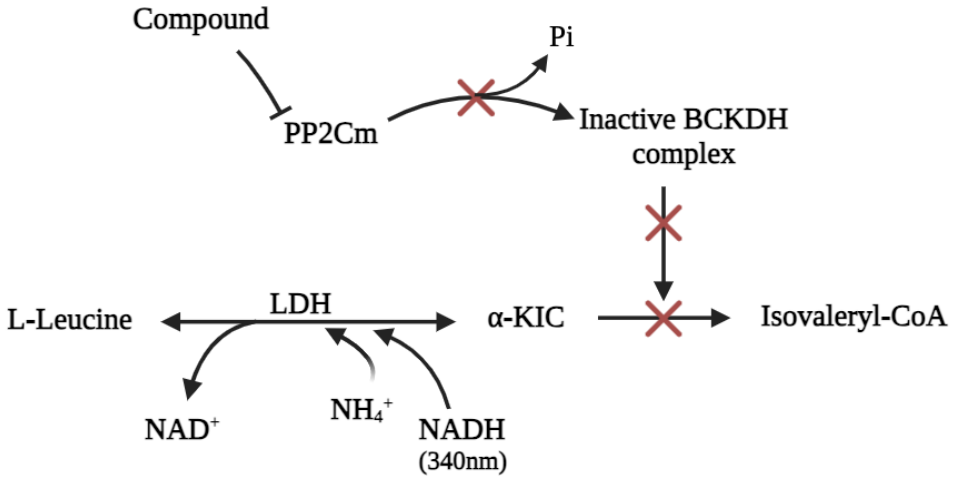

Figure 1.7. BCKA assay reaction with inhibition of PP2Cm. *Compound inhibition of PP2Cm results in an inactive BCKDH complex. When inactive, the BCKDH complex loses its ability to oxidatively decarboxylate BCKAs. The illustration demonstrates a halt in the decarboxylation of the BCKA α-KIC to isovaleryl-CoA, resulting in the accumulation of α-KIC. Excess α-KIC is subsequently converted to L-Leucine by the enzyme LDH in the presence of NADH and ammonium, leading to a stoichiometric oxidation of NADH. The decrease in NADH can be measured at 340 nm, serving as an indicator of PP2Cm inhibition.*

2 AIM OF STUDY

The overall aim of this master thesis was to target mitochondrial metabolism to combat pancreatic cancer by identifying and characterizing novel molecules inhibiting the activity of the human PP2Cm enzyme. The identification and characterization were determined through activity- and cytotoxicity analyses of 15 compound hits selected from high-throughput screening (HTS) of PP2Cm.

Potential inhibitory and activating compounds of PP2Cm were tested to investigate their ability to inhibit or activate PP2Cm activity. Additionally, the cytotoxicity of each inhibitory compound in PANC-1 cells was examined. Also, the aim was to perform structural analyses of PP2Cm with protein crystallography.

Potential PP2Cm inhibitors and activators were validated and characterized through the following objectives:

- Expression and purification of human PP2Cm
- Determination and analysis of the inhibitory effects of PP2Cm compounds using enzymatic activity assay.
- Analysis of the cytotoxicity of PP2Cm compounds to PANC-1 cells using Presto Blue assay.
- Characterization of the compound's ability to inhibit PP2Cm *in vivo* using BCKA assay.

3 MATERIALS AND METHODS

Information on buffers, medium, chemicals, and the materials used in the following methods are listed in the appendix. The figures and illustrations are made with Microsoft PowerPoint or Biorender.com.

3.1 Protein expression

For this project, two variants of the PP2Cm enzyme were expressed and purified: a SUMO-tagged full-length human PP2Cm, and a mutant truncated form consisting of amino acids 84-361. The two variants are referred to as full-length (FL) SUMO-PP2Cm and Δ SUMO-PP2Cm throughout this thesis, respectively. Both proteins were expressed and purified regularly using the same materials and methods. In addition, a previously transformed TEV-protease was purified to cleave the SUMO-tag off the proteins. The FL SUMO-PP2Cm was employed for enzymatic assays, and the Δ SUMO-PP2Cm was prepared for crystallization. The proteins were stored on ice during short-time storage to prevent possible degradation and denaturation of the proteins.

3.1.1 Transformation of expression plasmid

To enhance solubility and simplify purification, the PP2Cm enzymes were generated using the kanamycin-resistant pET-SUMO vector containing a hexa histidine-tag (His-tag) at the N-terminal, followed by SUMO and a tobacco etch virus (TEV) protease cleavage site (ENLYFQG) in front of the PP2Cm (**Figure 3.1**)(83). The expression plasmids for SUMO-PP2Cm were transformed into ArcticExpress (D3) competent cells, derived from Agilent BL21-CodonPlus (DE3)-RIPL competent cells, to enable efficient high-level expression of the enzymes in *Escherichia coli* (*E.coli*). FL SUMO-PP2Cm was already transformed and available as a glycerol stock in the lab.

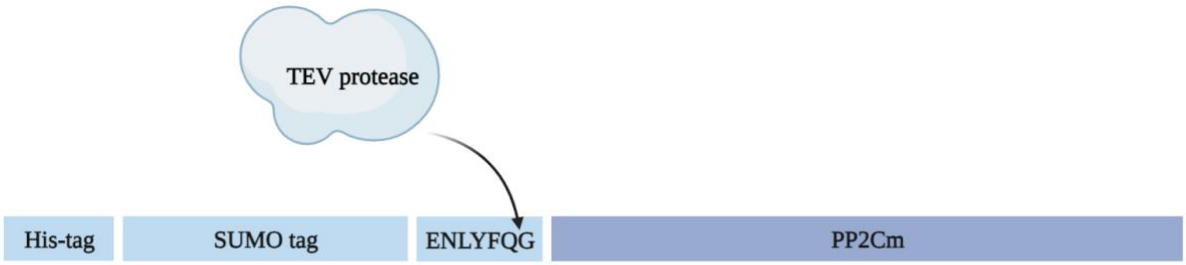

Figure 3.1. Construction plasmid of SUMO-PP2Cm*. The construct consists of a His-tag, followed by a SUMO tag, and the TEV protease cleavage site (ENLYFQG) in front of the PP2Cm protein sequence. The TEV protease cleaves between the glutamine and glycine residues.*

The Δ SUMO-PP2Cm plasmid was transformed by adding 1 µL of 50 ng/µL plasmid to One Shot BL21 chemically competent *E. coli* cells kept on ice. A heat shock was applied by subjecting the cells to 42°C for 20 seconds, followed by five minutes resting on ice. Subsequently, 1 mL of preheated Super Optimal broth with Catabolite repression (SOC) medium was added to the cells followed by 1-hour incubation at 37°C with shaking. The culture was spread onto Luria broth (8) agar plates containing 50 ng/µL kanamycin. Two plates were prepared: one plate with 75 µL culture, and one with 750 µL culture. The plates were incubated overnight at 37°C. Presence of a kanamycin resistance gene in the expression plasmids ensured that only bacteria carrying the plasmid could grow on the plates. From the resulting growth, one single colony was selected for preparation of a pre-culture for protein expression, and a small volume of the transformed cells was also stored with 20% glycerol at - 80°C for later use.

3.1.2 Protein expression

SUMO-PP2Cm transformed cells were inoculated in LB culture medium supplemented with 100 µg/mL kanamycin for overnight culture growth. **Figure 3.2** illustrates the different steps of the SUMO-PP2Cm protein expression. The overnight culture was incubated at 37°C in a 311DS shaking incubator at 120 rpm. A total of 10 mL of the overnight culture were transferred to 1 L autoclaved LB medium [25 g broth/ 1 L Milli-Q H_2O] supplied with 100 µg/mL kanamycin. A total of 6 L culture was prepared for each round of protein expression and purification. Cultures were incubated in a Multitron incubator rotary shaker at 37 °C and 180 rpm for ~2 hours until OD_{600} reached 0.5-0.6. Once the desired OD_{600} level was achieved, 1 mL 0.25 M isopropyl-β-D-1-thiogalactopyranoside (IPTG) was added to each liter culture for initiation of protein

expression (84). The cultures were incubated for another 2 hours at 37°C and 180 rpm. Cells were harvested by centrifugation of the cultures at 4 °C and 5000 rpm for 20 minutes in a Sorvall Lynx 6.000 centrifuge using a Fiberlite F9- 6x1.000 Lex angle rotor. The harvested cells were stored at -20 °C until further use.

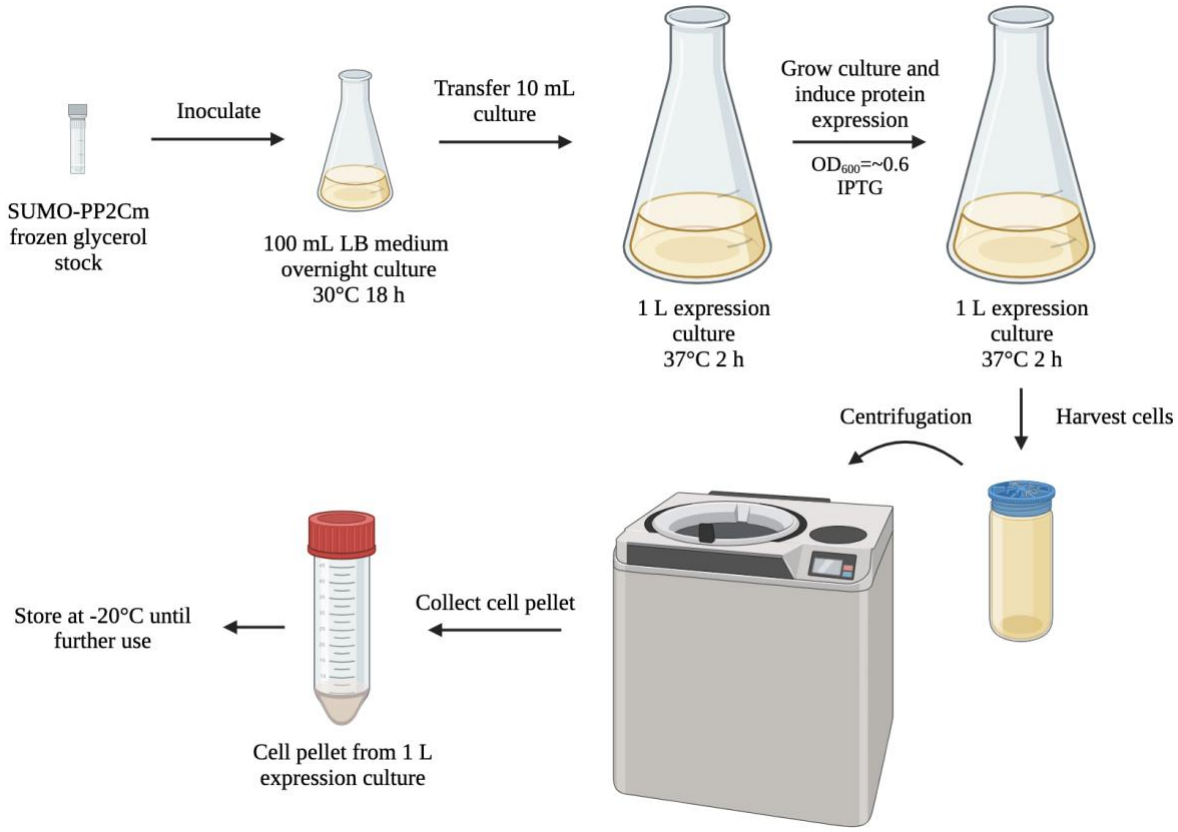

Figure 3.2. Illustration of SUMO-PP2Cm protein production. *The illustration shows the different steps of SUMO-PP2Cm protein expression and cell harvesting. SUMO-PP2Cm transformed cells are inoculated in 100 mL kanamycin-containing LB medium with overnight incubation at 30 ℃. Subsequently, 10 mL overnight culture is transferred to 1 L fresh LB medium. The expression culture incubates at 37 ℃ until OD_{600} reaches 0.5-0.6, and the protein expression is induced with IPTG. The expression culture is incubated for another 2 hours before cell harvesting by centrifugation. The cell pellet is collected and stored at -20 ℃.*

The TEV protease was expressed and purified to cleave the enzyme sequence from the SUMO tag. A glycerol stock of transformed TEV protease cells was available in the lab and used to prepare an overnight culture. The enzyme was expressed by transferring 10 mL overnight culture to 6x1 L LB culture supplemented with 100 µg/mL ampicillin. The culture was

incubated at 37°C until OD_{600} reached ~0.6, and the cell cultures were induced with IPTG and allowed to grow at 18°C for ~18 hours. The cells were harvested as described above for SUMO-PP2Cm.

3.1.3 Preparation of protein extract

The protein extract was prepared by resuspending and homogenizing harvested cells in 15 mL buffer A [10 mM Imidazole, 50 mM Tris pH 8, 300 mM NaCl] per liter of cell culture, followed by sonication. Complete lysis of bacterial cells is necessary for a good yield of purified protein. Sonication disrupts the cell walls by generating ultrasonic pressure waves that will free the protein (85). The sonication was performed with a Vibra Cell sonicator by applying ultrasonic vibration three times for 30 seconds on amplitude 60. To clarify the cell lysate, the cell suspension was centrifugated at 4°C and 15000 rpm for 20 minutes using a Fiberlite F21-8x50y angle rotor. The supernatant was collected in falcon tubes and stored on ice.

3.2 Protein purification

3.2.1 Immobilized metal affinity chromatography

Both variants of SUMO-PP2Cm and the TEV protease contain a His-tag with six histidine residues at the N-terminal end with high affinity to the Ni-NTA resin. Therefore, immobilized metal affinity chromatography (IMAC) was used as the first step of protein purification. An Econo-Column was packed with 1 mL Ni-NTA agarose beads slush [50% v/v] per 1 L cell culture. The immobilized metal was nickel (Ni^{2+}) which is bound to the chelator, nitrilotriacetic acid (NTA). When His-tagged proteins are applied to the agarose beads, binding occurs between the nickel and the His-tag, which enables the separation of proteins not containing a His-tag from proteins that do (86). Initially, the column was washed twice with 30 mL water and equilibrated with 10 mL of buffer A to remove the ethanol from the Ni-NTA slush. His-tagged SUMO-PP2Cm supernatant was added to the Ni^{2+}-containing column, and the unbound proteins (flowthrough) were collected. The column was washed with 50 mL buffer A to ensure the removal of unbound proteins, and the eluent was collected as a separate wash fraction.

Elution buffer B [300 mM NaCl, 50 mM Tris pH 8.0, 50 mM Imidazole] and buffer C [300 mM NaCl, 50 mM Tris pH 8.0, 300 mM Imidazole] were employed to elute the His-tagged protein. Buffer B was added first, and the eluate was collected in 3 x 5 mL fractions, followed by 15 mL of buffer C also collected in 3 x 5 mL fractions.

3.2.2 Protein evaluation

The level and purity of the target protein were evaluated with a sodium dodecyl sulfate-polyacrylamide gel electrophoresis (SDS-PAGE). SDS-PAGE separates proteins in a solution based on their size. SDS is a detergent that denatures proteins and gives them a negative charge proportional to their size. When applied to a polyacrylamide gel, an electric field is applied and negatively charged proteins move towards the positive electrode. Smaller proteins will move through the gel faster than larger proteins, thus the proteins are separated based on their molecular mass (87).

Eluates from IMAC were prepared by mixing aliquots of each fraction with NuPAGE® LDS Sample buffer [4 X] in a 3:1 ratio. Also, 1 µL of 40 mM β-mercaptoethanol (β-ME) was added to the samples to denature the proteins and reduce all cysteine residues (88). The samples were heated to 95°C for 10 minutes followed by 1 minute centrifugation. A Novex® Mini-Cell electrophoresis chamber was prepared and filled with 3-(N-morpholino) propane sulfonic acid buffer (MOPS buffer) [1 X]. The protein samples were loaded in a vertical SDS-PAGE system on an 8-12 % Bis-Tris plus 10-well gel alongside 3 µL SeeBlue® Prestained Standard [1X] or SeeBlue® Plus2 Standard [1X]. Electrophoresis was run using a 200 V constant voltage for 35 minutes at room temperature. The gel was stained with staining solution [40% methanol, 10% acetic acid, 0.1% Coomassie Blue] for 10-15 minutes and destained with destaining solution [4% glycerol, 10% acetic acid, 40% methanol] on a Multi-Shaker table for 30-40 minutes.

The purest SUMO-PP2Cm protein fractions were identified, pooled, and concentrated by ultra-filtration to a volume of ~500 µL (20-23 mg/mL) using Amicon® Ultra-15 Centrifugal Filter Unit. Further purification was conducted using a BioRad fast protein liquid chromatography (FPLC) system equipped with a gel filtration column.

3.2.3 Dialysis of TEV protease

To remove imidazole and salt after IMAC, the purest fractions of TEV protease, analyzed from SDS-PAGE, were pooled and dialyzed. Dialysis exchanges the buffer and desalts the protein sample by separating molecules based on their size, thus separating the imidazole and excess salt from the protein solution. The dialysis membrane is selective and permeable, allowing the smaller molecules to diffuse through the membrane until equilibrium is reached between the protein solution and the dialysis buffer (89).

The TEV protein fractions from the IMAC step were pooled in a Spectra/Por®2 semipermeable dialysis membrane with a 12-14 kDa cut-off and submerged in 2 L dialysis buffer [50 mM NaCl, 20 mM Tris pH 8, 10 mM ß- ME, 0.5 mM EDTA] at 4°C with swirling for two hours. The buffer was exchanged with a new fresh batch of dialysis buffer after 1 hour.

TEV protease cleavage of the fusion tag from Δ SUMO-PP2Cm protein was carried out using stoichiometric ratios of 1:5, 1:10, and 1:100 with overnight incubation. The cleavage was confirmed through SDS-PAGE analysis, and subsequent size exclusion chromatography was conducted to separate the fusion tag from the protein.

3.2.4 Size exclusion chromatography

Size exclusion chromatography (SEC) can be used to fractionate molecules and complexes in a sample into fractions with a particular size range. The SEC column contains beads with a defined pore size range (fractionation range). Thus, the molecules and complexes that are too large to enter the pores will stay in the mobile phase and move through the column with the flow of the buffer. Smaller molecules and complexes that can move into the pores, enter the stationary phase and will move through the column by a longer path through the pores of the beads (90).

SEC was performed using a Superdex® 75 10/300 GL gel filtration column and a 1 mL sample loop for the sample application. The proteins were eluted using a phosphate-buffered saline (PBS) [1 X] buffer. The SEC was performed at 4°C with a duration of 40 mL and 0.500 mL/min

flow rate using an NGC™ Quest 10 Chromatography System. The protein absorbance was measured at 280 nm. Purity analysis and identification of the protein-rich fractions was carried out by SDS-PAGE (see section 3.1.3.3).

3.2.5 Protein concentration measurement and storage

After purification, the Δ SUMO-PP2Cm protein solution was concentrated to a final concentration of approximately 19 mg/mL for crystallization. This concentration was achieved using an Amicon® Ultra Centrifugal filter with a 10 kDa pore size. Protein concentration was determined utilizing the NanoDrop One UV-Vis spectrophotometer with respective molar extinction coefficients (ε) of 38 000 M^{-1} cm^{-1} for FL SUMO-PP2Cm, 20 315 $M^{-1}cm^{-1}$ for Δ SUMO-PP2Cm, and 33 710 $M^{-1}cm^{-1}$ for TEV protease. For enzymatic assays, the protein solutions were stored at -20°C with a 1:1 ratio of 99.5% glycerol BioQuality. For crystallization, the protein solution was stored at 4°C without the addition of glycerol.

3.3 Enzymatic assay

Human PP2Cm exhibits phosphatase activity, leading to the design and execution of a phosphatase activity assay aimed at measuring the activity of FL SUMO-PP2Cm when mixed with different potential inhibitory compounds. Most phosphatases can dephosphorylate the generic substrate p-nitrophenyl phosphate (pNPP). As a result, pNPP was employed as the substrate of choice for rapid colorimetric measurement of the FL SUMO-PP2Cm activity. SUMO-PP2Cm catalyzes the hydrolysis of pNPP, generating inorganic phosphate and the para-nitrophenol (pNP) conjugate base. This reaction produces a yellow-colored phenolate compound and its highest absorbance is observed at 405 nm (91). Thus, the increase in absorbance was measured at 405 nm and is proportional to the activity of FL SUMO-PP2Cm. The assay was carried out in a 384-well plate, with all compounds being tested in quadruplicates, and both positive and negative controls were incorporated. Absorbance was continuously measured over 60 minutes using an Epoch microplate spectrophotometer. The identified positive hits were subsequently employed to determine the IC_{50} values for the set of

human PP2Cm inhibitors. Before conducting experiments with the compounds, the enzyme activity was separately tested to ensure enzyme stability.

3.3.1 Optimization of assay

An optimized PP2Cm activity assay was developed in the lab before transferring the enzyme to the NCMM platform for subsequent high-throughput screening. For the assay, an already-established assay protocol was employed as a template for optimization of the assay. Several parameters were examined and are summarized in **Table 3.1**. Alkaline phosphatase was included as a positive control in the assay to compare with the activity of FL SUMO-PP2Cm. In addition, Dithiothreitol (DTT) was introduced into the assay, a known agent that restores enzyme activity that may have been compromised by the oxidation of free sulfhydryl groups. This inclusion was for investigating its impact on enzyme stability (92). The impact of storing the enzyme with glycerol was also investigated to assess its effect on enzyme activity. DMSO was used to dissolve the compounds, thus DMSO was added to the assay mix to investigate its impact on FL SUMO-PP2Cm. Also, the following parameters were tested: different concentrations of substrate pNPP, different concentrations of the enzyme, and the presence of $MnCl_2$.

Table 3.1. The different parameters examined in the enzymatic assay. *Overview of the different concentrations of parameters examined in the enzymatic assay. Optimized results include the concentration of parameters used in the established assay. The parameters tested were the activity of alkaline phosphatase compared to FL SUMO-PP2Cm, different concentrations of substrate pNPP and FL SUMO-PP2Cm, the effect of DMSO, DTT, and FL SUMO-PP2Cm stored with 50% glycerol, and the presence of* $MnCl_2$.

Parameter	***Examined in assay***	***Optimized result***
Alkaline phosphatase	10 μM	-
[pNPP]	1 mM, 10 mM	10 mM
[FL SUMO-PP2Cm]	200-500 nM	220 nM
Effect of DMSO	5%	No effect
Effect of DTT	10 mM	No effect
Effect of enzyme storage with 50% glycerol	Yes	No effect
$MnCl_2$	0 mM, 10 mM, 20 mM	20 mM

DMSO, DTT, and storage with 50% glycerol did not affect enzyme activity or stability. Raw data from the assay investigating the effect of DTT, storage of enzyme with 50% glycerol, and no $MnCl_2$ are provided in **Supplementary Figure D2**. Three reaction mixes (RMs) were prepared and transferred to the screening platform after optimizing the protocol. The reaction mixes are listed in **Table 3.2** which also displays the final parameters and their concentrations used in assays with the different compounds.

Table 3.2. Final reaction mixes for enzymatic assay. *The optimized reaction mixes used in the enzymatic assays.*

Solutions		***[Stock]***	***[Assay]***
RM1*	*FL SUMO-PP2Cm*	488 nM	219.6 nM
	$MnCl_2$	20 mM	9 mM
	Tris-HCl pH 7.5	20 mM	8.4 mM
RM2*	*$MnCl_2$*	20 mM	9 mM
	Tris-HCl pH 7.5	20 mM	9.8 mM
RM3	*pNPP*	10 mM	5 mM

**The stock solutions were diluted with 20 mM Tris-HCl pH 7.5.*

3.3.2 Preparation of compound dilution series

A total of 15 compounds, resulting from the high-throughput (HT) screening of the ~28000 compound large Enamine library at the NorOpenscreen platform at NCMM, were analyzed. The HT screening suggests that 12 of the compounds work as inhibitors and 3 work as activators of the enzyme. To differentiate them from the other compounds, the 3 potential activators are denoted as A2, A3, and A4. Additional information about the 15 compounds is presented in Appendix C, including their structures provided in Appendix E.

All compounds were purchased from Enamine as dry powders (10 mg), dissolved in 100% DMSO to a final concentration of 25-100 mM depending on solubility, and stored at 4°C for short-time use, and at -20°C for long-time storage. An Assist Plus pipetting robot was programmed to prepare a 1:1 dilution series for each of the 15 compounds. The robot pipetted 20 µL 100% DMSO to each well, except column 3, in a Nunc™ 384-well non-treated flat-bottom microplate. Then 40 µL of compound was pipetted to column 3 and the robot started a 1:1 dilution series throughout the plate, giving 22 different concentrations of the compound. Columns 1 and 2 were filled with 100% DMSO to be used as the positive control (PC), without compound, and the negative control (NC), without PP2Cm, respectively. The outline of the 384-well plate with dilutions of compounds 1 and 2 is illustrated in **Figure 3.3**, while **Table 3.3** presents the final concentration range in the dilution series of each compound.

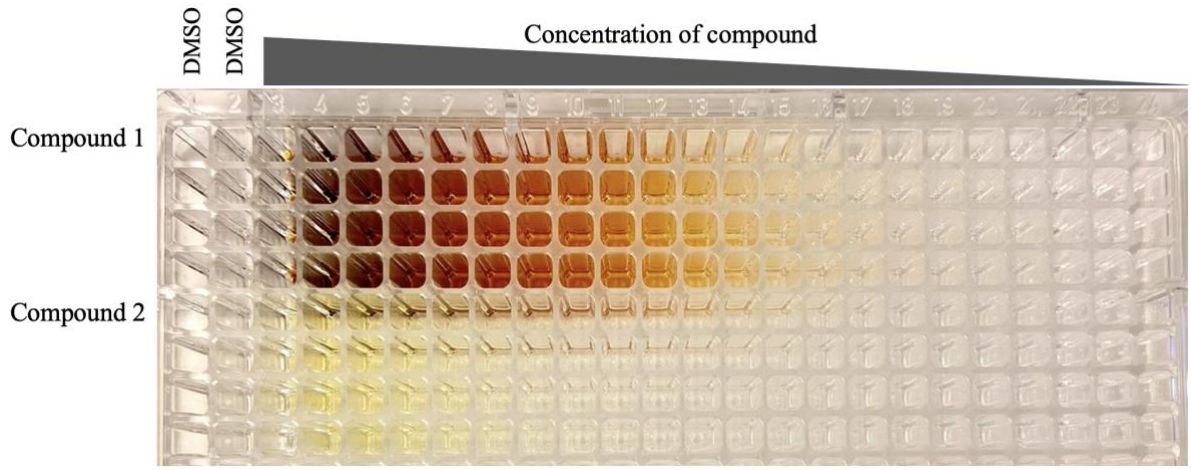

Figure 3.3. Dilution plate of compounds 1 and 2. *Schematic outline of the 384-well plate containing 22 dilutions of compounds 1 and 2.*

Table 3.3. An overview of the concentrations in the 384-well plates used for the dilution of the compounds. *The dilution plates were used in the enzymatic assays.*

Compound	***[Stock]***	***Concentration range***
1*, 3*, 4*	100 mM	100 mM – 24 nM
2*	50 mM	50 mM – 12 nM
1, 2, 3, 4, 5, 7, 8, 9, 10, 11, 12, 13, A2, A3, A4	25 mM	25 mM – 6 nM

** The compounds 1-4 were first tested at the given range as shown, however, substantial precipitation was observed for the highest concentrations. Thus, in the second round of assaying, all compounds were tested in the range of 25 mM – 6 nM.*

3.3.3 Dephosphorylation phosphatase activity assay with pNPP as substrate

To study the inhibitory effects of the various compounds on FL SUMO-PP2Cm, a dephosphorylation phosphatase activity assay was performed together with the prepared compound dilution series. The assay was carried out in a 384-well non-treated flat-bottom microplate and the pipetting was executed by an Assist Plus pipetting robot. The total assay reaction volume was 100 µL, and the different reaction mixes are listed in **Table 3.2**. All the RMs were diluted using 20 mM TRIS-HCl pH 7.5.

The reaction mixes ensure a more optimal assay but also control the reaction's initiation. For each compound, four parallels were included for each concentration of the 22 dilutions of the compound, including four parallels for the PC and the NC. For some of the compounds it was made several dilution plates starting at different concentrations, this was due to precipitation in the wells containing higher concentrations of compound when mixed with the RM. **Table 3.4** shows the different concentrations of the compounds in the assay.

Table 3.4: Concentration of the compounds in the assay. *Compounds 1, 2, 3, and 4 were first tested with their stock concentration. All compounds were tested with a concentration range of 1.25 mM – 0.3 nM in the assay.*

Compounds	***[Dilution plate]***	***[Assay]***
1, 3, 4	100 mM – 24 nM	5 mM – 1.2 nM
2	50 mM – 12 nM	2.5 mM – 0.6 nM
1, 2, 3, 4, 5, 7, 8, 9, 10, 11, 12, 13, A2, A3, A4	25 mM – 6 nM	1.25 mM – 0.3 nM

A program was made for the Assist Plus pipetting robot to prepare the activity assay. Initially, all RMs were prepared and added to a MASTERBLOCK® 96 Deep Well block that was placed on the Assist Plus pipetting robot together with the compound dilution plate and an empty 384-well microplate. The robot was programmed to perform the following steps:

1. Add 45 uL RM1 to all wells, except column 2 representing the negative control (NC).
2. Add 45 uL RM2 to column 2.
3. Add 5 uL compound dilution to columns 3-24. For positive (PC) and negative control (NC), columns 1 and 2 respectively, 5 uL 100% DMSO was added. Mix thoroughly.
4. Incubate for 10 minutes with the compounds.
5. Add 50 uL RM3 to all columns. Mix thoroughly.

As soon as the program finished, the 405 nm absorbance was measured every second minute for 1 hour using an Epoch microplate spectrophotometer.

3.3.4 Activity determination and analysis

The raw data obtained from the enzymatic activity assay were analyzed using the software Origin 2023b and Microsoft Excel. To determine the activity of FL SUMO-PP2Cm, the slope of the increase in absorbance was calculated in a time window of 15 minutes, where the slope is defined as the linear absorption change over time (i.e., rate of consumption of substrate pNPP). While pipetting, it takes approximately 16 minutes for the robot to distribute RM3 to the whole plate, thus the reaction in the first column starts earlier than the last columns. Therefore, this was adjusted for when calculating the slopes of every reaction. The activities were normalized in Excel by using the PC, representing maximum (100%) activity, and the NC, representing minimum (0%) activity. The normalized calculation is shown in Formula 3.1:

$$Normalized\ activity\ (\%) = 100\% \times \frac{(Slope(sample) - Slope(\mathrm{NC}))}{(Slope(PC) - Slope(NC))} \qquad 3.1$$

Formula 3.1 converts the slope values to the percentage of activity. *Slope(sample)* represents the calculated slope for the sample, while *Slope(NC)* and *Slope(PC)* represent the NC and PC, respectively. The mean activity with associated standard deviation was calculated for the normalized activity of the 4 parallels for each compound concentration and plotted in a scatter plot in Origin 2023b. A sigmoidal dose-response curve was then fitted to the data to calculate the IC_{50} values. The IC_{50} value represent the compound concentration that inhibits 50% of the PP2Cm activity. Formula 3.2 shows the formula for the dose-response curve:

$$y = A_1 + \frac{A_2 - A_1}{1 + 10^{(Log x_0 - x)p}} \qquad 3.2$$

Here, A_1 and A_2 represent the bottom asymptote and the top asymptote of the curve, respectively. *Log* x_0 is the IC_{50} value, where x is the variable compound concentration. The hill slope is represented as *p*, which describes any cooperativity.

For most compounds, it was not possible to fit a sigmoidal curve. Thus, the IC_{50} values were estimated directly from the graph at 50% activity, corresponding to 50% activity of PP2Cm

relative to the PC and NC. It is worth noting that a subset of the compounds did not inhibit down to 50% enzyme activity and the determination of their IC_{50} value was not obtainable.

3.4 Crystallization

Crystallographic experiments were performed with Δ SUMO-PP2Cm in an attempt to determine the 3D structure of PP2Cm with the compounds. The crystallization conditions for Δ SUMO-PP2Cm needed optimization before co-crystallization with the compounds. A screening of crystal conditions was analyzed using sitting-drop vapor diffusion. In addition, a hanging-drop vapor diffusion was set up using the previously published conditions. However, due to time limitations, the optimization was not completed and screening of Δ SUMO-PP2Cm crystal conditions gave no satisfactory results.

3.4.1 Screening and optimization of crystallization conditions

In this part of the project, the Δ SUMO-PP2Cm protein was used. For crystallization purposes, it was attempted to separate the protein from the SUMO tag by cleaving at the TEV protein sequence site using TEV protease. Only a partial cleavage was achieved, thus, the crystallization was instead attempted with the SUMO tag.

In the search for Δ SUMO-PP2Cm crystallization conditions, screening was conducted with specific crystallization kits and a Mosquito Crystal crystallization robot. Due to unsuccessful cleavage of the SUMO tag, a screening of Δ SUMO-PP2Cm with the SUMO tag intact was carried out using the Peg/Ion and JCSG+ crystallization kits. A concentration of ~19 mg/mL Δ SUMO-PP2Cm was used. A manual pipetting robot was used to fill a SWISSCI MRC 2-well plate with 30 µL well solution from each kit. Sitting drops were prepared at 4ºC by mixing 300 nL well-solution and 300 nL protein solution, performed by the Mosquito robot. Subsequently, the SWISS MRC 2-well plate was sealed with transparent duct tape and stored at 20ºC. Regular monitoring of the plate was carried out to observe crystal formation.

In addition, a hanging-drop vapor diffusion was set up with almost identical conditions as described in an article where SUMO-PP2Cm was crystallized (14). The conditions are listed in **Table 3.5**. The hanging drop vapor diffusion was performed in a 24-well VDX plate with sealant. The well-solution was prepared and then 2 µL of Δ SUMO-PP2Cm was mixed with 2 µL well-solution, followed by suspending the mixture over a reservoir of 0.5 mL of the precipitant solution. The plate was stored at 20°C and monitored regularly.

Table 3.5: Crystallization conditions for hanging-drop vapor diffusion of Δ SUMO-PP2Cm. *Stock solution of polyethylene glycol (PEG) 3350, $MgCl_2$, Tris-HCl, and β-ME. The different conditions were used as well-solutions 1-5.*

[Stock]	***1***	***2***	***3***	***4***	***5***
50 % PEG 3350	15%	17.5%	20%	22.5%	25%
3 M $MgCl_2$	0.2 M	0.2 M	0.2 M	0.2 M	0.2 M
1 M Tris-HCl pH 8.6	0.1 M	0.1 M	0.1 M	0.1 M	0.1 M
14 M β-ME	20 mM	20 mM	20 mM	20 mM	20 mM

3.5 Cellular testing of SUMO-PP2Cm compounds

To analyze the cytotoxicity of the compounds, a PANC-1 (ATCC® CRL-1469™) cell line was used as a pancreatic ductal adenocarcinoma (PDAC) model. The cells were used in a Presto Blue assay to assess the Lethal dose 50 (LD_{50}) when introduced to the different compounds. In addition, a branched-chain keto-acid (BCKA) assay was conducted to indirectly measure the intracellular activity of PP2Cm when the cells are exposed to the different compounds.

3.5.1 Cell cultivation

During this part of the project, the cells were cultured continuously in Dulbecco's Modified Eagle's Medium (DMEM) containing 4.500 mg/mL glucose, supplemented with 10% fetal bovine serum (FBS), and 1% pen-strep (100 U/mL penicillin and 100 U/mL streptomycin). For

cultivation, a 75 cm^2 Nunc™ cell culture flask was used, and the cells were incubated in a Forma Steri-Cycle CO_2 incubator at 37 °C with 5% CO_2. The cell lab had established a routine check of the Mycoplasma bacterium to prevent infection of cells by the bacterium. This is important because Mycoplasma is small enough to enter the filters that are supposed to protect cells from contamination. If infected, it can change the metabolism and physiology of the cells (93). Thus, the cells were tested before performing the assays.

To maintain cell viability and prevent nutrient depletion and overcrowding, the PANC-1 cells were continuously passaged when they reached 80-90% confluence (94). The passaging process involved using a split ratio of 1:5 or 1:10 for the PANC-1 cells, where the culture medium was first removed from the flask, and the cells were washed with 10 mL 1X PBS. Subsequently, 1 mL of a 0.25 % trypsin-ethylenediaminetetraacetic acid (EDTA) solution was added to the flask to detach the adherent cells. Trypsin functions as a proteinase that cleaves cell surface protein until it gets neutralized by an inhibitor like serum (94). Thus, the cells were incubated in the trypsin solution until detachment, verified using a DM IL microscope, and subsequently, 10 mL of DMEM was added to the flask to inactivate trypsin activity. The 1:5 split ratio involved removing 8 mL of the cell suspension, followed by the addition of 9 mL of fresh DMEM to the cell culture flask, resulting in a total volume of 11 mL.

3.5.2 Presto Blue cell viability assay

The PANC-1 cells were incubated with compounds to measure the drug cytotoxicity by using the Presto Blue™ cell viability assay. The Presto Blue® cell viability reagent quantitatively measures the proliferation of cells by using the reducing power of living cells (79). When introduced to cells, the reagent uses the reducing power of metabolically active cells to convert resazurin to fluorescent resorufin. The color change can be analyzed and evaluated quantitatively on an absorbance- or fluorescence-based microplate reader at maximum absorbance of 570 nm and 600 nm as reference wavelength, or 535-560/590-615 nm, respectively. Also, qualitative analysis can be evaluated by the visual color change of the solution from blue to red (**Figure 3.4)**(80).

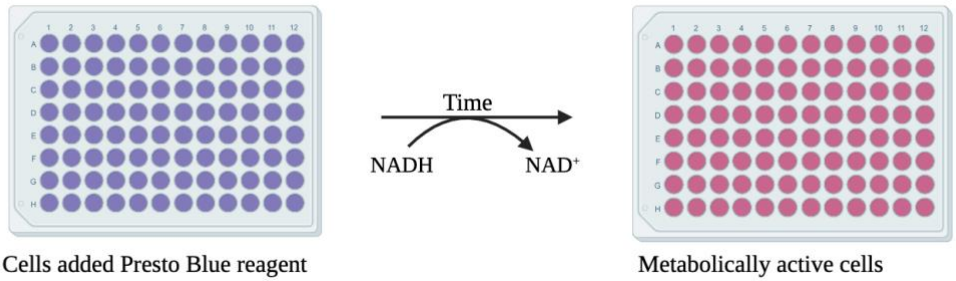

Figure 3.4. Visual color change of PrestoBlue reagent reaction*. Living metabolically active cells will convert resazurin to resorufin when introduced to the PrestoBlue reagent, causing a visual color change from blue to pink.*

The Presto Blue cell viability assay was performed in a 96-well culture microplate. An Assist Plus pipetting robot prepared a serial dilution of 10 dilutions of the compounds with a starting concentration of compounds at 25-100 mM, depending on their solubility. Cells were plated with a 2000 cells/well density. The cells were allowed to grow in DMEM for 24 hours in an incubator at 37°C and 5% CO_2 before 1 µL of each compound was added to each well by the Assist Plus pipetting robot. For each concentration of the compound, a total of four parallels were set up. Compound dilutions were added to columns 3-12, and 100% DMSO was added to columns 1 and 2 to represent the PC and NC, respectively. The cells were incubated with the compound for 48 hours before the medium was replaced with 100 µL DMEM containing 5% PrestoBlue® reagent. The plate was incubated for 4 hours before the absorbance was measured at 570 nm and 600 nm on an Epoch microplate spectrophotometer.

3.5.3 Analysis of Presto Blue Assay

To process and analyze the raw data from the PrestoBlue® assay, Excel and Origin 2023b were used. The background signal in the assay was corrected by subtracting the 570 nm absorbance from the 600 nm absorbance. The data was normalized using Formula 3.3. The average absorbance was calculated for each sample parallel, and the corresponding standard deviations were calculated using Formula 3.4.

$$V = 100\% \times \left(\frac{Abs(Sample) - Abs(NC)}{(Abs(PC) - Abs(NC))}\right) \quad 3.3$$

In **Formula 3.3,** *Abs(Sample)* represents the mean absorbance of the sample, and *Abs(NC)* and *Abs(PC)* represent the mean absorbance of the negative and positive control, respectively. The positive control is 100% viable cells that do not contain a compound, whereas the negative control is the wells not containing cells and thus equals 0% viability. The PC and NC had 8 parallels, and the samples had 4 parallels.

$$\delta V = \sqrt{\left(\frac{\delta Abs(PC)}{Abs(PC)}\right)^2 + \left(\frac{\delta Abs(Sample)}{Abs(Sample)}\right)^2} \times V \qquad 3.4$$

In **Formula 3.4**, δV corresponds to the standard deviation of the normalized viability (V). $\delta Abs(PC)$ and $\delta Abs(Sample)$ represent the standard deviation of the absorbance of the positive control (*Abs(PC)*) and the standard deviation of the mean absorbance of the sample parallel $Abs(Sample)$, respectively.

Origin 2023b was used to plot the calculated viability and its corresponding standard deviation as a function of the compound concentrations. A sigmoidal dose-response curve was fitted to the data and used to calculate the LD_{50} values. The LD_{50} values indicate which compound concentration gives 50% cell viability when compared to the PC and NC. For some of the samples, the data did not fit the sigmoidal dose-response curve, thus the LD_{50} value was estimated directly from the plot at 50% viability.

3.5.4 Activity assay of branched-chain α-keto acids – BCKA assay

This activity assay of branched-chain α-keto-acids (BCKA) evaluates cellular PP2Cm activity by measuring BCKAs. An inactive BCKDH complex accumulates BCKAs within cells. By measuring the level of extracellular BCKAs, inhibited enzyme activity can be detected (81). The process involves leucine dehydrogenase (LDH) converting α-KIC to L-Leucine in the presence of ammonium and NADH, monitored through stoichiometric oxidation of NADH and decreasing absorbance at 340 nm (82). This provides a quantitative measure of enzyme inhibition. The assay can also be performed by measuring the fluorescence of NADH at Ex/Em 355/460 nm.

3.5.5 Optimization of BCKA assay

The assay protocol needed optimization due to variable results. This assay can be conducted by measuring either the fluorescence or the absorbance of NADH. However, it exhibits greater sensitivity when measuring the fluorescence, necessitating lower concentrations of α-ketoisocaproic acid (KICA) and NADH. During optimization, absorbance measurements provided a more stable standard curve for KICA than fluorescence. Consequently, conditions for absorbance measurements were prioritized when conducting the assay with the compounds. Various concentrations of KICA, NADH, and LDH were tested to establish an optimized assay protocol, and the tested concentrations for absorbance and fluorescence are listed in **Table 3.6** and **Table 3.7**, respectively. Despite these efforts, the assay's variability did not improve, leading to the continued use of the initial concentrations.

Table 3.6. Parameters of BCKA assay measured at 340 nm absorbance. *The assay is supplied with NADH and NH_4^+. α-KIC is included as a standard curve, while LDH is applied for enzyme activity measurement. Various concentrations of NADH and KICA were tested.*

	Parameter	***Start***	***Examined***	***Final concentrations***
Absorbance	[NADH]	400 µM	0 µM, 25 µM, 50 µM, 100 µM, 150 µM, 200 µM, 300 µM, 400 µM	400 µM
	[NH_4^+]	50 mM	-	50 mM
	[KICA] standard	0 µM, 25 µM, 100 µM, 400 µM	0 µM, 25 µM, 50 µM, 100 µM, 200 µM, 400 µM	0 µM, 25 µM, 100 µM, 400 µM
	[LDH]	0.224 µM	-	0.224 µM

Table 3.7. Parameters of BCKA assay measured at Ex/Em 355/460 nm fluorescence. *The assay is supplied with NADH and NH_4^+. KICA is included as a standard curve, while LDH is applied for enzyme activity measurement. Various concentrations of NADH, KICA, and LDH were tested.*

	Parameter	***Start***	***Examined***	***Final concentrations***
Fluorescence	[NADH]	200 µM	0 µM, 25 µM, 50 µM, 100 µM, 150 µM, 200 µM	150 µM
	[NH_4^+]	50 mM	-	50 mM
	[KICA] standard	0 µM, 2 µM, 4 µM, 6 µM, 8 µM, 10 µM	0 µM, 2.5 µM, 5 µM, 10 µM, 20 µM, 50 µM	0 µM, 2 µM, 4 µM, 6 µM, 8 µM, 10 µM
	[LDH]	0.14 µM	0.7 µM	0.14 µM

3.5.6 BCKA assay

The compounds were incubated with PANC-1 cells to assess BCKA consumption. This assay quantitatively measures the amount of BCKA secreted by the cells by measuring the amount of NADH used by the leucine dehydrogenase (LDH) enzyme. The assay was carried out in a 96-well culture microplate. PANC-1 cells were plated with a density of 50 000 cells/well and incubated for 24 hours at 37°C and 5% CO_2. The compounds were diluted in 900 µL DMEM. Compounds 3-13 were diluted to a final concentration of 100 µM. Compounds 1 and 2 were diluted to a final concentration of 1 µM due to higher cytotoxicity. The medium was removed from the wells and 200 µL of DMEM containing compound was added to two wells/compound.

Additionally, a PC was added to four wells, containing DMEM with 100% DMSO free of compound. The cells were allowed to incubate with the DMEM-diluted compounds for 4 hours in an incubator at 37°C. After incubation, the medium (samples) was collected in PCR strips and stored at 2-4°C until usage.

The samples and fresh DMEM were subjected to a 5-minute denaturation step at 90°C to eliminate interfering serum proteins. A standard of 0 µM, 25 µM, 100 µM, and 400 µM KICA

was prepared in heat-treated DMEM for measuring absorbance. Subsequently, 100 µL of standards and samples were added to their respective wells. Both NADH and NH_4^+ were added to all wells, yielding a final concentration of 400 µM NADH and 50 mM NH_4^+. A 10X dilution of 35 µM LDH was made for absorbance measurement, and 6.4 µL was added to 100 µL in the assay. LDH was added to two of the wells for each compound, and the absorbance was immediately measured at 340 nm every minute for 30 minutes using an Epoch microplate spectrophotometer.

The assay was additionally monitored by fluorescence. In this context, a standard series of 0 µM, 2 µM, 4 µM, 6 µM, 8 µM, and 10 µM KICA was prepared, and 200 µM NADH was used instead of 400 µM NADH. Also, a 5X dilution of 35 µM LDH was prepared, and 2 µL of this diluted LDH was added to 100 µL in the assay. The fluorescence was measured at Ex/Em 355/460 nm using a Fluoroskan microplate fluorometer.

3.5.7 Quantification of BCKA levels by BCKA assay

The raw data from the BCKA assay was processed and analyzed using Microsoft Excel. The difference in absorbance of the sample with and without LDH was calculated at 30 minutes and provided the signal for α-KIC concentration. Formula 3.5 provides the calculation for the signal of α-KIC concentration:

$$\Delta Abs = Abs(Sample) - Abs(Sample\ LDH) \qquad 3.5$$

ΔAbs is the difference in absorbance between the sample without and with LDH. *Abs(Sample)* is the absorbance of the sample, while *Abs(Sample LDH)* is the absorbance of the sample containing LDH.

A control without LDH was included to assess the level of keto acids in the presence of NADH when LDH, which consumes NADH, is not present. As a result, the difference in absorbance between non-LDH-containing samples and the LDH-containing samples was plotted to evaluate keto acid levels against the standard curve. Furthermore, a positive control (PC) of non-treated cells was included to examine the BCKA secretion of cells not exposed to any compound.

3.6 Ethical considerations

In this project, only the PANC-1 cell line was used for cellular testing of the compounds. The PANC-1 cell line is commercial, thus no approval was required.

4 RESULTS AND DISCUSSION

The BCKDH complex is required for pancreatic cancer cell proliferation (34). As the activator of the BCKDH complex, PP2Cm is a highly relevant target to reduce the activity of the BCKDH complex (12) and consequently, cancer cell growth and proliferation in pancreatic ductal adenocarcinoma (PDAC) patients. Therefore, High-Throughput screening of recombinant fusion protein (SUMO-PP2Cm) against a 28000 compound library was performed, giving 15 candidate compound hits that were further analyzed in this project. Both enzymatic inhibition and cell toxicity (IC_{50} and LD_{50} values, respectively) have been determined for each compound, in addition to an analysis of the *in vivo* inhibitory effects of the compounds. A crystallization screening of Δ SUMO-PP2Cm was performed with the aim of structural analysis. In the truncated variant, a long sequence representing a long tail on the PP2Cm protein has been removed because it is suspected to be non-functional. These analyses give novel knowledge about the inhibitory effects of these compounds on SUMO-PP2Cm.

4.1 Protein purification

Various methods were performed for the isolation and purification of SUMO-PP2Cm. The protein must be as pure as possible for optimal results in determining IC_{50} values (95) and crystallization performance (67). The two protein variants were purified regularly using already-established protocols for Immobilized Metal Ion Affinity Chromatography (IMAC) and size exclusion (SEC). The purification and identification of the target protein were analyzed with SDS-PAGE. In addition to SUMO-PP2Cm, TEV protease was purified once, however, this is not included in the results. Only the optimal purification methods are included in the results.

4.1.1 Immobilized metal affinity chromatography

IMAC is a protein purification method that captures his-tag on proteins by the tag's affinity to the Ni^{2+}-NTA resin (86). The two variants of SUMO-PP2Cm were expressed with an N-terminal his-tag, making them suitable for purification with IMAC. The protein was eluted

using an increasing gradient of imidazole buffer. The collected fractions were analyzed with SDS-PAGE to identify the purest and most protein-rich fractions. Polyacrylamide gels from electrophoresis analysis of both variants of SUMO-PP2Cm after IMAC are presented in **Figure 4.1**. The SeeBlue standard was used as a molecular-weight size marker to compare molecular masses and loaded in lane 1. Lane 2 contains the collected flow-through fraction which contains the proteins that did not bind the resin in IMAC. The column was washed with elution buffer A [10 mM imidazole], containing the lowest concentration of imidazole. The collected wash fraction was loaded in lane 3 and represents the unspecific bound proteins. Lanes 4-6 and 7-9 contain proteins eluted by elution buffers B [50 mM imidazole] and C [300 mM imidazole], respectively.

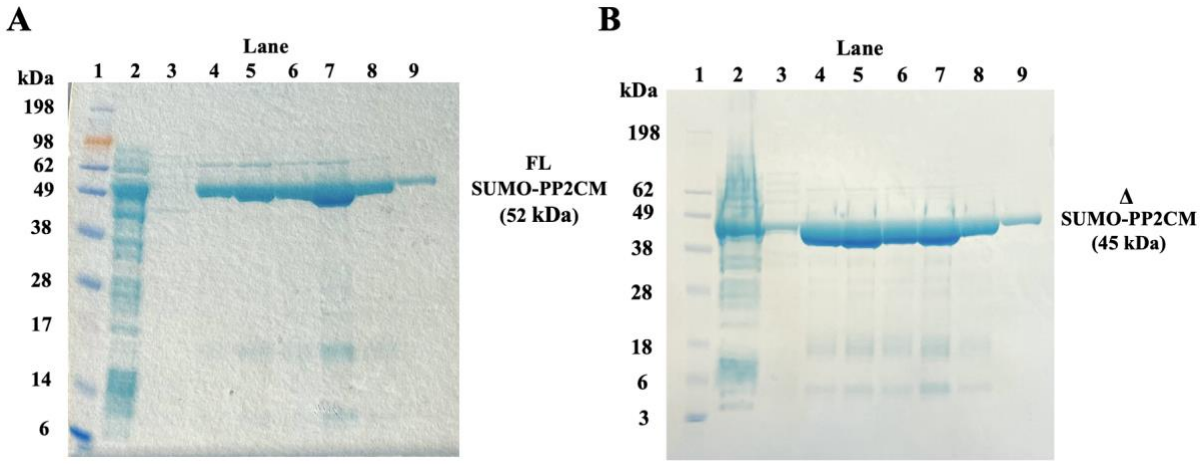

Figure 4.1. SDS-PAGE result of SUMO-PP2Cm after IMAC purification*. The ladder, SeeBlue Plus2 standard (**A**), and SeeBlue pre-stained standard (**B**) were loaded in lane 1. The flowthrough and wash fractions were loaded in lanes 2 and 3, and fractions from elution with elution buffer B and C were loaded in lanes 4-6 and 7-9, respectively. (**A**) Polyacrylamide gel of FL SUMO-PP2Cm (52 kDa). The protein eluted in lanes 4-9. (**B**) Polyacrylamide gel of Δ SUMO-PP2Cm (45 kDa). The protein eluted in lanes 4-9.*

The molecular mass of FL SUMO-PP2Cm is 52.484 kDa and has been identified in **Figure 4.1A**, whereas Δ SUMO-PP2Cm has been identified in **Figure 4.1B** with a molecular mass of 45.013 kDa. The thick bands above (**Figure 4.1A**) and below (**Figure 4.1B**) the 49 kDa mark in lanes 4-8 represent large amounts of SUMO-PP2Cm and are smeared out because of high protein concentration. SUMO-PP2Cm eluted both with elution buffer B and C, i.e., 50 mM and 300 mM imidazole, respectively. Lane 4-9 shows an efficient purification where major impurities have been removed compared to the flowthrough fraction in lane 2. There are some

weak bands with higher and lower molecular mass, but the purity was estimated to be above 90%. Due to the smeared bands, it would have been more precise to perform an SDS-PAGE with a lower protein concentration to determine if other bands appear around this molecular mass. The purest fractions with the highest SUMO-PP2Cm concentration were merged, concentrated to ~ 0.5 mL, and further purified by SEC. The truncated variant, Δ SUMO-PP2Cm, was treated with TEV protease before further purification.

4.1.2 SUMO tag removal

SUMO tag removal was only attempted with the 45 kDa long Δ SUMO-PP2Cm. Removal of the fusion tag, especially his-tags, has been shown to be important for crystal formation (83). Δ SUMO-PP2Cm is expressed with a hexahistidine tag, followed by a SUMO tag, and the TEV protease recognition site (ENLYFQG) at the N-terminal end. The TEV protease cleaves between the glutamine (Q) and glycine (G) residues in the recognition sequence. Therefore, cleavage will remove both the his-tag and SUMO tag from the protein. To be used in crystallization, Δ SUMO-PP2Cm was treated with TEV protease for cleavage of this fusion tag. SDS-PAGE was performed to confirm the cleavage, and the result is presented in **Figure 4.2A-C**. The SeeBlue pre-stained standard was used as a ladder and loaded in lane 1. SUMO-tagged PP2Cm and TEV protease-digested SUMO-PP2Cm are seen in lanes 2 and 3, respectively (**Figure 4.2A** and **B**). **Figure 4.2C** shows digested Δ SUMO-PP2Cm in both lanes 2 and 3, where the protein in lane 3 was treated with a higher concentration of TEV protease. Δ SUMO-PP2Cm has a molecular mass of 45 kDa before digestion with TEV protease, and a molecular mass of approximately 31 kDa after digestion.

In **Figure 4.2A** a batch of TEV protease stored with 50% glycerol at -20°C was used, and the stoichiometric ratio between TEV protease and Δ SUMO-PP2Cm was 1:10. The solution with protein and protease was incubated overnight. The digestion was not successful, as no band appeared around 31 kDa and we can still see a thick band around 45 kDa. Digestion by TEV protease usually requires a ratio of 1:100 (96), thus this batch of TEV protease enzyme seems to be inactive. Therefore, a freshly purified batch of TEV protease was prepared and used in the digestions shown in **Figures 4.2B** and **4.2C**. The purification of TEV protease is described in the Materials and Methods section.

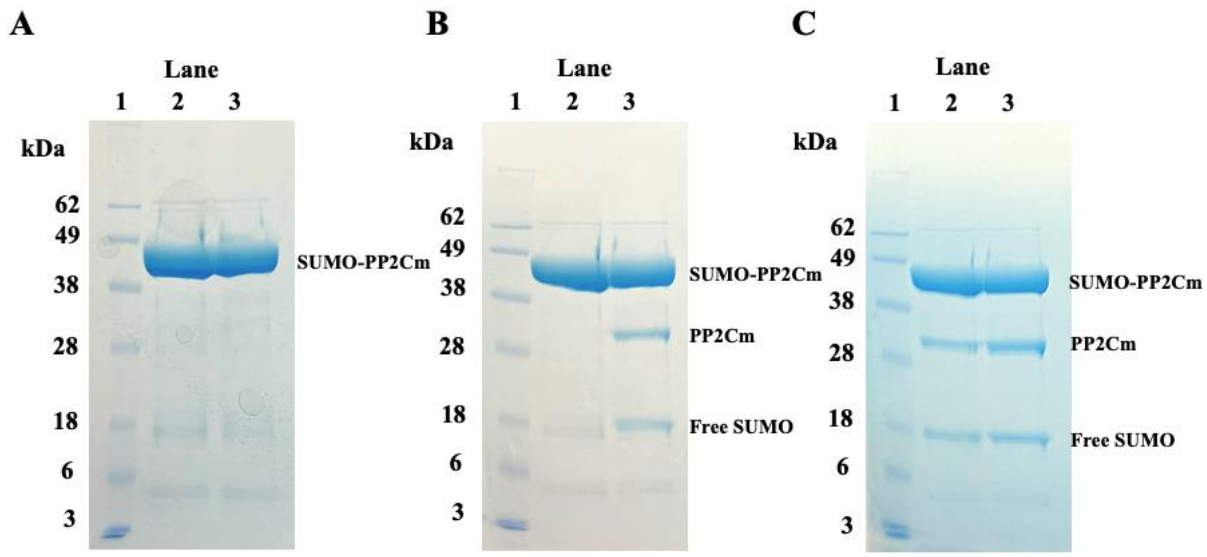

Figure 4.2. SDS-PAGE result of Δ SUMO-PP2Cm (41 kDa) after digestion by TEV protease. *Lane 1 is loaded with the SeeBlue pre-stained standard [1X], lane 2 contains truncated SUMO-PP2Cm, and lane 3 contains TEV protease-treated Δ SUMO-PP2Cm. (**A**) Δ SUMO-PP2Cm was loaded in lane 2, while Δ SUMO-PP2Cm treated with TEV protease in a 1:10 ratio was loaded in lane 3. (**B**) Lane 2 contains Δ SUMO-PP2Cm, while lane 3 contains Δ SUMO-PP2Cm treated with TEV protease in a 1:100 ratio. (**C**)Δ SUMO-PP2Cm treated with TEV protease in a 1:100 and 1:5 ratio was loaded in lanes 2 and 3, respectively.*

The molecular mass of PP2Cm without the SUMO tag is approximately 31 kDa, as the fusion tag has a molecular weight of ~14 kDa. The band corresponding to the molecular mass of digested Δ SUMO-PP2Cm can be seen in **Figures 4.2B** and **4.2C** between the 28-38 kDa mark. However, the protein was only partially cleaved as there is a much higher concentration of the SUMO-tagged protein than the digested protein, indicated by the thicker band below 49 kDa. A protease:protein ratio of 1:100 and 1:5 is presented in lane 3 of **Figure 4.2B** and **C**, respectively. Both lane 2 and 3 were loaded with digested Δ SUMO-PP2Cm in **Figure 4.2C**, but lane 2 contain Δ SUMO-PP2Cm digested with 1% TEV protease, and lane 3 contain Δ SUMO-PP2Cm digested with 20% TEV protease. When comparing the bands in lanes 2 and 3, the increased concentration of TEV protease did not cause substantially more cleavage. Regardless of this, it was attempted to separate the digested protein from the tag and the tagged protein by SEC with PBS [1X] buffer.

4.1.3 Size exclusion chromatography

SEC was performed for buffer exchange and further purification of both variants of SUMO-PP2Cm and TEV protease-cleaved PP2Cm. The purification by SEC was monitored by measuring the absorbance at 280 nm. The protein was eluted with 1X PBS buffer and collected in 0.5 mL fractions. FL SUMO-PP2Cm eluted in fractions A13-A23, as seen in the chromatogram in **Figure 4.3**. The peak tails, a reason can be that the protein is hydrophobic or electrostatic.

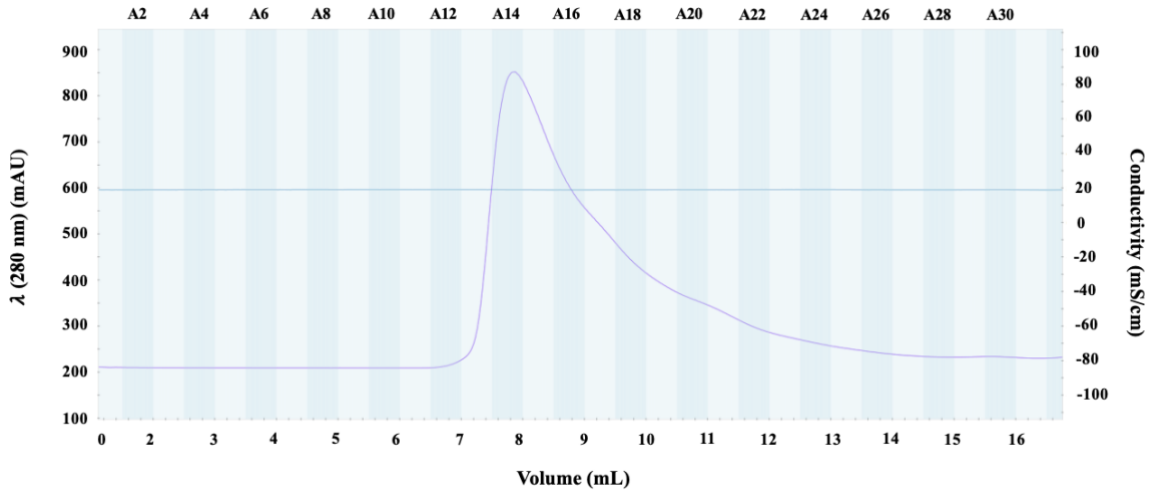

Figure 4.3. SEC chromatogram of FL SUMO-PP2Cm. *The 280 nm absorbance is shown in purple, correlating with the elution of SUMO-PP2Cm. SUMO-PP2Cm eluted in fractions A13-A23.*

The protein-containing fractions were analyzed with SDS-PAGE to identify the purest fractions containing high protein concentrations. **Figure 4.4** presents the SDS-PAGE results of the fractions. In **Figure 4.4A**, the SeeBlue Plus 2 standard was loaded in lane 1, and the FL SUMO-PP2Cm fractions were loaded in lanes 2-11. **Figure 4.4B** shows the results from SEC of Δ SUMO-PP2Cm in lanes 2-10, with SeeBlue prestained standard [1X] as a protein ladder in lane 1. Lanes 3-6 (**Figure 4.4A**) and lanes 3-8 (**Figure 4.4B**) have the strongest bands around 52 kDa and 45 kDa, containing the highest protein concentration. Both the truncated and full-length forms of SUMO-PP2Cm show weak bands around 62 kDa, but their identity is unknown.

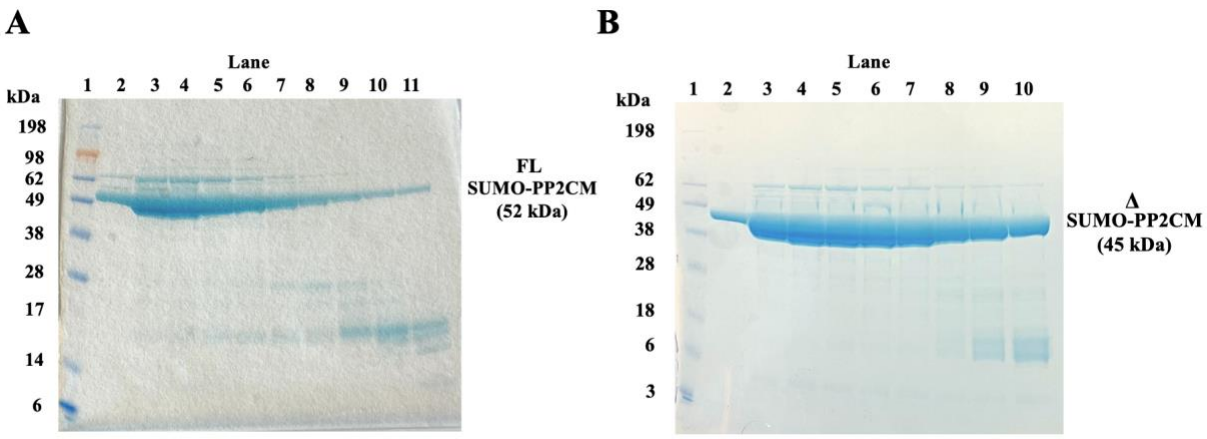

Figure 4.4. SDS-PAGE polyacrylamide gel after SEC of SUMO-PP2Cm. *Lane 1: SeeBlue Plus 2 standard (**A**)/ SeeBlue pre-stained standard [1X] (**B**). Lane 2-10/11: Protein-containing fractions from SEC. (**A**) SDS-PAGE gel of fraction A13-A23 from SEC of FL SUMO-PP2Cm. (**B**) SDS-PAGE gel of fraction A14-A23 from SEC of Δ SUMO-PP2Cm.*

No more purification was considered necessary after SEC, and the purest fractions were merged, concentrated (if needed), and used for enzymatic assay (FL SUMO-PP2Cm) or crystallization screening (Δ SUMO-PP2Cm) and stored at 4°C for further use.

SEC was also conducted to separate the digested Δ PP2Cm protein from the SUMO tag and the tagged protein. The SEC chromatogram for this is shown in **Figure 4.5**. The fusion tag has a smaller molecular weight than the protein, thus it will move into the pores of the beads in the gel filtration column, i.e., the stationary phase. The tag will move through the column by a longer path and elute later than the protein, enabling the separation of the protein from the fusion tag. Also, Δ PP2Cm has a lower molecular mass than Δ SUMO-PP2Cm and thus elutes later. Ideally, there should have been three distinct peaks in the chromatogram, representing Δ SUMO-PP2Cm, Δ PP2Cm, and the fusion tag. However, the chromatogram shows a long tail with a very small peak occurring in fractions A18-A19 and in fractions A21-A22.

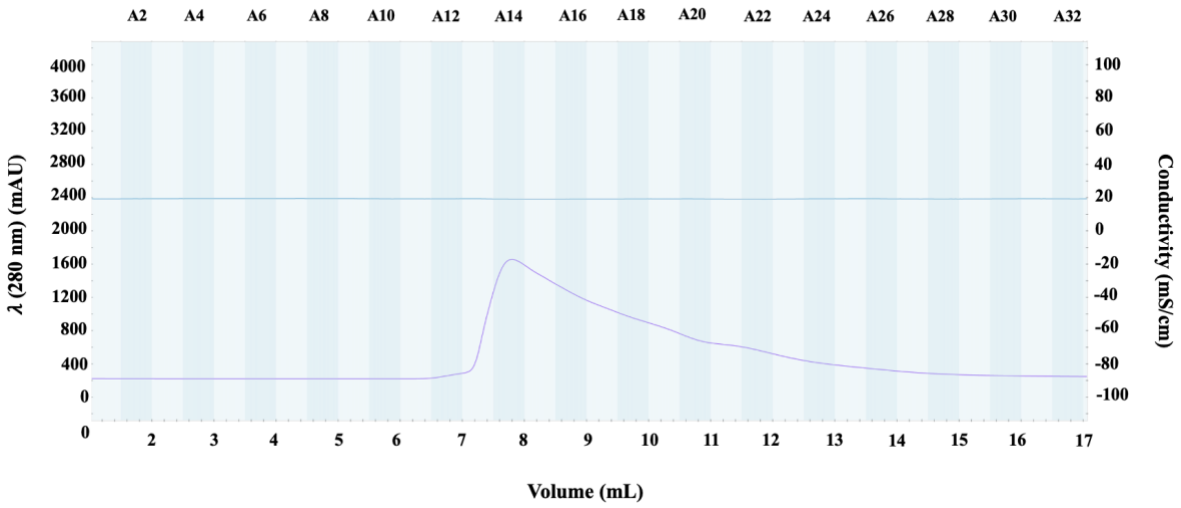

Figure 4.5. SEC chromatogram of TEV protease digested Δ SUMO-PP2Cm. *The 280 nm absorbance is shown in purple, correlating with the elution of Δ SUMO-PP2Cm, Δ PP2Cm, and the fusion tag. The proteins and the fusion tag eluted in fractions A13-A24.*

The result from SDS-PAGE of fractions A13-A22 from SEC is shown in **Figure 4.6**.

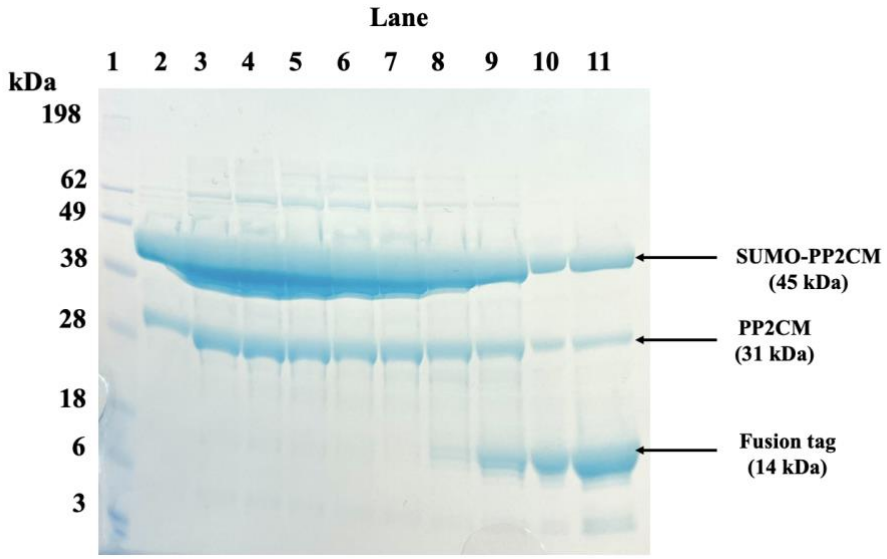

Figure 4.6. SDS-PAGE result after SEC to separate Δ PP2Cm from Δ SUMO-PP2Cm and the fusion tag*. Lane 1 was loaded with SeeBlue pre-stained standard [1X] while lane 2-11 was loaded with protein-containing fractions from SEC.*

Separation of Δ PP2Cm from Δ SUMO-PP2Cm was not successful, as the bands for both proteins appear in all the lanes of the gel (**Figure 4.6**). However, lanes 2-7 show a successful separation of the proteins from the fusion tag. Although this separation was successful, the protein solution is suboptimal for crystallization, as mixes of proteins or protein variants rarely give crystals. In addition, the Δ PP2Cm protein has a much lower protein concentration than Δ SUMO-PP2Cm, indicated by the weaker and thinner bands on the gel. Protein crystallization requires high protein concentration for crystal formation (67), thus there is a bigger chance for crystal formation using Δ SUMO-PP2Cm.

4.2 Enzymatic assay

An enzymatic dephosphorylation phosphatase activity assay was performed to assess the inhibitory and possible activating effects of the 15 compounds on SUMO-PP2Cm. The assay was conducted to determine IC_{50} values for each compound to identify the most potent compounds. The IC_{50} values were determined manually from sigmoidal dose-response curves in Origin 2023b. Four replicates were included for each compound.

4.2.1 Optimization

The assay was optimized before testing the different compounds. This was to ensure stable enzyme activity. DMSO was used to solubilize the chemicals used in the assay. Tris-HCl pH 7.5 was used to dilute the reaction mix 1 and 2. Different concentrations of $MnCl_2$ and the substrate pNPP were tested to ensure that it was not a limiting factor. These and other factors that were tested are summarized in **Table 3.1**. The final composition of the reaction mixes used in the enzymatic assay is listed in **Table 3.2**, and the concentration range of the compounds is listed in **Table 3.4** in the Materials and Methods section.

It is important to note that FL SUMO-PP2Cm has been shown to have variable activity from each purification. Therefore, the assay was performed with the same protein batch while testing all compounds.

A total of 17 compounds were ordered from HT screening. However, compounds 6 and A1 were not delivered and are thus not included in this project.

4.2.2 Dose-response analysis

An Integra plus pipetting robot was used to perform the pipetting of the different components of the assay. The usage of a robot ensures low variability, high accuracy, and lower standard deviations compared to manual pipetting. The compounds were tested in a dilution series of 22 dilutions, where every reaction had four replicates to make the results more representative.

The slope of the linear absorption change over time was calculated using the increase in absorbance, representing the rate of consumption of substrate pNPP. The raw data obtained from the enzymatic assay with one of the compounds is provided in **Supplementary Figure D1**. For generating the graphs of normalized activity (%), Origin 2023b was employed, with the compound concentrations expressed in μM. The expected outcome was to observe 100% activity at the lowest compound concentrations in the nM range, while the highest compound concentrations were expected to have 0% activity at the mM level. Determination for IC_{50} values typically involves fitting the data to a sigmoidal dose-response curve, with the IC_{50} values calculated automatically within Origin 2023b. However, in this case, the data could not fit a sigmoidal dose-response function. Thus, IC_{50} values were determined manually by approximating the concentration of the compound at which the activity of FL SUMO-PP2Cm reached a 50% inhibition level. Precipitation occurred in the wells with high compound concentrations for compounds 1, 2, 5, 10, 11, 13, and A4, therefore, the data for these concentrations were not plotted.

All results from the enzymatic assay of compounds 1-4, 5 and 7-9, 10-13, and activators 2-4 are plotted in **Figure 4.7A**, **B**, **C**, and **D**, respectively. Unfortunately, none of the results conformed to a sigmoidal dose-response function, and the representation of compound data is restricted to data points alone.

A

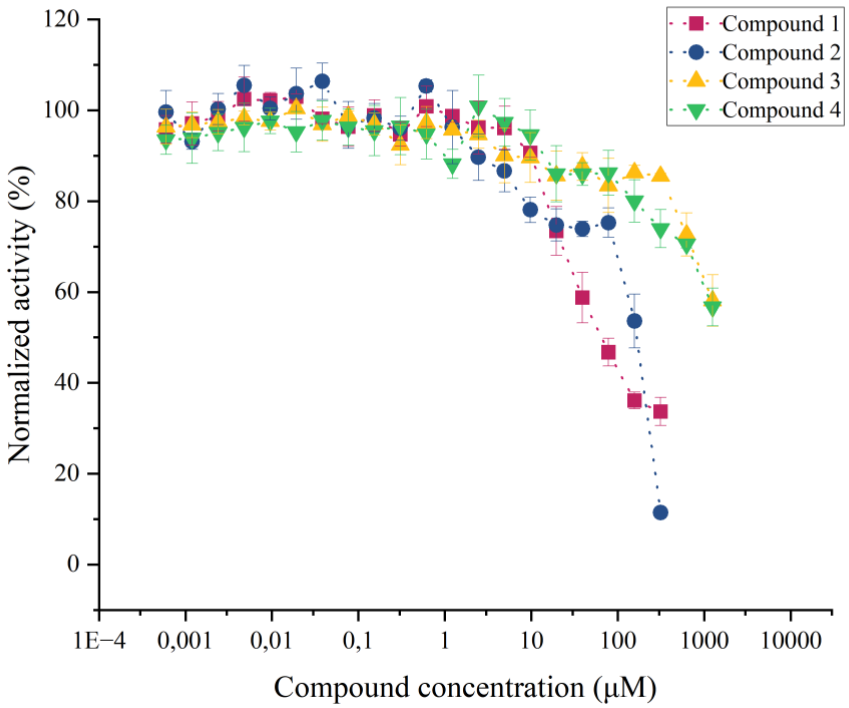
Compound 1
Compound 2
Compound 3
Compound 4
Normalized activity (%)
120
100
80
60
40
20
0
1E−4
0,001
0,01
0,1
1
10
100
1000
10000
Compound concentration (μM)

B

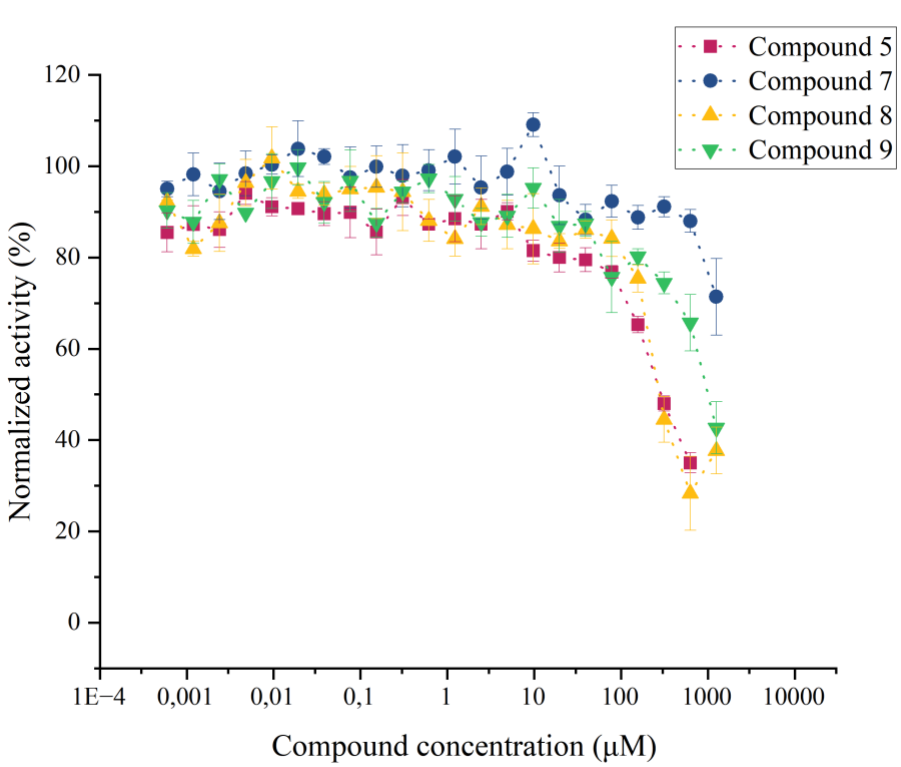
Compound 5
Compound 7
Compound 8
Compound 9
Normalized activity (%)
120
100
80
60
40
20
0
1E−4
0,001
0,01
0,1
1
10
100
1000
10000
Compound concentration (μM)

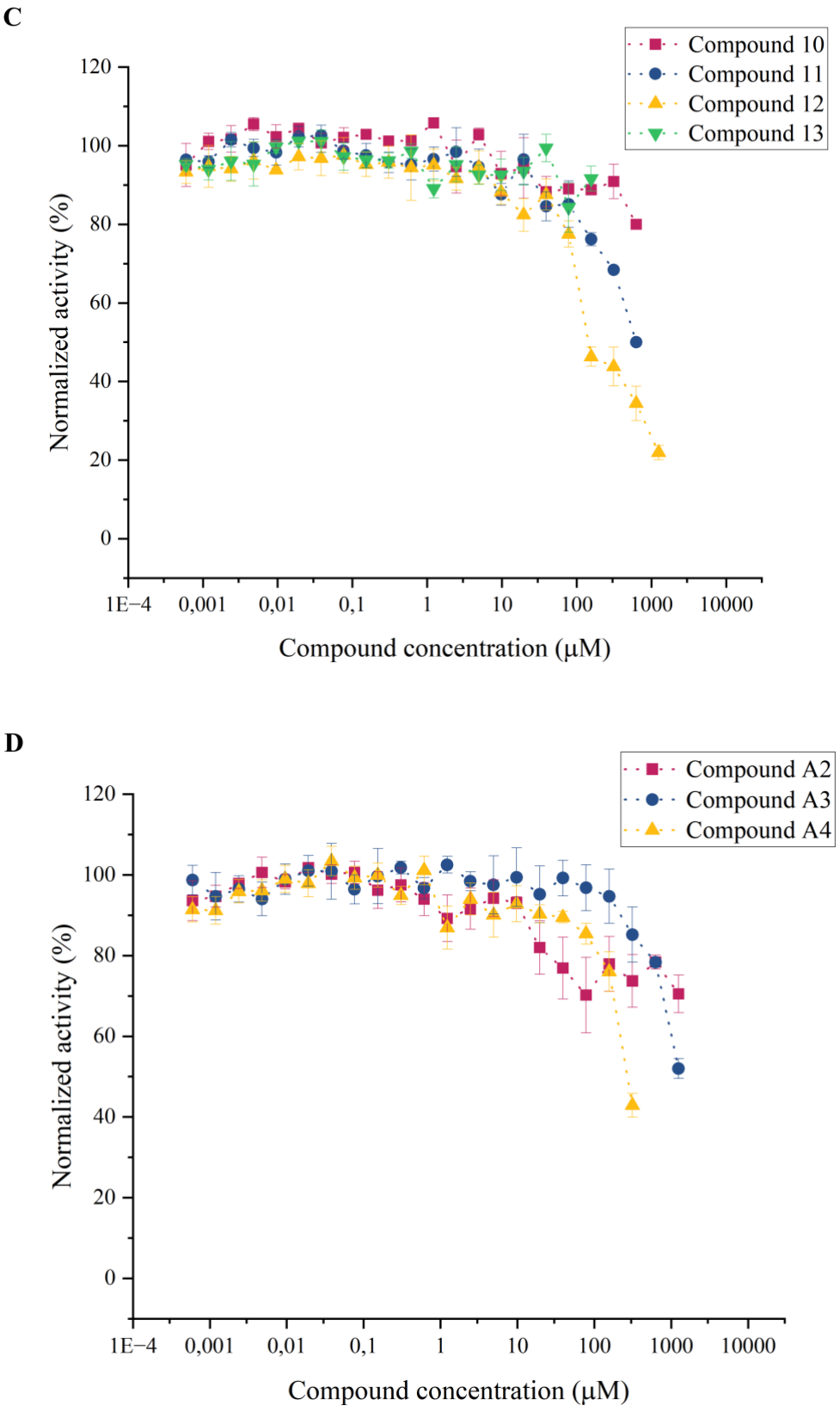

Figure 4.7. Dephosphorylation phosphatase activity assay results of FL SUMO-PP2Cm incubated with 15 compounds*. SUMO-PP2Cm incubated with compounds 1-4 (**A**), 5 and 7-9 (**B**), 10-13 (**C**), and A2-A4 (**D**).*

Normalized enzyme activity is plotted as a function of compound concentration in μM. The data is plotted with standard deviations for each concentration of the compounds.

Additionally, the determination of the IC_{50} value for all compounds proved unfeasible, as some compounds did not achieve the desired inhibition of enzyme activity to the extent of 50%. A subset of the compounds, including compounds 2, 8, and 12, demonstrated a gradual increase from around 20% to 100% in SUMO-PP2Cm activity as the compound concentration decreased, showing that the compounds were able to inhibit FL SUMO-PP2Cm activity. However, most compounds initiate at 40-60 % enzyme inhibition, with enzyme activity subsequently increasing to 100% with lower compound concentrations. This pattern was observed for compounds 3, 4, 8, 9, 11, and A4. Compounds 1, 5, and 12 inhibit enzyme activity down to 20-30%, but the goal is to achieve full inhibition of FL SUMO-PP2Cm. Among the 15 compounds studied, only compound 2 exhibited a noteworthy capability to bring the enzyme activity close to 0%, doing so at its highest concentration of 625 μM. Compounds 7, 10, and 13 were not able to inhibit FL SUMO-PP2Cm at the tested concentrations. Higher concentrations of the compounds could not be assessed due to limitations such as their solubility in DMSO or the occurrence of precipitation in the wells. Overall, high compound concentrations were required before any significant reduction in FL SUMO-PP2Cm activity was observed, making most of the compounds weak inhibitors at high concentrations, resulting in high IC_{50} values in the high μM range.

Regarding the proposed activators depicted in **Figure 4.7D**, none of these compounds exhibited the expected behavior of enhancing enzyme activity. Instead, they demonstrated weak inhibition at higher compound concentrations. In contrast to the anticipated outcome, it is evident that compounds A2-A4 are notably ineffective as activators at the tested concentrations.

4.2.3 IC_{50} determination

The IC_{50} values determined from the phosphatase activity assay are viewed in **Table 4.1**. The estimation of IC_{50} values for all compounds was performed manually by looking at the compound concentration inhibiting 50% of FL SUMO-PP2Cm activity. Standard deviations are not included for this reason.

Out of the 15 compounds, compounds 1, 2, and 12 have the lowest IC_{50} values. For the compounds that were unable to determine an IC_{50} value, the highest concentration available in 100% DMSO was not able to inhibit FL SUMO-PP2Cm activity down to more than 60-80%, thus higher concentrations could not be tested. Potential novel drug compounds should have an IC_{50} value lower than 10 μM (47). The lower the IC_{50} value, the more potent the drug. Thus, testing with higher compound concentrations for IC_{50} determination would not be reasonable with the compounds provided in this project. It is worth mentioning that all these IC_{50} values are substantially higher than the values estimated through the HT screening process. It is somewhat surprising that the IC_{50} and the inhibitory effects could not be confirmed in this project. The reason for this is not known, however, it cannot be ruled out that there are differences in the compounds between the HT screening library and the compounds we ordered. In other words, the results indicate a less favorable outcome in comparison to the initial high-throughput screening, which necessitates a closer examination of the compounds' integrity and effectiveness.

The HT screening platform provided estimated IC_{50} values for each compound. It is expected that these estimates will become more refined and accurate as the compounds undergo larger-scale testing with the target enzyme. The estimated IC_{50} values are listed in **Table 4.1** together with the IC_{50} values determined from the enzymatic assay in this project.

Table 4.1. IC_{50} values of compounds 1-5 and 7-13 for FL SUMO-PP2Cm. *The estimated IC_{50} values from the initial HT screening and the estimated IC_{50} values from the enzymatic assay in this project. All values are estimated from the sigmoidal curves of the enzymatic assay with each compound. Compounds with values shown in bold were tested in a second assay performed by manual pipetting.*

Compound	**Estimated IC_{50} (μM) from HT screening of FL SUMO-PP2Cm**	**FL SUMO-PP2Cm activity assay IC_{50} (μM)**
1	5.7	**64***
2	8.2	**162***
3	11.5	>1000
4	15	>1000
5	16.4	286*
7	22.5	>1000
8	22.7	280*
9	23	990*
10	23.5	>625
11	26.7	649*
12	33.9	**147***
13	37.8	>156

**Estimated IC_{50} value based on a manual reading of the graph.*

In addition, an assay was performed with manual pipetting of 10, 30, 60, and 75 μM compound concentration with compounds 1, 2, and 12 to investigate lower IC_{50} values. These values were chosen based on the estimated IC_{50} values from HT screening. However, none of the compounds inhibited the enzyme activity down to 50% at these concentrations, thus the IC_{50} values for compounds 2 and 12 are still above 75 μM. For compound 1, the initial assay resulted

in a lower IC_{50} value of 64 μM but based on this second assay this value cannot be trusted. The result of this assay is provided in **Supplementary Figure D3**.

After the lab work in this project finished, other people in the lab expressed FL SUMO-PP2Cm by increasing the incubation time after induction with IPTG during protein expression. Using this batch of protein, they managed to get an IC_{50} value of ~25 μM for compound 1. However, the rest of the IC_{50} values for the other compounds have not improved. A reason for the different IC_{50} values of compound 1 can be the variability in FL SUMO-PP2Cm activity from batch to batch. This can also explain the much higher IC_{50} values compared to the estimated values from HT screening.

4.3 Crystallization

Crystallization was performed with the aim of obtaining a 3D structure of Δ PP2Cm and to further co-crystallize PP2Cm with the different compounds to investigate binding properties in the active site of PP2Cm. Earlier publications show that the full-length human SUMO-PP2Cm are resistant to crystallization, thus a truncated variant where flexible segments of amino acids are deleted from the protein construct was used. In addition, the published structure of PP2Cm with intact SUMO tag contains holes at the site where the SUMO tag resides (14). Thus, we wanted to crystallize PP2Cm without SUMO. Δ SUMO-PP2Cm was digested with TEV protease to remove the fusion tag, but the separation of Δ PP2Cm from Δ SUMO-PP2Cm was unsuccessful (**Figure 4.6**). The Δ SUMO-PP2Cm with SUMO tag was thus used to screen crystallization conditions.

4.3.1 Crystallization screening

Three different structures of PP2Cm based on protein crystal analyses have been published at UniProt.org, in addition to a predicted structure (AlphaFold). The first structure of PP2Cm was published in 2006 with 274 amino acids and one Mg^{2+} ligand bound in the active site (97). However, the article did not include the crystallization conditions. A more recent structure was released in 2019, with a diffraction resolution of 2.60 Å. The article detailing this structure has not been published, and the crystallization conditions remain undisclosed. The third structure

was published back in 2012, where Mg^{2+} and β-ME are bound in the active site. This structure was obtained from PP2Cm with SUMO tag because it confers solubility on the protein (14). The conditions for hanging drop vapor diffusion, as outlined in this article, were tested in this master project to obtain crystals. The conditions are listed in **Table 3.5** under the Materials and Methods section.

In addition, a screening of crystallization conditions was tested with different crystallization kits. Unfortunately, crystallization conditions were not identified as no crystals were formed during this project. One reason may be the attached fusion tag, or because of the removal of flexible segments of amino acids. As no crystals of Δ SUMO-PP2Cm were formed, co-crystallization with compounds was not attempted. Without crystals, X-ray diffraction cannot be performed, thus structural analyses were excluded from the project.

4.4 Cellular testing of compounds

Even though the enzymatic assay resulted in high IC_{50} values, it is still interesting to test the compounds in cells to investigate the compound's cytotoxicity in a biological model. PANC-1 cells were used because of the overexpression and important function of branched-chain amino acid (BCAA) metabolic enzymes in these cells (31). These cells are important in the tumor microenvironment in pancreatic cancer, making them important target cells to combat PDAC. The most interesting compounds are the ones with cytotoxicity towards PANC-1 cells. The compounds are assumed to influence the cells based on their IC_{50} values. Lower IC_{50} values suggest a stronger inhibitory effect on the cells.

A Presto Blue assay was conducted on PANC-1 cells to investigate cell viability when exposed to compounds. To calculate the viability of the cells, the absorbance of treated cells relative to non-treated cells was plotted as a function of increasing compound concentration. As for the determination of the compound's IC_{50} values, the Origin software was used to plot the data with sigmoidal dose-response functions to determine LD_{50} values. However, the data could not be fitted with a dose-response function, and manual reading of the graphs was used to determine

the approximate LD_{50}, defined as 50% of the remaining signal relative to mock. All compounds were tested with four replicates and the results shown represent the average. Ideally, these experiments should have been repeated ($n \geq 3$) to calculate an average LD_{50} value with an estimate of experimental variation. However, only one experiment was executed with all compounds due to time limitations. Some of the compounds reduced cell viability by 100% even at the lowest concentration in the initial run, thus these compounds were tested again at lower concentrations.

Branched-chain keto acids accumulate upstream of the BCKDH complex, and increased secretion of BCKA is known from MSUD, caused by a low activity of BCKDH (38). To evaluate whether extracellular BCKA is affected by the inhibitors, a BCKA assay was conducted to investigate the compound's effect *in vivo*. For each compound, one well was supplemented with LDH, and one was not. A control without LDH was included to look at the level of keto acids with NADH when LDH is not present to consume NADH. Thus, the difference in absorbance between non-LDH-containing samples and LDH-containing samples was plotted with the control to compare the level of keto acids.

4.4.1 Compound sensitivity for PANC-1 cells

PANC-1 cells were tested for compound sensitivity by determining the cell viability of exposed cells with the Presto Blue assay. The results for each compound of the assay are plotted in **Figure 4.8A-D**. Some of the compounds exhibit an impact on cell viability more than others, which is especially seen for compounds 1, 2, and 13, being the most cytotoxic and interesting inhibitors. Among the compounds, the most intriguing ones are those that demonstrate the highest cytotoxicity against PANC-1 cells. Compounds 1 and 2 are highly cytotoxic and kill all cells at all tested concentrations, while compounds 4 and A2 are the least cytotoxic, where LD_{50} values could not be determined as they did reduce viability down to 50%. Other interesting compounds are compounds 5-9 (**Figure 4.8B**) which all affect the cell viability in full range from 0-100% at the tested concentrations. In general, compounds 3, 5-9, and 10-12 show a dose-response effect. Compound A3 shows low cytotoxicity only affecting the viability at its highest concentrations. The graph for compound 3 shows a decreased viability at the lowest compound concentration compared to the second lowest compound concentration, which is likely due to an experimental error. This can also apply to compounds 13, A2, A3, and A4.

A

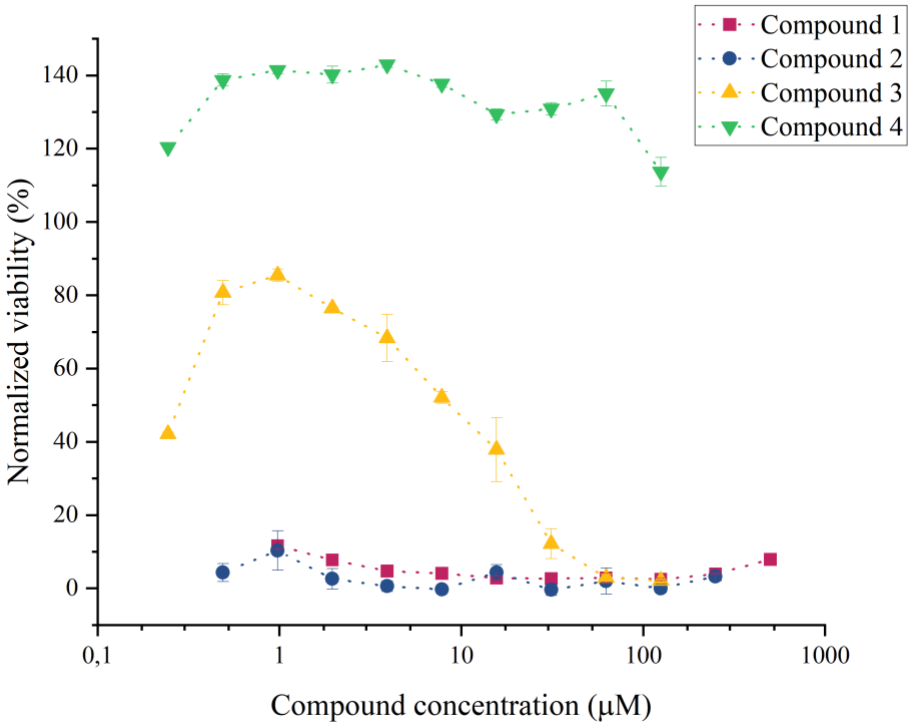
Compound 1
Compound 2
Compound 3
Compound 4
Normalized viability (%)
140
120
100
80
60
40
20
0
0,1
1
10
100
1000
Compound concentration (µM)

B

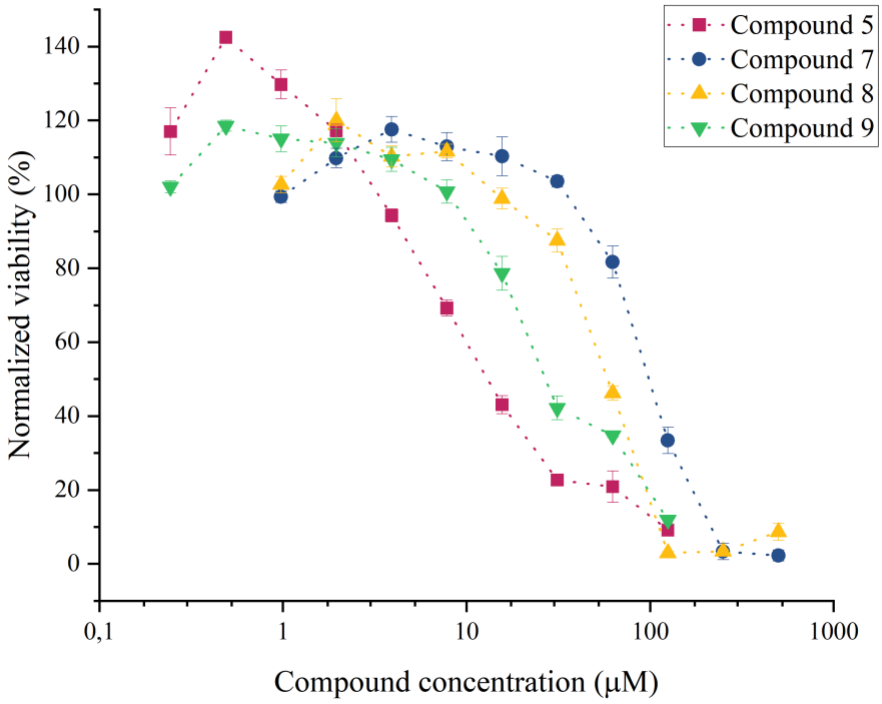
Compound 5
Compound 7
Compound 8
Compound 9
Normalized viability (%)
140
120
100
80
60
40
20
0
0,1
1
10
100
1000
Compound concentration (µM)

C

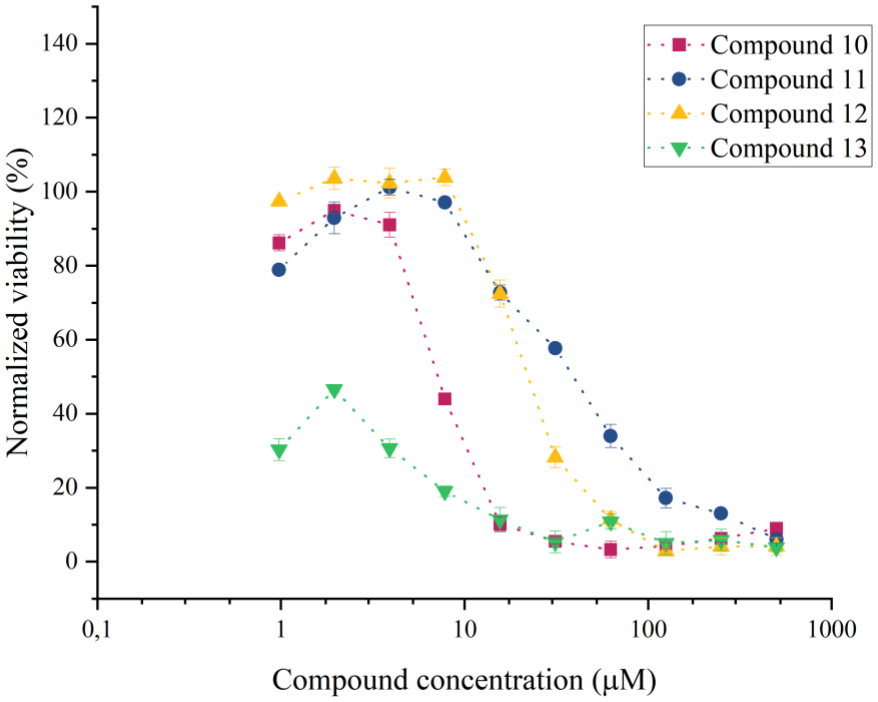

D

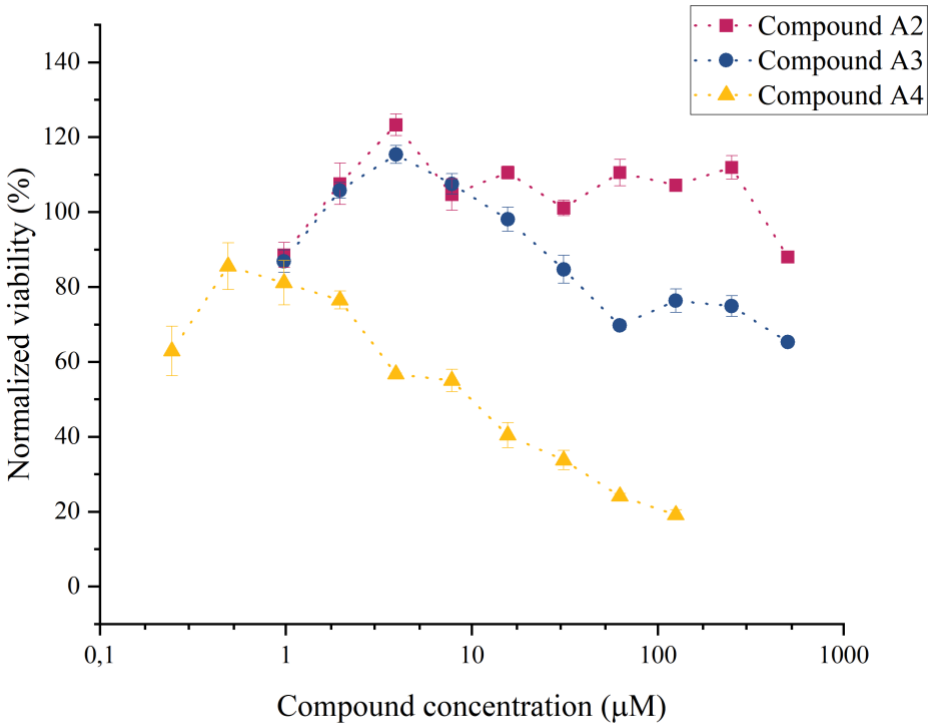

Figure 4.8. Presto Blue cell viability assay results for PANC-1 cells incubated with compounds 1-5, 7-13, and A2-A4. *The graphs illustrate the normalized viability (%) of PANC-1 cells with standard deviations, plotted on a*

*logarithmic scale depicting increasing compound concentration. The compounds are shown in figure panels: (**A**) Compounds 1-4, (**B**) compounds 5-9, (**C**) compounds 10-13, (**D**) compounds A2-A4.*

Due to the pronounced cytotoxicity of compounds 1 and 2 observed at the initial tested concentrations, a subsequent assay was conducted with these compounds at lower concentrations. The results of the subsequent assay are presented in **Figure 4.9A**. Notably, both compounds 1 and 2 demonstrated substantial cytotoxicity at the highest concentrations tested, affecting 90-100% of the cells, while the second highest concentration yielded a 90% viability rate. **Figure 4.9B** displays the combined data from **Figure 4.8A** and **Figure 4.9A**, with the omission of two data points pertaining to the lowest concentration. These combined data clearly show a sigmoidal dose-response curve. Remarkably, the graph exhibits a steep decline in viability from approximately 90% down to 10-20%, suggesting that further testing of concentrations within this range would be needed for a more precise determination of LD_{50}. Due to time limitations, this additional analysis was not pursued.

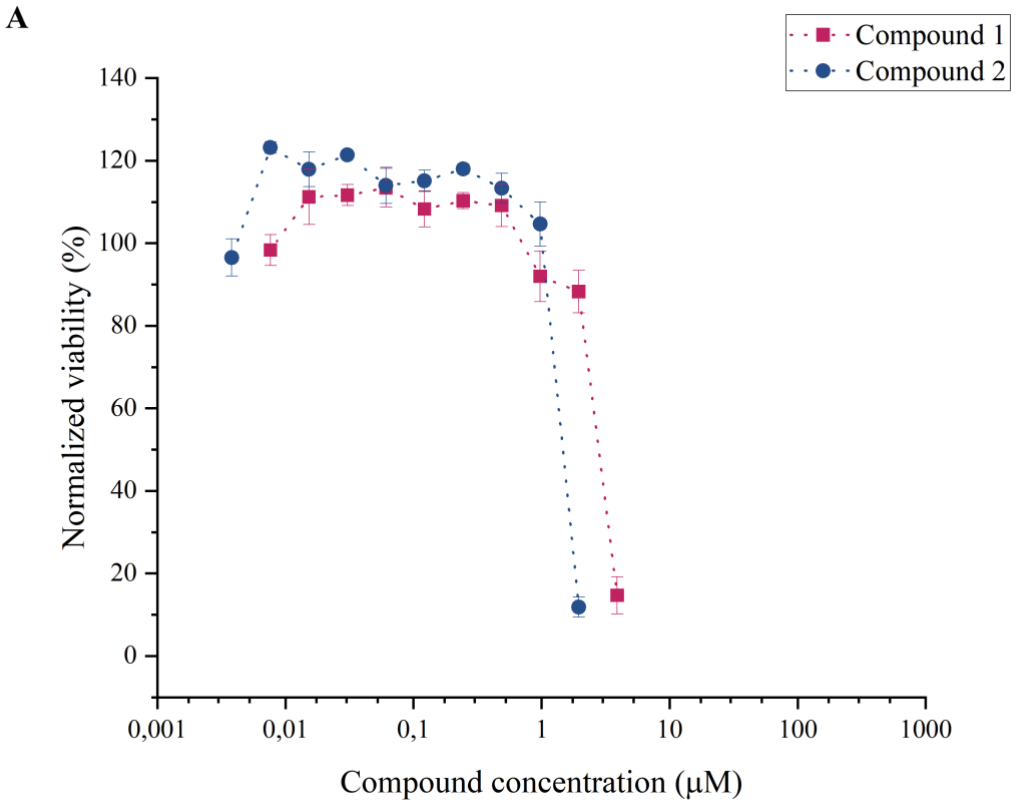

B

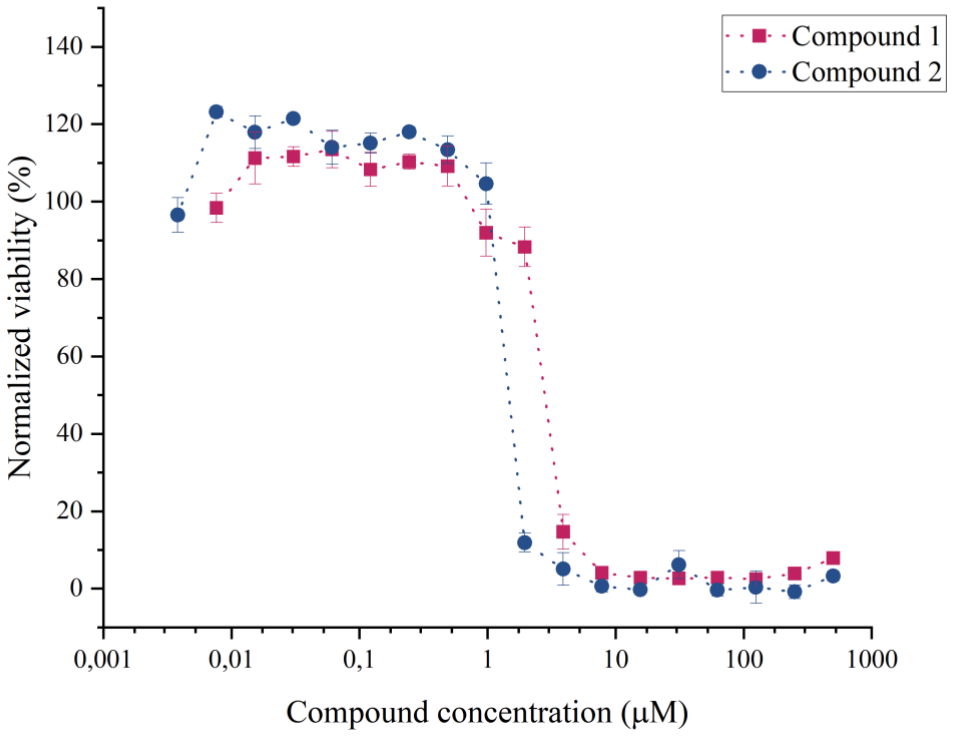

Figure 4.9. Presto Blue assay result for PANC-1 cells incubated with compounds 1 and 2*. (**A**) Subsequent assay with lower concentrations of compounds 1 and 2 compared to the initial assay. (**B**) The initial result of compounds 1 and 2 plotted with the result of the subsequent assay with lower compound concentrations. The data is plotted with standard deviations.*

4.4.2 LD_{50} determination

The LD_{50} values were estimated manually by reading the graph at 50% cell viability. The resulting LD_{50} values obtained from the Presto Blue assay are summarized in **Table 4.2**. Standard deviations are not included because of manual reading of the LD_{50} determination.

Table 4.2. LD_{50} values of compounds 1-13 and activators A2-A4 for SUMO-PP2cm. *All values are estimated from the sigmoidal curves of the Presto Blue assay with each compound. Compounds with values shown in bold were tested in a second assay with lower compound concentrations.*

Compound	**SUMO-PP2Cm LD_{50} (μM)**
1	**3***
2	**2***
3	9*
4	>125
5	13*
7	98*
8	59*
9	27*
10	7*
11	39*
12	22*
13	< 2
A2	>500
A3	>500
A4	10*

**Estimated LD_{50} value based on a manual reading of the graph.*

Among the compounds giving LD_{50} values, compounds 1, 2, and 13 are the most interesting compounds with LD_{50} values of 3 μM**,** 2 μM, and < 2 μM, respectively. Other compounds with

LD_{50} values below 20 μM are compounds 3, 5, 10, 13, and A4. Compounds 4, A2, and A3 exhibit the lowest cytotoxicity, and LD_{50} values could not be determined as they did not reduce viability to below 50%. In general, the estimated LD_{50} values are lower than the IC_{50} values obtained from the enzymatic assay.

It would be interesting to evaluate the compounds on different cell lines, for example, fibroblast cells as a control. This could provide information on whether the observed cytotoxicity is caused by PP2Cm inhibition or off-target effects. The most interesting compounds would have been the ones that show high cytotoxicity to PANC-1 cells and low cytotoxicity to fibroblast cells. However, as the IC_{50} values are much higher than the LD_{50} values for the best compounds, the cause of toxicity is likely to be other than PP2Cm inhibition. When IC_{50} values exceed the concentration required to reduce cell viability to 50%, the inhibition of PP2Cm will not be efficient at a level where cells are still alive. It can also imply that off-target effects on other proteins in the cancer cells are responsible for the toxicity. Further, a lower IC_{50} value than LD_{50} value is desirable because the opposite may inflict challenges.

4.4.3 Compound effect *in vivo*

The BCKA assay was conducted to investigate the compound's effect *in vivo*. The BCKA assay uses the activity of the LDH enzyme to measure the level of extracellular BCKA secreted by compound-incubated PANC-1 cells in the cell media. BCKAs, like α-KIC can be converted to L-Leucine by LDH in the presence of NH_4^+ and NADH, causing stoichiometric oxidation of NADH (**Figure 1.7**)(81). Thus, NADH and NH_4^+ are supplied to all samples in the assay, together with LDH added to half of the samples, leaving the other half as a control without LDH. Increased BCKA levels will lead to a decreasing level of NADH that can be measured spectrophotometrically with both fluorescence and absorbance. In this project, measuring absorbance gave more stable standard curves than for fluorescence, thus the final assay was measured by absorbance and is included in the result.

The potential activators, A2-A4, were excluded from this assay due to their weak inhibition of SUMO-PP2Cm. Although compounds 3, 4, 7, 10, and 13 also displayed weak inhibition of SUMO-PP2Cm, they were included for comparison with the control. PANC-1 cells were

exposed to 100 μM of compounds 3-13, and 1 μM of compounds 1 and 2 due to their higher cytotoxicity. However, it became evident that most compounds exhibited high cytotoxicity after analyzing the Presto Blue assay, indicating that lower concentrations should have been used for all compounds, except for compound 4. Conversely, the results from the enzymatic assay indicated a requirement for higher compound concentrations for effective PP2Cm inhibition. Ideally, this assay should have been performed with compounds with lower IC_{50} and higher LD_{50} values than observed in this project.

One can determine BCKA production from the measured absorbance by looking at the standard curve. The standard curve was established for one set of 25, 100, and 400 μM of KICA in DMEM. In addition, a blank sample (0) with DMEM is included to look at the absorbance of DMEM supplied with NADH, ammonium, and LDH to ensure no signals with no KICA present in the sample. **Figure 4.10A** shows the result from the standard curve. Enzymatic conversion of α-KIC by LDH was completed after 14 min, and the difference in absorbance of the sample without and with LDH at 30 minutes provides the signal for KICA concentration. The difference in absorbance is plotted against KICA concentration. Notably, the measurement for 100 μM KICA appears to be out of the linear relationship and thereby causes a shift in the trendline. Since the absorbance equivalent to 0 μM KICA is 0.122, all values above this are quantified with a small margin of error. The rate of increase is 0.0033 and can be used as concentration dependency, however, due to variation in the standard curve the absolute values should be taken into account at low concentrations.

Figure 4.10B presents the difference in absorbance for cells incubated with 1 μM of compounds 1 and 2, together with nontreated cells (control). The difference in absorbance with and without LDH is 0.141 for non-treated cells. This value is 0.019 higher than the absorbance for 0 μM KICA and is equivalent to α-KIC concentration of ~ 6 μM when accounting for the rate of increase. Cells exposed to compounds 1 and 2 show a remaining absorbance difference of 0.056 and 0.231, respectively, implying less BCKA secretion in the compound 1 exposed cells, and increased BCKA secretion in cells exposed to compound 2. An absorbance difference of 0.231 is equivalent to ~ 33 μM KICA according to the standard curve. Compounds 3-13 are presented in **Figure 4.10C**. These compounds collectively exhibit less BCKA secretion in comparison to

the control, and compounds 4, 5, 7, 8, 9, 10, and 13 even display negative values between 0 and -0.25. The negative values may be attributed to cell death resulting from too high compound concentrations. Moreover, the assay should be tested for counteractivity to investigate if the compounds affect the activity of LDH.

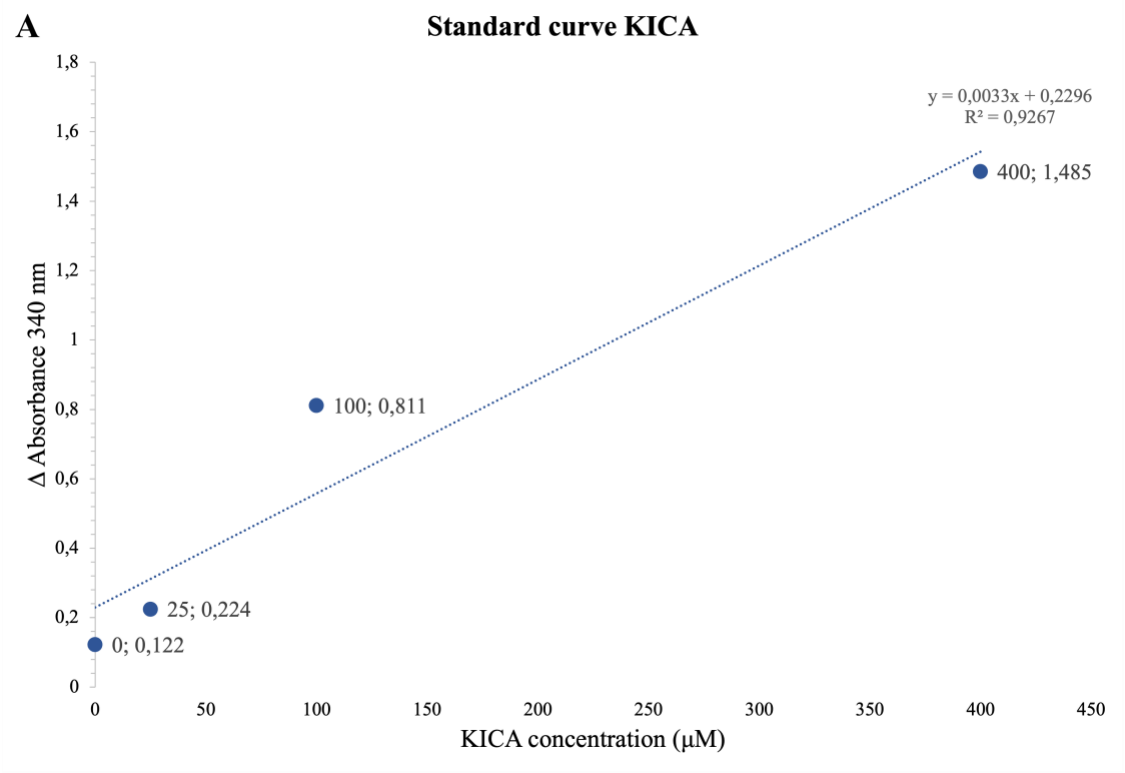

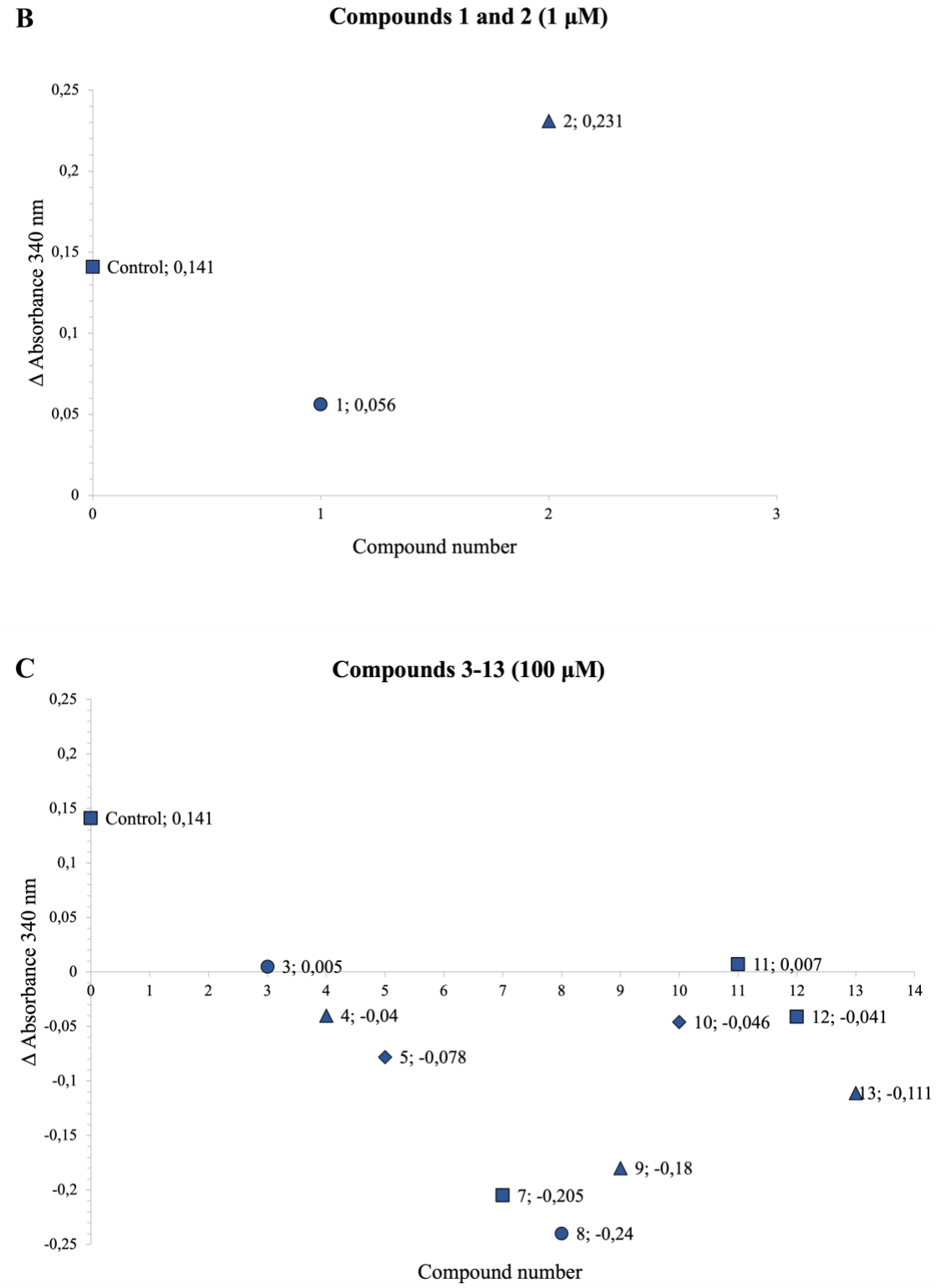

Figure 4.10. Result of BCKA assay with compounds 1-5 and 7-13, including standard curves and control. *(A) Standard curve for conversion of 25, 100, and 400 µM KICA in DMEM. (**B**) The difference in absorbance between samples with and without LDH of cells incubated with 1 µM of compounds 1 and 2. The control (non-treated cells)*

*is included for comparison. (**C**) The difference in absorbance between samples with and without LDH of cells incubated with 100 μM of compounds 3-13.*

Overall, the testing revealed that cells exposed to the compounds secreted less BCKAs than the control cells, which runs contrary to the expected behavior of a potent PP2Cm inhibitor. The samples containing LDH were expected to convert NADH to NAD^+ with a decrease in absorbance compared to control samples without LDH, given that the cells secreted BCKAs as a consequence of PP2Cm inhibition. Except for compound 2, the result does not imply that the cells have increased secretion of BCKAs since samples containing a compound show lower or negative differences in absorbance than the control sample. There are several reasons why an expected decrease in absorbance was not observed. One reason for a non-decreasing absorbance of NADH can be that the assay is not sufficiently optimized, or that the inhibitors are not reaching the target enzyme inside the mitochondria. Also, the amount of produced and secreted α-KIC as a consequence of PP2Cm inhibition might be below the detection limit for the assay. The experiment was conducted in a volume of 200 μL with approximately 50 000 cells/well, which may be a limiting factor. Upon examination of the standard curves, it becomes evident that a minimum secretion of approximately 25-100 μM BCKA by the cells is required for accurate measurement through absorbance. Hence, it would be advisable to optimize the assay for fluorescence, given its heightened sensitivity for NADH detection. In addition, an LDH counter assay should be conducted to investigate the counteractivity of the compounds. Given that there is at best a weak signal from the samples containing compounds, it becomes apparent that the assay in its current form is not suitable for measuring the *in vivo* effect of these compounds. Another more elaborate assay, e.g., by using ^{14}C isotopically labeled leucine as substrate and tracing the radioactive product, one could possibly detect PP2Cm inhibition *in vivo*.

5 CONCLUSION AND FUTURE ASPECTS

During this project, a total of 15 compounds have been validated in their ability to inhibit or activate the SUMO-PP2Cm enzyme. The validation involved determining enzymatic IC_{50} values and conducting LD_{50} analyses with the PANC-1 cell line. Additionally, an assay measuring the intracellular activity of PP2Cm was conducted.

The enzymatic assay was established to assess the effect of the different compounds on enzyme activity within a biochemical system. The determination of IC_{50} involved manual reading of the graphs at which enzyme activity was inhibited by 50%. Notably, several compounds did not achieve the desired 50% inhibition of enzyme activity, which was observed with compounds 3, 4, 7, 10, 13, A2, and A3. Compound 1 emerged as the most effective inhibitor with an IC_{50} value of approximately 64 μM. Generally, IC_{50} values for most compounds were much above 100 μM. Subsequently, all compounds were employed in cell cytotoxicity analyses to determine the LD_{50} values of each compound. Most of the compounds displayed pronounced cytotoxicity toward PANC-1 cells, with compounds 1, 2, 3, 5, 10, 13, and A4 demonstrating LD_{50} values below 20 μM. However, the high cytotoxicity may be due to off-target effects. In contrast, compounds 4, A2, and A3 exhibited minimal cytotoxicity, to the extent that their LD_{50} values could not be determined as they did not influence cell viability down to 50%. An additional cell-based assay was implemented to assess the intracellular effect of the compounds. The results revealed an overall decrease in BCKA secretion compared to the control, which is the opposite of the expected behavior of a potent PP2Cm inhibitor. However, cells incubated with compound 2 were the only sample showing increased BCKA secretion, indicating off-target effects of the other compounds, counteractivity, or too high cytotoxicity. However, this assay and our preliminary results should be fully optimized to be employed to determine the effects of the compounds *in vivo*, as the assay could provide vital information about *in vivo* inhibition of PP2Cm.

In future research, it would be advantageous to establish a protein expression protocol that ensures consistent enzyme activity across different protein batches. Furthermore, the IC_{50} and the inhibitory effects of the compounds could not be confirmed in this project. It cannot be ruled out that there are differences in the compounds between the HT screening library and the compounds we ordered, thus the quality of our compounds should be investigated. The findings of this project provide valuable insights for advancing the research on identifying and designing compounds with inhibitory effects at a low μM scale. The pursuit of more effective inhibitors is of interest, and testing analogs of the most potent compounds may lead to the discovery of new compounds with improved IC_{50} and LD_{50} values. Future research should include testing all compounds against control fibroblasts and other cell lines derived from pancreatic cancer to determine their toxicity profiles. Additionally, it is essential to explore potential off-target effects for all compounds. In terms of structural analyses, there is a need to screen SUMO-PP2Cm against various crystallization conditions using different crystallization kits. Also, other variants (truncations or other fusions) of PP2Cm should be tested to find good and reproducible crystallization conditions. Obtaining crystals of truncated PP2Cm without the SUMO tag for a deeper investigation of protein structure and potential co-crystallization with inhibitory compounds is of interest.

Finally, it would be valuable to assess the binding affinities of all compounds, employing techniques such as MicroScale Thermophoresis (MST), surface plasmon resonance (SPR), and bio-layer interferometry (BLI). Such experiments could support the notion that we indeed have identified a set of PP2Cm binding molecules, despite the deviating results between the HTS assay and the targeted assay in this thesis.

BIBLIOGRAPHY

1. Wu G. **Amino acids: metabolism, functions, and nutrition**. Amino Acids. 2009;37(1):1-17.
2. Neinast M, Murashige D, Arany Z. **Branched Chain Amino Acids**. Annu Rev Physiol. 2019;81:139-64.
3. Nie C, He T, Zhang W, Zhang G, Ma X. **Branched Chain Amino Acids: Beyond Nutrition Metabolism**. Int J Mol Sci. 2018;19(4).
4. Hutson SM, Sweatt AJ, Lanoue KF. **Branched-chain amino acid metabolism: implications for establishing safe intakes**. J Nutr. 2005;135(6 Suppl):1557s-64s.
5. Du C, Liu WJ, Yang J, Zhao SS, Liu HX. **The Role of Branched-Chain Amino Acids and Branched-Chain α-Keto Acid Dehydrogenase Kinase in Metabolic Disorders**. Front Nutr. 2022;9:932670.
6. Holeček M. **Branched-chain amino acids in health and disease: metabolism, alterations in blood plasma, and as supplements**. Nutrition & Metabolism. 2018;15(1):33.
7. Mayers JR, Torrence ME, Danai LV, Papagiannakopoulos T, Davidson SM, Bauer MR, et al. **Tissue of origin dictates branched-chain amino acid metabolism in mutant Kras-driven cancers**. Science. 2016;353(6304):1161-5.
8. White PJ, Lapworth AL, An J, Wang L, McGarrah RW, Stevens RD, et al. **Branched-chain amino acid restriction in Zucker-fatty rats improves muscle insulin sensitivity by enhancing efficiency of fatty acid oxidation and acyl-glycine export**. Mol Metab. 2016;5(7):538-51.
9. Lotta LA, Scott RA, Sharp SJ, Burgess S, Luan J, Tillin T, et al. **Genetic Predisposition to an Impaired Metabolism of the Branched-Chain Amino Acids and Risk of Type 2 Diabetes: A Mendelian Randomisation Analysis**. PLoS Med. 2016;13(11):e1002179.
10. Manoli I, Venditti CP. **Disorders of branched chain amino acid metabolism**. Transl Sci Rare Dis. 2016;1(2):91-110.
11. Chuang JL, Davie JR, Chinsky JM, Wynn RM, Cox RP, Chuang DT. **Molecular and biochemical basis of intermediate maple syrup urine disease. Occurrence of homozygous G245R and F364C mutations at the E1 alpha locus of Hispanic-Mexican patients**. J Clin Invest. 1995;95(3):954-63.
12. Lu G, Sun H, She P, Youn JY, Warburton S, Ping P, et al. **Protein phosphatase 2Cm is a critical regulator of branched-chain amino acid catabolism in mice and cultured cells**. J Clin Invest. 2009;119(6):1678-87.
13. Mann G, Mora S, Madu G, Adegoke OAJ. **Branched-chain Amino Acids: Catabolism in Skeletal Muscle and Implications for Muscle and Whole-body Metabolism**. Front Physiol. 2021;12:702826.
14. Wynn RM, Li J, Brautigam CA, Chuang JL, Chuang DT. **Structural and biochemical characterization of human mitochondrial branched-chain alpha-ketoacid dehydrogenase phosphatase**. J Biol Chem. 2012;287(12):9178-92.
15. Lu G, Sun H, Korge P, Koehler CM, Weiss JN, Wang Y. **Functional characterization of a mitochondrial Ser/Thr protein phosphatase in cell death regulation**. Methods Enzymol. 2009;457:255-73.
16. Pan BF, Gao C, Ren SX, Wang YB, Sun HP, Zhou MY. **Regulation of PP2Cm expression by miRNA-204/211 and miRNA-22 in mouse and human cells.** Acta Pharmacol Sin. 2015;36(12):1480-6.

17. Lu G, Ren S, Korge P, Choi J, Dong Y, Weiss J, et al. **A novel mitochondrial matrix serine/threonine protein phosphatase regulates the mitochondria permeability transition pore and is essential for cellular survival and development**. Genes Dev. 2007;21(7):784-96.
18. Lian K, Guo X, Wang Q, Liu Y, Wang RT, Gao C, et al. **PP2Cm overexpression alleviates MI/R injury mediated by a BCAA catabolism defect and oxidative stress in diabetic mice**. Eur J Pharmacol. 2020;866:172796.
19. Lian K, Du C, Liu Y, Zhu D, Yan W, Zhang H, et al. **Impaired adiponectin signaling contributes to disturbed catabolism of branched-chain amino acids in diabetic mice. Diabetes**. 2015;64(1):49-59.
20. Lu G, Wang Y. **Functional diversity of mammalian type 2C protein phosphatase isoforms: new tales from an old family**. Clin Exp Pharmacol Physiol. 2008;35(2):107-12.
21. Dolatabad MR, Guo LL, Xiao P, Zhu Z, He QT, Yang DX, et al. **Crystal structure and catalytic activity of the PPM1K N94K mutant.** J Neurochem. 2019;148(4):550-60.
22. Liu Y, Sun Y, Guo Y, Shi X, Chen X, Feng W, et al. An Overview: **The Diversified Role of Mitochondria in Cancer Metabolism**. Int J Biol Sci. 2023;19(3):897-915.
23. Lieu EL, Nguyen T, Rhyne S, Kim J. **Amino acids in cancer**. Exp Mol Med. 2020;52(1):15-30.
24. Ananieva EA, Wilkinson AC. **Branched-chain amino acid metabolism in cancer**. Curr Opin Clin Nutr Metab Care. 2018;21(1):64-70.
25. Joyce C, Rayi A, Kasi A. **Tumor-Suppressor Genes**. StatPearls. Treasure Island (FL): StatPearls Publishing Copyright © 2023, StatPearls Publishing LLC.; 2023.
26. Yao CC, Sun RM, Yang Y, Zhou HY, Meng ZW, Chi R, et al. **Accumulation of branched-chain amino acids reprograms glucose metabolism in CD8(+) T cells with enhanced effector function and anti-tumor response**. Cell Rep. 2023;42(3):112186.
27. Ilic M, Ilic I. **Epidemiology of pancreatic cancer**. World J Gastroenterol. 2016;22(44):9694-705.
28. Chen Q, Pu N, Yin H, Zhang J, Zhao G, Lou W, et al. **A metabolism-relevant signature as a predictor for prognosis and therapeutic response in pancreatic cancer**. Exp Biol Med (Maywood). 2022;247(2):120-30.
29. Rawla P, Sunkara T, Gaduputi V. **Epidemiology of Pancreatic Cancer: Global Trends, Etiology and Risk Factors**. World J Oncol. 2019;10(1):10-27.
30. Geng Y, Guan R, Hong W, Huang B, Liu P, Guo X, et al. I**dentification of m6A-related genes and m6A RNA methylation regulators in pancreatic cancer and their association with survival.** Ann Transl Med. 2020;8(6):387.
31. Zhu Z, Achreja A, Meurs N, Animasahun O, Owen S, Mittal A, et al. **Tumour-reprogrammed stromal BCAT1 fuels branched-chain ketoacid dependency in stromal-rich PDAC tumours**. Nat Metab. 2020;2(8):775-92.
32. Kurmi K, Haigis MC. **Nitrogen Metabolism in Cancer and Immunity**. Trends Cell Biol. 2020;30(5):408-24.
33. Nong X, Zhang C, Wang J, Ding P, Ji G, Wu T. **The mechanism of branched-chain amino acid transferases in different diseases: Research progress and future prospects**. Front Oncol. 2022;12:988290.
34. Lee JH, Cho YR, Kim JH, Kim J, Nam HY, Kim SW, et al. **Branched-chain amino acids sustain pancreatic cancer growth by regulating lipid metabolism**. Exp Mol Med. 2019;51(11):1-11.

35. Blackburn PR, Gass JM, Vairo FPE, Farnham KM, Atwal HK, Macklin S, et al. **Maple syrup urine disease: mechanisms and management**. Appl Clin Genet. 2017;10:57-66.
36. Ozcelik F, Arslan S, Ozguc Caliskan B, Kardas F, Ozkul Y, Dundar M. **PPM1K defects cause mild maple syrup urine disease: The second case in the literature**. Am J Med Genet A. 2023;191(5):1360-5.
37. Strauss KA, Carson VJ, Soltys K, Young ME, Bowser LE, Puffenberger EG, et al. **Branched-chain α-ketoacid dehydrogenase deficiency (maple syrup urine disease): Treatment, biomarkers, and outcomes**. Mol Genet Metab. 2020;129(3):193-206.
38. Xu J, Jakher Y, Ahrens-Nicklas RC. **Brain Branched-Chain Amino Acids in Maple Syrup Urine Disease: Implications for Neurological Disorders**. Int J Mol Sci. 2020;21(20).
39. Sun R, Liu M, Lu L, Zheng Y, Zhang P. **Congenital Heart Disease: Causes, Diagnosis, Symptoms, and Treatments**. Cell Biochem Biophys. 2015;72(3):857-60.
40. Wu W, He J, Shao X. **Incidence and mortality trend of congenital heart disease at the global, regional, and national level, 1990-2017**. Medicine (Baltimore). 2020;99(23):e20593.
41. Sun H, Lu G, Ren S, Chen J, Wang Y. **Catabolism of branched-chain amino acids in heart failure: insights from genetic models**. Pediatr Cardiol. 2011;32(3):305-10.
42. Zhou SF, Zhong WZ. **Drug Design and Discovery: Principles and Applications.** Molecules. 2017;22(2).
43. Berdigaliyev N, Aljofan M. **An overview of drug discovery and development**. Future Med Chem. 2020;12(10):939-47.
44. Ferreira LG, Dos Santos RN, Oliva G, Andricopulo AD. **Molecular docking and structure-based drug design strategies**. Molecules. 2015;20(7):13384-421.
45. Tang Y, Zhu W, Chen K, Jiang H. **New technologies in computer-aided drug design: Toward target identification and new chemical entity discovery**. Drug Discov Today Technol. 2006;3(3):307-13.
46. Doytchinova I. **Drug Design-Past, Present, Future**. Molecules. 2022;27(5).
47. Hughes JP, Rees S, Kalindjian SB, Philpott KL. **Principles of early drug discovery**. Br J Pharmacol. 2011;162(6):1239-49.
48. Anderson AC. **The process of structure-based drug design**. Chem Biol. 2003;10(9):787-97.
49. Chen D, An X, Ouyang X, Cai J, Zhou D, Li QX. **In Vivo Pharmacology Models for Cancer Target Research**. Methods Mol Biol. 2019;1953:183-211.
50. Méndez-Lucio O, Baillif B, Clevert DA, Rouquié D, Wichard J. **De novo generation of hit-like molecules from gene expression signatures using artificial intelligence**. Nat Commun. 2020;11(1):10.
51. Gimeno A, Ojeda-Montes MJ, Tomás-Hernández S, Cereto-Massagué A, Beltrán-Debón R, Mulero M, et al. **The Light and Dark Sides of Virtual Screening: What Is There to Know?** Int J Mol Sci. 2019;20(6).
52. Talevi A. **Computer-Aided Drug Design: An Overview**. Methods Mol Biol. 2018;1762:1-19.
53. Rees DC, Congreve M, Murray CW, Carr R. **Fragment-based lead discovery**. Nat Rev Drug Discov. 2004;3(8):660-72.
54. Carr RA, Congreve M, Murray CW, Rees DC. **Fragment-based lead discovery: leads by design**. Drug Discov Today. 2005;10(14):987-92.

55. Sonawane R, Wagh R, Dhumane J, Deore A. **The Stages of Drug Discovery and Development Process**. Asian Journal of Pharmaceutical Research and Development. 2019;7(6):62-7.
56. Yonchev D, Bajorath J. **Integrating computational lead optimization diagnostics with analog design and candidate selection**. Future Sci OA. 2020;6(3):Fso451.
57. Brake K, Gumireddy A, Tiwari A, Chauhan H, Kumari D. **In vivo Studies for Drug Development via Oral Delivery: Challenges, Animal Models and Techniques**. 2017;08(09):1-11.
58. Ma C, Peng Y, Li H, Chen W. **Organ-on-a-Chip: A New Paradigm for Drug Development**. Trends Pharmacol Sci. 2021;42(2):119-33.
59. Tamimi NA, Ellis P. **Drug development: from concept to marketing!** Nephron Clin Pract. 2009;113(3):c125-31.
60. Bisswanger H. **Enzyme assays.** Perspectives in Science. 2014;1(1-6):41-55.
61. Boeckx J, Hertog M, Geeraerd A, Nicolai B. **Kinetic modelling: an integrated approach to analyze enzyme activity assays**. Plant Methods. 2017;13:69.
62. Greis KD. **Mass spectrometry for enzyme assays and inhibitor screening: an emerging application in pharmaceutical research**. Mass Spectrom Rev. 2007;26(3):324-39.
63. Li M, Chou J, King KW, Jing J, Wei D, Yang L. **ICECAP: an integrated, general-purpose, automation-assisted IC50/EC50 assay platform**. J Lab Autom. 2015;20(1):32-45.
64. Lorenz U. **Protein tyrosine phosphatase assays**. Curr Protoc Immunol. 2011;93:11.7.1-.7.2.
65. Smyth MS, Martin JH. **x ray crystallography**. Mol Pathol. 2000;53(1):8-14.
66. Parker MW. **Protein structure from x-ray diffraction**. J Biol Phys. 2003;29(4):341-62.
67. McPherson A, Gavira JA. I**ntroduction to protein crystallization**. Acta Crystallogr F Struct Biol Commun. 2014;70(Pt 1):2-20.
68. Pascual E, Addadi L, Andrés M, Sivera F. **Mechanisms of crystal formation in gout-a structural approach**. Nat Rev Rheumatol. 2015;11(12):725-30.
69. Erdemir D, Lee AY, Myerson AS. **Nucleation of crystals from solution: classical and two-step models**. Acc Chem Res. 2009;42(5):621-9.
70. Delmar JA, Bolla JR, Su CC, Yu EW. **Crystallization of membrane proteins by vapor diffusion**. Methods Enzymol. 2015;557:363-92.
71. Russo Krauss I, Ferraro G, Pica A, Márquez JA, Helliwell JR, Merlino A. **Principles and methods used to grow and optimize crystals of protein-metallodrug adducts, to determine metal binding sites and to assign metal ligands**. Metallomics. 2017;9(11):1534-47.
72. Forsythe EL, Maxwell DL, Pusey M. **Vapor diffusion, nucleation rates and the reservoir to crystallization volume ratio**. Acta Crystallogr D Biol Crystallogr. 2002;58(Pt 10 Pt 1):1601-5.
73. Segeritz C-P, Vallier L. **Cell culture**. Basic Science Methods for Clinical Researchers. 2017:151-72.
74. Niepel M, Hafner M, Chung M, Sorger PK. **Measuring Cancer Drug Sensitivity and Resistance in Cultured Cells.** Curr Protoc Chem Biol. 2017;9(2):55-74.
75. Riss TL, Moravec RA, Niles AL, Duellman S, Benink HA, Worzella TJ, et al. **Cell Viability Assays**. In: Markossian S, Grossman A, Brimacombe K, Arkin M, Auld D, Austin C, et al., editors. Assay Guidance Manual. Bethesda (MD): Eli Lilly & Company and the National Center for Advancing Translational Sciences; 2004.

76. Wei F, Wang S, Gou X. **A review for cell-based screening methods in drug discovery**. Biophys Rep. 2021;7(6):504-16.
77. Watanabe M, Sheriff S, Lewis KB, Cho J, Tinch SL, Balasubramaniam A, et al. **Metabolic Profiling Comparison of Human Pancreatic Ductal Epithelial Cells and Three Pancreatic Cancer Cell Lines using NMR Based Metabonomics**. J Mol Biomark Diagn. 2012;3(2).
78. Lieber M, Mazzetta J, Nelson-Rees W, Kaplan M, Todaro G. **Establishment of a continuous tumor-cell line (panc-1) from a human carcinoma of the exocrine pancreas**. Int J Cancer. 1975;15(5):741-7.
79. Lall N, Henley-Smith CJ, De Canha MN, Oosthuizen CB, Berrington D. **Viability Reagent, PrestoBlue, in Comparison with Other Available Reagents, Utilized in Cytotoxicity and Antimicrobial Assays**. Int J Microbiol. 2013;2013:420601.
80. Xu M, McCanna DJ, Sivak JG. **Use of the viability reagent PrestoBlue in comparison with alamarBlue and MTT to assess the viability of human corneal epithelial cells**. J Pharmacol Toxicol Methods. 2015;71:1-7.
81. Indo Y, Kitano A, Endo F, Akaboshi I, Matsuda I. **Altered kinetic properties of the branched-chain alpha-keto acid dehydrogenase complex due to mutation of the beta-subunit of the branched-chain alpha-keto acid decarboxylase (E1) component in lymphoblastoid cells derived from patients with maple syrup urine disease**. J Clin Invest. 1987;80(1):63-70.
82. Mahdizadehdehosta R, Kianmehr A, Khalili A. **Isolation and characterization of Leucine dehydrogenase from a thermophilic Citrobacter freundii JK-91strain Isolated from Jask Port**. Iran J Microbiol. 2013;5(3):278-84.
83. Bell MR, Engleka MJ, Malik A, Strickler JE. **To fuse or not to fuse: what is your purpose?** Protein Sci. 2013;22(11):1466-77.
84. Gomes L, Monteiro G, Mergulhão F. **The Impact of IPTG Induction on Plasmid Stability and Heterologous Protein Expression by Escherichia coli Biofilms.** Int J Mol Sci. 2020;21(2).
85. Shehadul Islam M, Aryasomayajula A, Selvaganapathy P. **A Review on Macroscale and Microscale Cell Lysis Methods**. Micromachines. 2017;8(3).
86. Block H, Maertens B, Spriestersbach A, Brinker N, Kubicek J, Fabis R, et al. **Immobilized-metal affinity chromatography (IMAC): a review**. Methods Enzymol. 2009;463:439-73.
87. Nowakowski AB, Wobig WJ, Petering DH. **Native SDS-PAGE: high resolution electrophoretic separation of proteins with retention of native properties including bound metal ions.** Metallomics. 2014;6(5):1068-78.
88. Kielkopf CL, Bauer W, Urbatsch IL. **Sodium Dodecyl Sulfate-Polyacrylamide Gel Electrophoresis of Proteins**. Cold Spring Harb Protoc. 2021;2021(12).
89. Andrew SM, Titus JA, Zumstein L. **Dialysis and concentration of protein solutions**. Curr Protoc Toxicol. 2002;Appendix 3:A.3h.1-5.
90. Hagel L. **Gel-filtration chromatography**. Curr Protoc Mol Biol. 2001;44:10.9.1-.9.2.
91. McAvoy T, Nairn AC. **Serine/threonine protein phosphatase assays**. Curr Protoc Mol Biol. 2010;92:18.7.1-.7.1.
92. Lukesh JC, 3rd, Palte MJ, Raines RT. **A potent, versatile disulfide-reducing agent from aspartic acid**. J Am Chem Soc. 2012;134(9):4057-9.
93. Nikfarjam L, Farzaneh P. **Prevention and detection of Mycoplasma contamination in cell culture**. Cell J. 2012;13(4):203-12.
94. Masters JR, Stacey GN. **Changing medium and passaging cell lines**. Nat Protoc. 2007;2(9):2276-84.

95. Scott JE, Williams KP. **Validating Identity, Mass Purity and Enzymatic Purity of Enzyme Preparations**. In: Markossian S, Grossman A, Brimacombe K, Arkin M, Auld D, Austin C, et al., editors. Assay Guidance Manual. Bethesda (MD): Eli Lilly & Company and the National Center for Advancing Translational Sciences; 2004.
96. Raran-Kurussi S, Cherry S, Zhang D, Waugh DS. **Removal of Affinity Tags with TEV Protease**. Methods Mol Biol. 2017;1586:221-30.
97. Almo SC, Bonanno JB, Sauder JM, Emtage S, Dilorenzo TP, Malashkevich V, et al. **Structural genomics of protein phosphatases**. J Struct Funct Genomics. 2007;8(2-3):121-40.

APPENDIX

Appendix A: Materials, instruments, chemicals, and software

A1 Materials and instruments

Material and instrument	*Manufacturer*
ARCTIC EXPRESS DE3/pETSUMO PP2Cm *E. coli* cells	Agilent Technologies
BL21 OneShot/pET-SUMO PP2Cm *E. coli* cells	Agilent Technologies
BL21-RIL/PCS563 6-His-TEV protease *E. coli* cells	Agilent Technologies
Luria Broth	Invitrogen
311DS shaking incubator	Labnet International
Multitron incubator rotary shaker	Infors HT
Eppendrof Biophotometer	VWR
Sorvall lynx 6.000 centrifuge	Thermo Scientific
Fiberlite F9- 6x1.000 Lex angle rotor	Thermo Scientific
Vibra Cell sonicator	Sonics & Meterials Inc.
Fiberlite F21-8x50y angle rotor	Thermo Scientific
Econo-Column	Bio-Rad
Nickel agarose	Goldbio
Novex Mini-Cell electrophoresis chamber	Invitrogen
8-12 % Bis-Tris plus 10 well gel	Invitrogen
8-12 % Bis-Tris plus 17 well gel	Invitrogen
Eppendorf heater	Eppendorf
Centrifuge galaxy mini	VWR
Multi-Shaker table	Biosan
Spectra/Por2 semipermeable dialysis membrane 12-14 kDa	Spectrum Labs
Magnet stirrer	IKA
Amicon Ultra-15 centrifugal filter unit	Sigma-Aldrich
Superdex 75 10/300 GL gel filtration column	Cytiva
NGC Quest 10 Chromatography system	Bio-Rad
Amicon Ultra Centrifugal filter 10 kDa	Merck Millipore

Nanodrop One UV-Vis spectrophotometer	Thermo Scientific
Epoch microplate spectrophotometer	Biotek
Integra Assist Plus pipetting robot	Integra Biosciences
Nunc 384-well non-treated flat-bottom microplate	Thermo Scientific
Masterblock 96 Deep Well	Hampton Research
SWISSCI MRC 2-well plate	Hampton Research
96-well manual pipette	Mettler Toledo
Mosquito Crystal crystallization robot	SPT Labtech
24-well VDX crystallization plate with sealant	Hampton Research
Circle cover slides 22 mm	Hampton Research
Microscope	Olympus
PANC-1 cells	ATCC, CRL-1469™
75 cm^2 Nunc cell culture flask	Thermo Scientific
Forma Steri-Cycle CO_2 incubator	Thermo Scientific
96-well culture microplate	Corning
Microscope	Leica Microsystems
Centrifuge, Megafuge 1.0	Heraeus instruments
Fluoroskan Microplate Fluorometer	Thermo Scientific

A2 Chemicals

Chemical	***Manufacturer***
Kanamycin	Sigma-Aldrich
$MnCl_2$	Sigma-Aldrich
MQ	Merck Millipore
IPTG	Apollo Scientific
Glycerol	VWR prolabo chemicals
Imidazole	Sigma-Aldrich
NaCl	Oslo University Hospital
Tris pH 8	Oslo University Hospital
NuPAGE LDS Sample buffer	Life Technologies

ß-mercaptoethanol	Sigma-Aldrich
SeeBlue Prestained standard	Invitrogen
SeeBlue Plus2 standard	Invitrogen
PBS	Oslo University Hospital
PNPP	Thermo Scientific
DTT	Sigma-Aldrich
DMSO	Sigma-Aldrich
Peg/Ion kit	Hampton Research
JCSG+ kit	Molecular Dimensions
PEG 3350	Sigma-Aldrich
$MgCl_2$	Sigma-Aldrich
DMEM	Sigma-Aldrich
Trypsin	Sigma-Aldrich
FBS	Sigma-Aldrich
PrestoBlue™ cell viability reagent	Invitrogen
NADH	Sigma-Aldrich
Ammonium sulfate	Sigma-Aldrich
KICA	Sigma-Aldrich

A3 Software

Software	***Manufacturer***
Gen5	BioTek
VIALAB	Integra Biosciences
Excel	Microsoft Office
Origin 2023b	OriginLab Corporation
Chromlab	Bio-Rad
Mosquito	SPT LabTech
ChemDraw 19.0	PerkinElmer

Appendix B: Buffers, staining, de-staining solution, and media

Buffer A	*Concentration*
NaCl	300 mM
Tris-HCl pH 8	50 mM
Imidazole	10 mM

Buffer B	*Concentration*
NaCl	300 mM
Tris-HCl pH 8	50 mM
Imidazole	50 mM

Buffer C	*Concentration*
NaCl	300 mM
Tris-HCl pH 8	50 mM
Imidazole	300 mM

MOPS buffer	*Mass/Volume*
EDTA pH 7.2, 0.5M	2 mL
Natrium acetate	1.36 g
MOPS	8.38 g
MQ water	1 L as a final volume

Destaining solution	*%*
Methanol	40 %
Acetic acid	10 %
Glycerol	4 %

Staining solution	*%*
Methanol	40 %
Acetic acid	10 %
Coomassie blue	0.1 %

Dialysis buffer	*Concentration*
NaCl	50 mM
Tris-HCl pH 8	20 mM
β-ME	10 mM
EDTA	0.5 mM

LB medium	*g/L*
LB broth	25 g
MQ water	1 L

Appendix C: SUMO-PP2Cm compounds

Compound	Molport ID	Manufacturer	Molecular mass (g/mol)	[Stock (85)]
1	Molport-044-207-680	ENAMINE Ltd.	306,3551	100
2	Molport-009-623-110	ENAMINE Ltd.	464,5847	50
3	Molport-005-744-015	ENAMINE Ltd.	402,8795	100
4	Molport-005-776-273	ENAMINE Ltd.	380,5032	100
5	Molport-004-451-630	ENAMINE Ltd.	458,6017	25
7	Molport-009-455-290	ENAMINE Ltd.	336,4705	100
8	Molport-009-628-078	ENAMINE Ltd.	487,6562	100
9	Molport-044-259-683	ENAMINE Ltd.	358,4561	25
10	Molport-005-781-848	ENAMINE Ltd.	480,6686	100
11	Molport-005-799-115	ENAMINE Ltd.	644,6496	100
12	Molport-044-291-795	ENAMINE Ltd.	411,4525	100
13	Molport-044-398-921	ENAMINE Ltd.	301,385	100
A2	Molport-005-774-734	ENAMINE Ltd.	440,7	100
A3	Molport-005-764-551	ENAMINE Ltd.	370,9	100
A4	Molport-009-473-565	ENAMINE Ltd.	288,3	50

Appendix D: Supplementary figures

D1 Raw data from dephosphorylation phosphatase activity assay

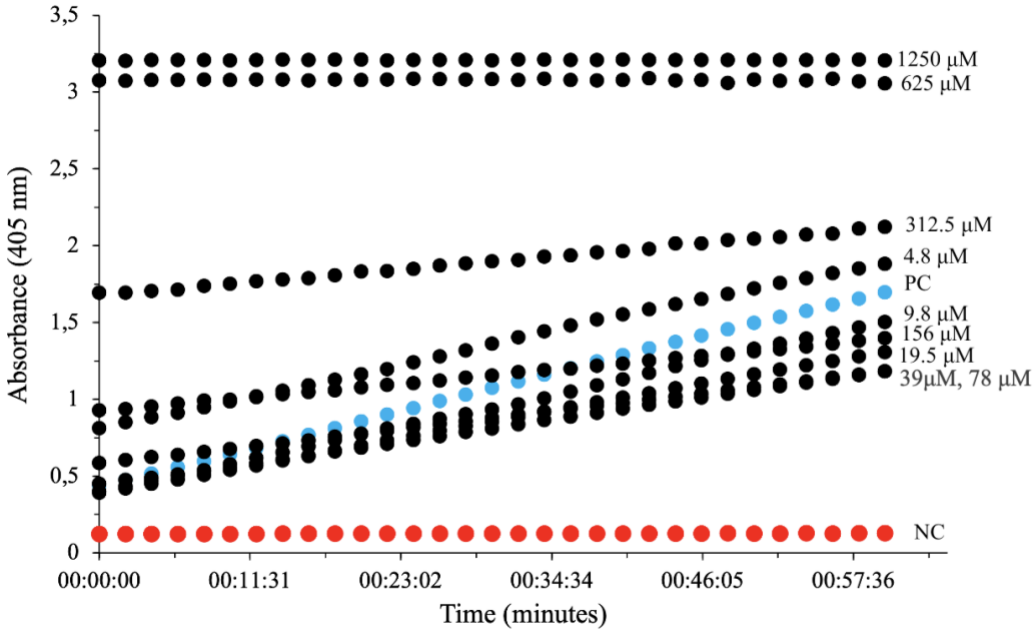

Figure D1. Raw data from dephosphorylation phosphatase assay with one of the compounds. *The positive (PC) and negative (NC) controls are presented in blue and red, respectively. Black color represents different concentrations of the compound. PC equals to 100% activity, while NC equals to 0% activity. The absorbance of pNPP was measured spectrophotometrically at 405 nm for one hour, reading every second minute. The increasing curves represent the increasing consumption of pNPP, which is stoichiometrically parallel to SUMO-PP2Cm activity. The slope of the increase in absorbance was calculated in a time window of 15 minutes. The data was normalized to determine SUMO-PP2Cm activity.*

D2 Raw data from optimization of FL SUMO-PP2Cm activity assay

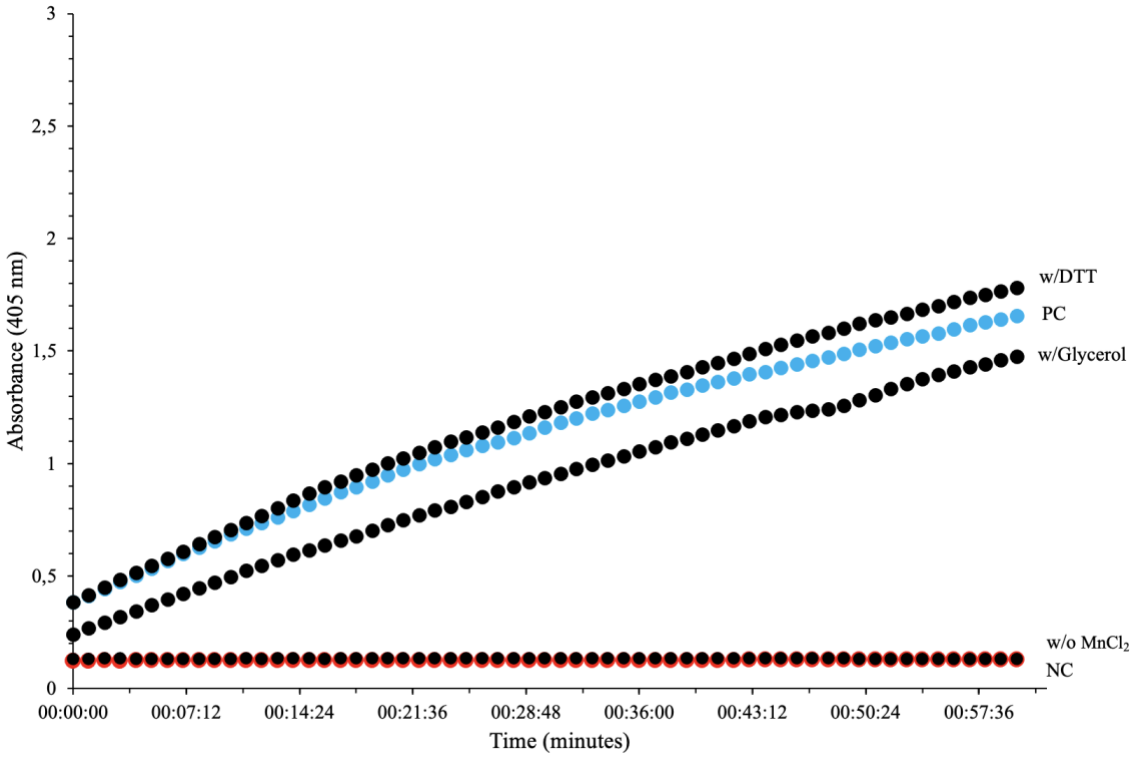

Figure D2. Raw data from optimization of FL SUMO-PP2Cm activity assay. *The positive (PC) and negative (NC) controls are presented in blue and red, respectively. The black curves represent the different parameters tested. This assay looked at the effect of DTT on FL SUMO-PP2Cm activity, if the enzyme activity was affected when stored with 50% glycerol, and the enzymes' dependency on* $MnCl_2$.

D3 Dephosphorylation phosphatase activity assay with compounds 1, 2, and 12.

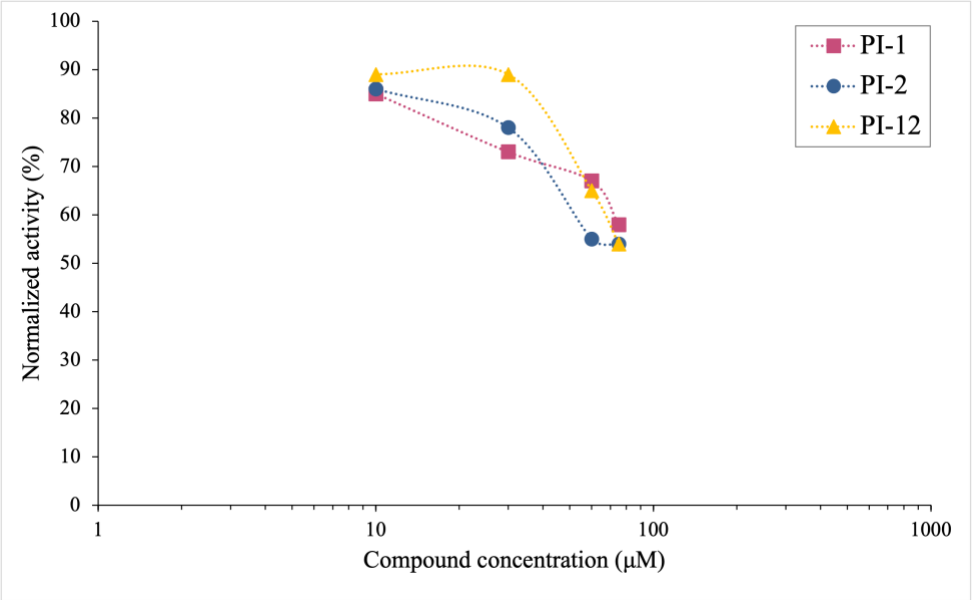

Figure D3. Dephosphorylation phosphatase activity assay with compounds 1, 2, and 12. *Different concentrations of 10, 30, 60, and 75 µM compound concentrations with compounds 1, 2, and 12 were manually tested to investigate lower* IC_{50} *values. Four parallels were included for each concentration of the compounds. The compound concentrations are plotted against the normalized activity. None of these compound concentrations reduced enzyme activity to below 50%.*

Appendix E: Compound number and structure

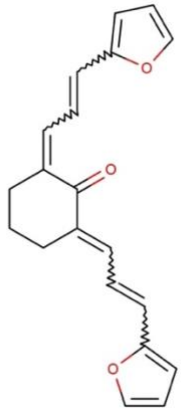

1

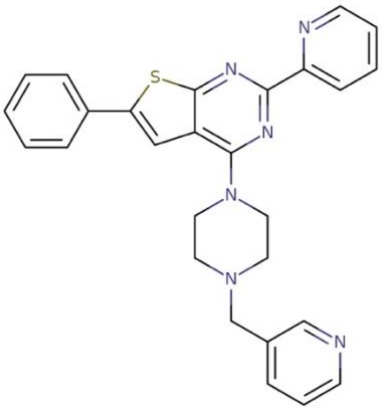

2

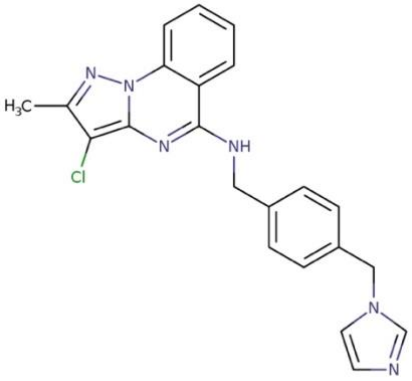

3

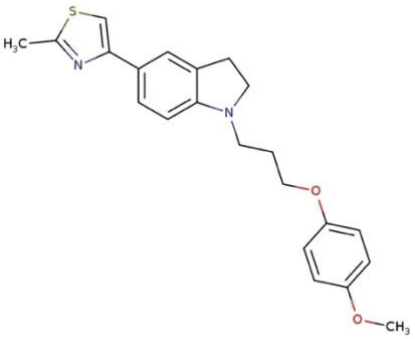

4

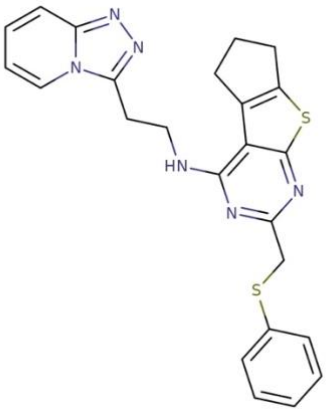

5

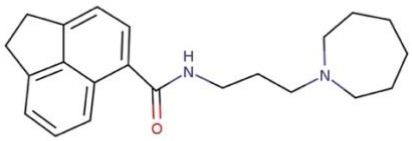

7

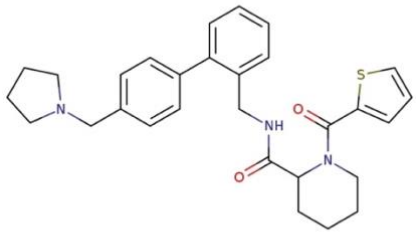
N
NH
O
S
O
N

8

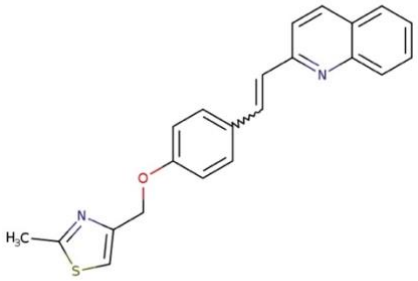
N
O
N
S
H3C

9

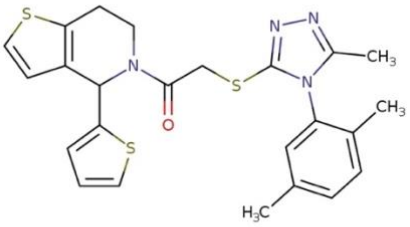
S
N
N
N
CH3
S
O
S
CH3
H3C

10

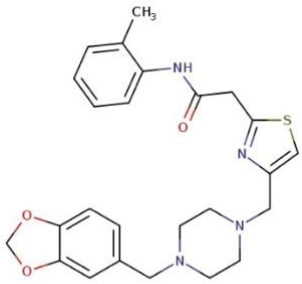
CH3
NH
O
S
N
O
O
N
N

11

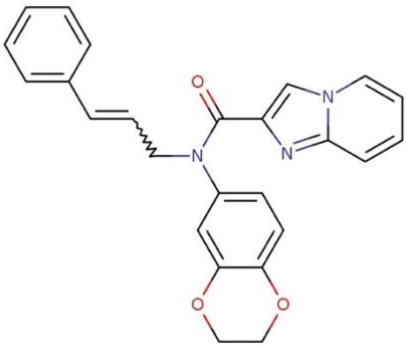
O
N
N
O
O
O

12

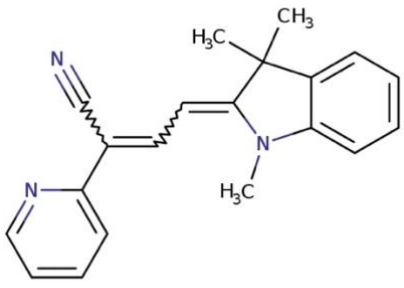
CH3
H3C
N
N
N
H3C

13

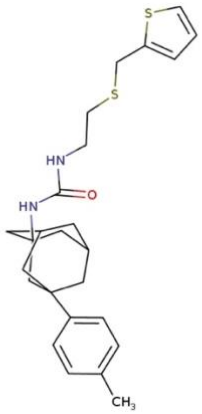

A2

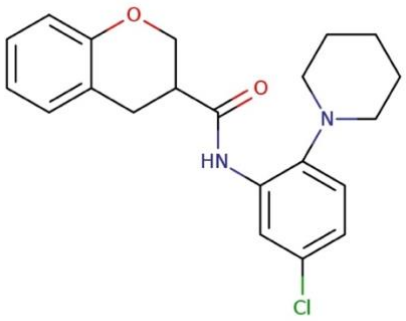

A3

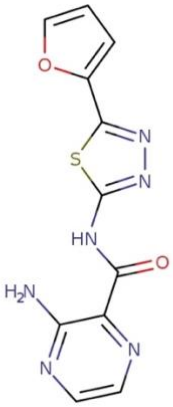

A4